THESIS

QUANTIFICATION OF VOLATILE ORGANIC COMPOUND EMISSIONS FROM UNCONVENTIONAL OIL AND GAS DEVELOPMENT

Submitted by

Weixin Zhang

Department of Atmospheric Science

In partial fulfillment of the requirements

For the Degree of Master of Science

Colorado State University

Fort Collins, Colorado

Fall 2024

Master's Committee:

Advisor: Jeffrey L. Collett, Jr.

Da Pan
Jeffrey R. Pierce
Jay M. Ham

ABSTRACT

QUANTIFICATION OF VOLATILE ORGANIC COMPOUND EMISSIONS FROM UNCONVENTIONAL OIL AND GAS DEVELOPMENT

Oil and gas (O&G) development in the U.S. has accelerated in the past two decades, aided by unconventional extraction techniques including hydraulic fracturing and horizontal drilling. Potential environmental and health impacts of volatile organic compounds (VOCs) originating from O&G activities in populated regions have raised concerns. In Broomfield, Colorado, six new O&G well pads were approved for development in 2017 and an air monitoring program was established in October 2018 to collect weekly and later plume-triggered air samples. This study addresses the limited existing knowledge of activity-specific VOC emission rates from unconventional O&G development (UOGD), utilizing these observations and dispersion model simulations through emission inversion methods. Emissions are characterized from well drilling, hydraulic fracturing, coiled tubing/millout, flowback, and production operations.

Substantial variations in average VOC emission rates, determined using weekly canister observations, are observed across different UOGD phases. Drilling and coiled tubing/millout operations exhibit the highest total VOC emission rates, attributed to hydrocarbon release from shale formations and drilling mud. In contrast, hydraulic fracturing gives lower emission rates, consistent with injection of fluids into the well during this operation, minimizing the probability of subsurface hydrocarbon emissions. Diesel-powered engines are identified as the primary ethyne sources during hydraulic fracturing. Production was characterized by lower VOC emission rates than pre-production phases but remains an important emission category due to its long duration (decades). Variations of emission rates within each phase highlight the complexity of factors and activities influencing emission rates, including, for example, vertical vs. horizontal drilling and periodic maintenance activities. VOC emission rates associated with drilling mud volatilization and

hydraulic fracturing suggest that previously published emission estimates (EPA (2022), and Hecobian et al. (2019)) underestimate average VOC emission rates during these activities. Significantly lower emission rates during flowback compared to previous work (Hecobian et al., 2019) reveal how improved management practices, including tankless, closed-loop fluid handling systems have effectively reduced what used to be a dominant source of pre-production VOC emissions. Plume-triggered samples, capturing transient high-concentration plumes, reveal short-term VOC emission rates approximately an order of magnitude higher for drilling and flowback than determined from weekly samples. In the case of flowback, short-term emission pulses have been linked to periodic emptying of sand canisters used to trap fracking sand emerging from previously fracked wells.

ACKNOWLEDGEMENTS

The four-year field observation data from the Broomfield Air Quality Monitoring Program (AQM) is an important component of this thesis. AQM, a collaborative effort between Ajax Analytics and the Collett Research Group in the Department of Atmospheric Science at Colorado State University, was funded by the City and County of Broomfield.

I would like to express my sincere gratitude to Dr. Da Pan, Dr. Jeffrey Pierce, and Dr. Jay Ham for serving on my Master's committee and providing valuable feedback on this work. A special acknowledgment goes to Da Pan for his mentorship during both my research and fieldwork endeavors. I owe my deepest thanks to my advisor, Dr. Jeffrey Collett, whose support and guidance have been the foundation of this academic pursuit. Gratitude is extended to Dr. Yong Zhou, Dr. Arsineh Hecobian, Dr. Katie Benedict, and Dr. I-Ting Ku, whose contributions to AQM were indispensable.

Lastly, I want to thank my mother, whose unwavering love, support, and encouragement have been the guiding light throughout my academic journey. Though she is no longer with me, her presence and influence continue to shape my life and accomplishments.

DEDICATION

Dedicated to my mother, with heartfelt thanks for everything she had given me.

TABLE OF CONTENTS

LIST OF TABLES

LIST OF FIGURES

Chapter 1

Introduction

1.1 Volatile Organic Compounds

Pervasive in the atmosphere, volatile organic compounds (VOCs) are reactive chemicals emitted from biogenic and anthropogenic sources. Biogenic VOCs are often abundant, and their sources include vegetation, wildfires, soils, and oceans. Anthropogenic VOCs are emitted from fossil fuel use and production, chemical products, oil and gas (O&G) operations, and biomass combustion (Atkinson et al., 2003; Reimann et al., 2007; Gilman et al., 2009; Lachenmayer, 2022; Ku et al., 2024).

VOCs can cause direct adverse health effects and are precursors of secondary air pollutants. The U.S. Environmental Protection Agency (EPA) classifies some VOCs as hazardous air pollutants (HAPs), which can cause cancer and/or other serious health impacts (EPA, 2015a). VOC emissions from O&G operations contain several HAPs – benzene, toluene, ethylbenzene, xylenes (BTEX), and hexane (EPA, 2015b). Atmospheric oxidation of VOCs produces tropospheric ozone and secondary organic aerosol (Gkatzelis et al., 2021), contributing to air pollution and adverse health effects (De Gouw et al., 2009; Stevenson et al., 2013; Mochizuki et al., 2015; Gu et al., 2021).

In recent years, regions near O&G producing basins have experienced air quality issues caused by VOC emissions (Buzcu and Fraser, 2006; Rutter et al., 2015; Prenni et al., 2016; Hecobian et al., 2019; Roest and Schade, 2020; Ku et al., 2024). One such region is the Colorado Northern Front Range (CNFR) near the Denver-Julesburg (DJ) O&G basin, where summertime ozone concentrations exceed the National Ambient Air Quality Standards (Cheadle et al., 2017). Air toxics emitted during O&G activities have also been raising concerns in the region. Previous studies conducted in the DJ basin showed that O&G operations are major contributors to VOC emissions in the CNFR (Pétron et al., 2012, 2014; Gilman et al., 2013; Swarthout et al., 2013; Thompson et

al., 2014; Halliday et al., 2016; McKenzie et al., 2018; Ku et al., 2024). However, VOC emissions from specific O&G activities are poorly constrained, and more accurate emission estimates are needed to facilitate policymaking and effective design of emission reduction strategies.

1.2 Oil and Gas in Colorado

As of January 2024, Colorado is the 6^{th} largest O&G producing state in the U.S. (ShaleXP, https://www.shalexp.com/colorado, accessed on 2024-04-07). Annual crude oil production and natural gas gross withdrawals in Colorado from 1981 to 2022 are shown in Figure 1.1 (Data credit: U.S. Energy Information Administration). The rapid increase of O&G production after 2000 was aided by unconventional extraction techniques (Lachenmayer 2022), including hydraulic fracturing and directional drilling. Currently, there are approximately 35,000 active O&G wells in Colorado. The locations of all O&G wells (active & abandoned) in Colorado and the CNFR are shown in Figure 1.2 (Data obtained on 2024-01-04 from Colorado Energy & Carbon Management Commission). O&G well density is high in many residential communities.

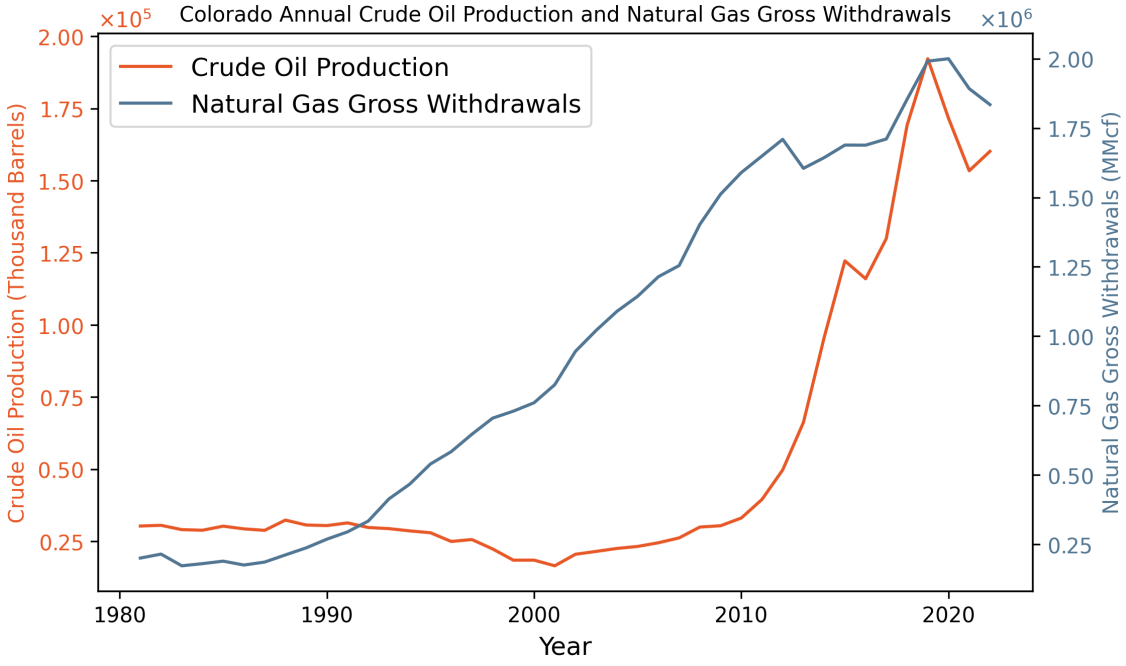

Figure 1.1: Annual crude oil production and natural gas gross withdrawals in Colorado from 1981 to 2022 (Data credit: U.S. Energy Information Administration).

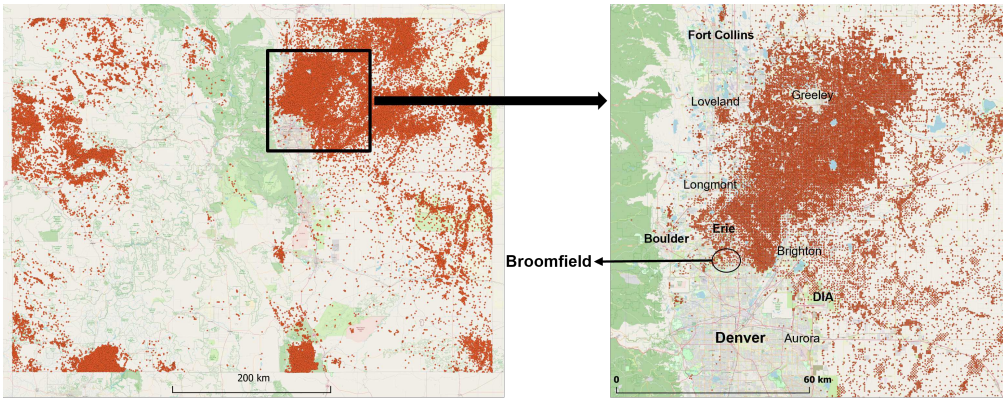

Figure 1.2: Locations of O&G wells in Colorado (left panel) and the CNFR (right panel). Data obtained from Colorado Energy & Carbon Management Commission.

1.3 UOGD and Potential Emission Sources

The United States became the world's largest producer of oil and natural gas in 2014, primarily aided by the improvement and incorporation of unconventional O&G extraction techniques (horizontal drilling and hydraulic fracturing) (Allen, 2016). Unconventional O&G development (UOGD) includes several phases: (1) well pad preparation, (2) drilling, (3) hydraulic fracturing (fracking), (4) coiled tubing/millout, (5) production tubing installation, (6) flowback, and (7) production. The descriptions of each phase are provided below, and more detailed information can be found in the report by EPA (2019): Management of Exploration, Development and Production Wastes: Factors Informing a Decision on the Need for Regulatory Action. The typical durations of different operations provided below are based on the timelines for the six large well pads developed in Broomfield, each with a varying number of wells ranging from 4 to 18. Different O&G development phases have different emission sources with different VOC emissions. (MacDonald, 2015; Hecobian et al., 2019; Orak et al., 2021; Lachenmayer, 2022; Ku et al., 2024).

The first phase is well pad preparation, which includes constructing the well pad, installing sound walls to reduce light and noise pollution, building roads to the pad, and installing required machines/instruments.

The second phase is drilling. Typically, a wellbore is drilled vertically first until the target depth is reached and is then drilled horizontally through the desired shale or tight sand formation. There are multi-casing layers surrounding the wellbore, preventing the collapse of the wellbore and the leakage of O&G into subterranean aquifers. Drilling mud is circulated to lubricate and cool the drill bit and to help bring drill cuttings back up to the surface through the space between the drill pipe and the wellbore. Drilling often takes one to four months. During this phase, potential air pollutant emission sources include drilling mud as it's being recycled on-site and handled by shale shakers and centrifuges (MacDonald, 2015; Ku et al., 2024), fugitive emissions of natural gas, truck traffic, and diesel or natural gas drilling rigs (Orak et al., 2021; Lachenmayer, 2022; Ku et al., 2024). Increasingly, some operators use electric drilling rigs instead of diesel/natural gas rigs to reduce on-site emissions (Ku et al., 2024) and noise.

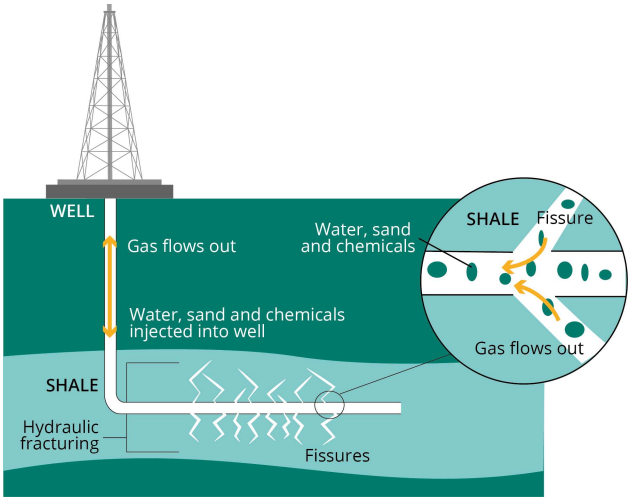

Figure 1.3: Schematic of hydraulic fracturing (fracking). Figure credit: European Environment Agency (https://www.eea.europa.eu/media/infographics/shale-gas-extraction-through-hydraulic-fracturing/view).

Once drilling is completed, a perforated gun with explosives is used to create holes in the casing. Then, hydraulic fracturing can start – a large volume of hydraulic fracturing fluid made with water, sand and chemicals (e.g., surfactants) is injected into the well and pressurized to create/expand tiny fissures in the shale rock. The sand acts as a proppant holding the fractures open and allowing O&G to eventually flow into the well. The hydraulic fracturing process is shown in

Figure 1.3. Fracking operation can last from weeks to two months. Truck traffic, diesel-powered compressors, and power generators can be major contributors to the emissions during hydraulic fracturing (MacDonald, 2015; Orak et al., 2021). It is currently challenging to electrify the fracking processes to reduce emissions because of the high-power requirements.

The next two phases are coiled tubing/millout and production tubing installation, which together can last from days to weeks. Coiled tubing is used to perforate pressure plugs inserted between well stages during fracking and facilitates the circulation of fluids via a jet nozzle, transporting both fluid and debris to the surface. Production tubing installation – the final tubing phase, typically extends through the entire well depth, effectively isolating the production zone from surrounding formations. Ku et al. (2024) observed high-concentration VOCs during coiled tubing/millout operations in Broomfield from unidentified sources.

Before production starts, fluids injected to the well during fracking need to be removed during the flowback phase, which often lasts three to six months. The waste water returned from the well includes both water injected during fracking operations and produced water that comes from the formation and is directed to pits, storage tanks, or piped off-pad before being either disposed or recycled for further fracking use. The flowback water can contain proppant sands used in fracking, which are separated and stored in sand cans. These sand cans are cleaned frequently at the beginning of the flowback phase when sand loads in the flowback fluids are high. During flowback, emissions of VOCs from water separation tanks, venting, and degassing of produced waters can occur (Orak et al., 2021). And for the well pads using an on-site open tank/pit to store waste water, the hot fluids returning to the surface can increase the concentration of dissolved organic compounds that can volatilize during the process. In areas with stricter environmental regulations or concerns, closed-loop fluid handling systems with off-pad storage are sometimes employed. This approach is intended to decrease fugitive emissions, although emissions can still occur during the periodic emptying of sand cans (MacDonald, 2015; Lachenmayer, 2022; Ku et al., 2024).

After the flowback phase, the well goes into production, which can last from years to decades. Even in production, a well can still be a VOC emission source (MacDonald 2015; Wilde et al.,

2021). Potential emission sources include, but are not limited to, on-pad separators and their maintenance operations, heater, compressor, wellhead, flaring, dehydration systems and fugitive emissions from equipment leaks (Allen et al., 2015; Zavala-Araiza et al., 2015; MacDonald 2015; Ku et al., 2024).

1.4 VOC Emissions from Oil and Gas

O&G industry is the largest industrial emission source of VOCs (EPA, 2023a). EPA's emission inventories have been compiled using the 2020 Nonpoint Oil and Gas Emission Estimation Tool (EPA Emission Tool) (Eastern Research Group, Inc., 2022). There are concerns, however, about the representativeness of this tool's emission factors for current operational practices. For example, the drilling mud degassing emission factor was based on a 1977 EPA report for offshore oil and gas development (Energy Resources Co, Inc., 1977), which considered different drilling muds than those used today for onshore UOGD under very different working conditions. In addition, several sources were not considered in the EPA Emission Tool, such as coiled tubing/millout operations and closed loop, tankless flowback operations and associated emptying of the sand cans.

To better constrain the impact of VOC emissions from different UOGD operations, previous field campaigns and model studies have been conducted (e.g., Leuchner and Rappenglück, 2010; Rutter et al., 2015; Hecobian et al., 2019; Roest and Schade, 2020; Ku et al., 2024). Several studies focusing on the DJ Basin have been conducted to apportion VOC sources (Pétron et al., 2012; Gilman et al., 2013; Swarthout et al., 2013; Thompson et al., 2014; Abeleira et al., 2015; Pollack et al., 2021) and concluded O&G operations are major contributors to VOCs in the region.

Despite these efforts, few studies have constrained the emission rates of VOCs from specific UOGD operations (MacDonald, 2015; Hecobian et al., 2019). Emission rates have several advantages over the ambient concentration values reported in many previous studies. Emission rates (factors), combined with activity data, can be used to estimate quantitative emission inventories. Accurate emission inventories are critical for predictive modeling for exposure assessments and

the design of effective emission control and remediation strategies. (Ekuland, 1992; MacDonald, 2015).

Based on the emission factors provided in the 1977 EPA report for offshore oil and gas development (Energy Resources Co, Inc., 1977), Wilson et al. (2007) estimated methane and non-methane total VOC emission rates during drilling from the degassing of synthetic based drilling muds to be 0.68 and 0.36 g/s, respectively. Campbell et al. (2021) estimated substantially lower onshore synthetic drilling mud degassing emission factors according to American Petroleum Institute comments to EPA (Koblitz, 2020) with estimated emission rates for methane and non-methane total VOCs of 0.119 and 0.064 g/s, respectively. The EPA Emission Tool estimates that flowback green completion techniques produce no emissions of VOC. MacDonald (2015) used a tracer ratio method to quantify the emission rates of 50 VOCs during drilling, hydraulic fracturing and flowback. It was found that well pads in pre-production phases emitted much more VOCs than well pads in the production phase. Hecobian et al. (2019) reported the emission rates of as many as 46 individual VOCs during different UOGD operations using a tracer ratio method. They concluded that VOC emission rates can vary greatly between different operations and even between well pads undergoing the same operation type. The highest emission rates for most VOCs were measured during flowback while emission rates during hydraulic fracturing and production were much lower. Median emission rates for non-methane total VOC during drilling, fracking, flowback and production phases were 0.43, 0.08, 6.33, and 0.33 g/s, respectively. Notably, the flowback operations studied by Hecobian et al. in the DJ Basin between 2014 and 2016 were so-called green completions but were not the closed-loop, tankless systems now used by some operators in the region.

There remains a considerable knowledge gap in the emission factors of VOCs during different UOGD phases despite some information provided by the limited studies mentioned above. This is due to both a lack of detailed VOC speciation in some prior studies as well as ongoing changes in UOGD operations, many of which are aimed at reducing environmental impacts. Therefore, this thesis will focus on quantifying the emission rates of VOCs from UOGD between 2019 and 2022

in the city and county of Broomfield, Colorado and linking emission rates to on-site activities for future development of emission factors.

1.5 Emission Rate Measurement Methods

Although there is a lack of studies specifically designed to characterize VOC emission rates during all pre-production UOGD phases, several quantification methods (summarized in the following paragraphs) have been developed and implemented to measure emission rates of methane or other compounds. While these methods are most often applied to production emissions, they can sometimes be useful for characterizing emissions from pre-production operations.

The flux chamber method developed by the US EPA can be used to directly measure air pollutants emissions (fluxes) from a source to the atmosphere. The accuracy and precision of this approach have been evaluated and discussed (EPA, 1986; Eklund, 1992; CalEPA, 2011; Ma et al., 2020). However, this method has not frequently been used in the field to study pre-production emissions since it requires the installation of a chamber on top of the source and measuring changing concentrations of VOCs inside the chamber (EPA, 1986; Ma et al., 2020).

The tracer ratio method is more broadly used in the field to quantify emission rates of VOCs from different sources (Howard et al., 1992; Lamb et al., 1995; Taylor et al., 2016; Hecobian et al., 2019). This method releases a tracer gas with a constant emission rate at the source and collects whole air samples downwind within a certain distance. Then, the emission rate of a compound of interest is calculated as the product of the tracer's constant emission rate and the ratio of the background-corrected concentrations of the compound of interest to the tracer (Hecobian et al., 2019).

On a larger scale, a top-down mass balance method using airborne data has been used to estimate methane emissions from O&G production regions (Karion et al., 2013; Pétron et al., 2014; Peischl et al., 2015; Karion et al., 2015). The method determines the difference of integrated concentrations between vertical curtains upwind and downwind of targeted regions to determine

fluxes of measured chemical species (White et al., 1976; Peischl et al. 2016, 2018; Francoeur et al. 2021).

Mobile sampling methods are sometimes used along with Gaussian plume inversion to fill survey emissions from individual well pads (Edie et al., 2020). For example, EPA OTM33A is a mobile measurement method developed by the US EPA to estimate fluxes of methane from O&G facilities and landfills (Thoma, 2012; EPA 2014; Thoma and Squier, 2014; Brantley et al., 2014, 2015; Robertson et al., 2017; Edie et al., 2020).

These methods have several limitations. On-site measurement methods (flux chamber method & tracer ratio method) have difficulty in including all emission sources, such as tanks and generators. Accessing the well pad might also induce changes to the operations – for example, the workers are likely to be more cautious when the measurement teams are on-site, creating a bias that is difficult to determine (Alvarez et al., 2018). The tracer ratio method requires downwind accessibility of roadways within a certain distance which could vary from meters to hundred meters and requires steady wind direction during the measurement period (Omara et al., 2018; Hecobian et al., 2019; Edie et al., 2020). The top-down mass balance method requires favorable meteorological conditions such as consistent wind direction and boundary layer height (White et al., 1976; Peischl et al., 2016; Peischl et al., 2018; Francoeur et al., 2021). The mobile plume sampling with Gaussian inversion method also needs favorable wind direction & roadway access and is not able to capture all emission sources (Edie et al., 2020). Moreover, many of these methods only provide a snapshot of the emissions and can easily miss sporadic emission events with high emission rates.

In this study, we aim to develop emission characterization methods that do not require well pad access and, in the meantime, retain the long-term characteristics and provide insights into the characteristics of transient high-concentration VOC plumes sometimes observed in the field.

1.6 Thesis Overview

This thesis uses observation data (weekly & plume-triggered samples) together with simulations by a dispersion model (AERMOD) to quantify the emission rates of 51 VOCs during different

UOGD operations conducted at several large, multi-well pads developed in Broomfield, Colorado. The Broomfield dataset provides a good opportunity to test this approach since it includes observations at several locations near UOGD, in adjacent neighborhoods, and at a reference background site several kilometers distant from UOGD operations (Ku et al., 2024). We first evaluate methods for quantifying VOC emission rates using observations from drilling operations with unique VOC composition. Multiple linear regression (MLR) and observation-simulation ratio methods are developed and evaluated for weekly samples and plume-triggered event samples, respectively. These methods are then applied to all UOGD operations, and the VOC emission rates obtained are compared with previous studies where possible.

The following chapter describes the methods used in this thesis to quantify VOC emissions, including application of the AERMOD dispersion model. Chapter 3 reports and discusses results, while Chapter 4 presents conclusions and recommends future topics of study.

Chapter 2

Methods

2.1 Observation Data

2.1.1 Broomfield Air Quality Monitoring Program

The rapid increase of O&G activities in Colorado raised people's concerns, especially for residents living in close proximity to O&G well pads. To ensure a sustainable future for Broomfield, the Broomfield Comprehensive Plan was adopted. The plan consists of eleven different sections including O&G development in Broomfield. The O&G chapter of the Broomfield Comprehensive Plan mainly focuses on air quality impacts from O&G development (Byers et al., n.d.).

After six O&G well pads were approved for development in Broomfield and considering the goals and actions set in the O&G chapter of the Broomfield Comprehensive Plan, an extensive air quality monitoring network (Broomfield Air Quality Monitoring Program (AQM), n.d.) was funded by the City and County of Broomfield. This program was initially designed by Ajax Analytics and the Department of Atmospheric Science, Colorado State University to monitor air pollutant concentrations within and beyond residential areas before and after UOGD. Subsequent modifications to the monitoring approach and locations were made in consultation with Broomfield staff and approved by Broomfield Council.

Based on O&G development schedules, the air quality monitoring program began in October 2018, prior to the start of development of the first well pad and consisted of 19 monitoring sites. Some of these sites were set up near the well pads, others were established in nearby neighborhoods, and one was set at a background/reference location several kilometers from the new UOGD activities. The locations of the 6 newly developed O&G well pads and the air monitoring sites are shown in Figure 2.1. The six O&G well pads (marked as brown boxes with well pad names), from left to right in Figure 2.1, are Livingston (LS), Northwest A (NWA), Northwest B (NWB), United (UT), Interchange A (ICA) and Interchange B (ICB), respectively. In Figure 2.1, the locations of

air monitoring sites are labeled as dots with site names. The background site (Commons), selected to represent regional conditions without local impact of O&G development, is located approximately 5 km south of the region shown in Figure 2.1. Air monitoring observations from 10 sites in Broomfield were used in this thesis. The 10 sites are Commons (COM), Interchange 01 (ITC01), Interchange 02 (ITC02), Interchange 03 (ITC03), Livingston 01 (LS01), Livingston 02 (LS02), NWPKWY 02 (NWP02), NWPKWY 03 (NWP03), United 01 (UT01), and United 02 (UT02).

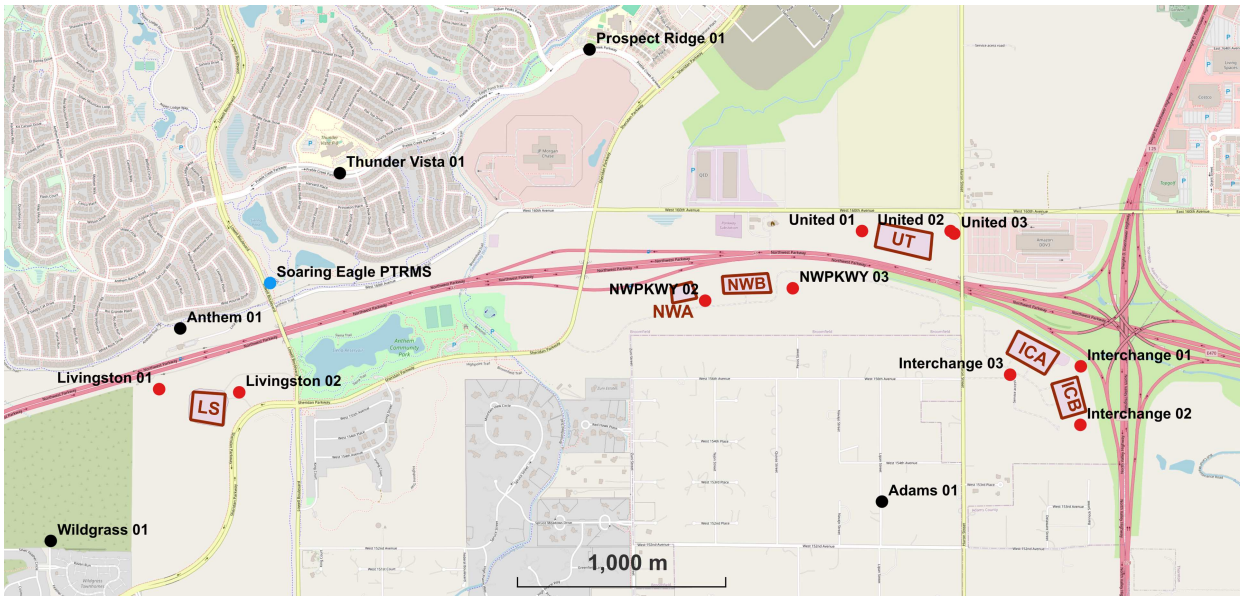

Figure 2.1: O&G well pads and monitoring sites in Broomfield, Colorado. O&G well pads are marked in brown boxes (the well pads, from left to right, are Livingston (LS), Northwest A (NWA), Northwest B (NWB), United (UT), Interchange A (ICA) and Interchange B (ICB), respectively). Monitoring sites are labeled as dots with site names. The background site – Commons (COM) is located about 5 km south of this region. Soaring Eagle site (blue dot) provides in-situ wind measurements.

Weekly, time-integrated samples collected at these sites were scheduled based on the operational timelines of nearby O&G well pads. Therefore, the sampling schedules varied from site to site. Table 2.1 lists the number of weekly canister samples collected at the 10 monitoring sites in Broomfield between the listed start date and end date. Figure 2.2 depicts the sampling timeline for each site in Broomfield. Samples were collected at COM, the background/reference site, continuously active throughout the whole period except for two weeks. Weekly samples at other

monitoring sites were not always continuous because the quantity of active monitoring sites for each week varied in accordance with operations at nearby O&G well pads.

Table 2.1: Number of weekly integrated canisters (weekly samples) collected at 10 monitoring sites in Broomfield between the listed start date and end date.

Site	Sampling Start Date	Sampling End Date	# of Weekly Samples
COM	2018-10-04	2022-12-29	220
ITC01	2018-10-04	2022-12-29	217
ITC02	2019-01-17	2022-09-22	78
ITC03	2019-01-17	2022-12-23	108
LS01	2018-10-11	2022-12-29	191
LS02	2018-11-29	2022-09-22	150
NWP02	2019-01-17	2022-09-22	50
NWP03	2019-01-17	2022-12-23	102
UT01	2019-01-17	2022-12-23	43
UT02	2019-01-17	2022-12-29	115

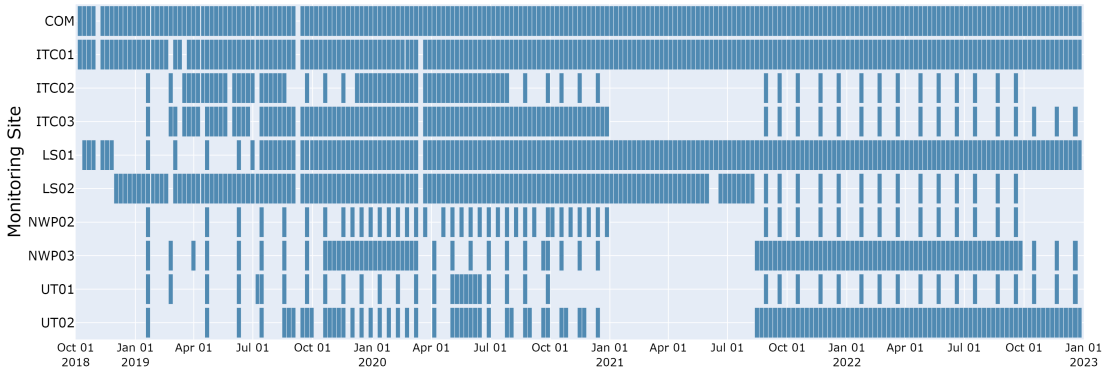

Figure 2.2: Weekly sampling timelines for 10 air monitoring sites in Broomfield.

2.1.2 Instrumentation

Weekly samples were collected with weekly integrated 6.0L canisters and were analyzed by a 5-channel gas chromatograph (GC) system. Photoionization Detector (PID) sensors provided 1-minute total VOC monitoring data in real-time. The PID sensors were coupled with a triggering

system which can collect 15-second triggered samples. A general description of the instrumentation is provided below. The limits of detection of the instruments and uncertainties of the data are provided in Lachenmayer (2022) and Ku et al. (2024).

Weekly Integrated Canister

Evacuated 6.0L Silonite®-coated canisters coupled with a flow controller (Entech Instruments Inc., Simi Valley, CA, USA) was used to collect weekly whole air samples (Figure 2.3). The flow controller maintains a constant inflow rate, such that the canister is steadily filled across a 7-day sampling period. LeBouf et al. (2012) have shown that Silonite-coated canisters can hold VOC concentrations stable for more than a month. After being retrieved back to the lab at the end of the sampling period, the weekly samples were analyzed within one week using a 5-channel GC with 3 Flame Ionization Detectors (FID), an Electron Capture Detector (ECD), and a quadrupole mass spectrometer (MS) for the concentrations of 51 VOCs. The list of 51 VOCs can be found in Figure C.3. Detailed information about the integrated canister's cleaning & evacuation, the flow controller's calibration, and the GC system can be found in Weber (2018).

Figure 2.3: Weekly integrated canister with flow controller (Picture credit: Entech Instruments).

Real-Time PID Monitoring System

Real-time PID monitoring systems (APIS, Inc., OR, USA) were deployed across the monitoring network in Broomfield at sites near O&G well pads starting in 2020. Each unit was equipped with a cup and vane anemometer to provide wind speed and wind direction data, meteorological

sensors to provide temperature, pressure, and humidity data, and a PID sensor. The PID sensor uses a 10.6 eV high sensitivity (MiniPIDs-HS, ION Science Inc., TX, USA) lamp and is sensitive to a suite of VOCs that can be photoionized at the lamp energy. It has a 15-second sampling rate and reports 1-minute integrated concentrations that are commonly referred to as total VOC (TVOC). Calibration information, bump tests, and response factors for individual VOCs can be found in Ku et al. (2024). Figure 2.4 shows the components and deployment of the real-time PID monitoring system.

The PID system was coupled with an automatic canister triggering flow controller to collect whole air samples in evacuated 1.4L Silonite®-coated canisters (Entech Instruments, CA, USA) in approximately 15 seconds fill time. In general, when the PID sensor detects a plume with a TVOC concentration higher than a pre-set threshold, the system will automatically trigger collection of a whole air sample: the flow controller opens the valve, and ambient air rapidly fills the evacuated 1.4L canister. The triggered canister is then retrieved and analyzed using the same GC system used to analyze the weekly canister.

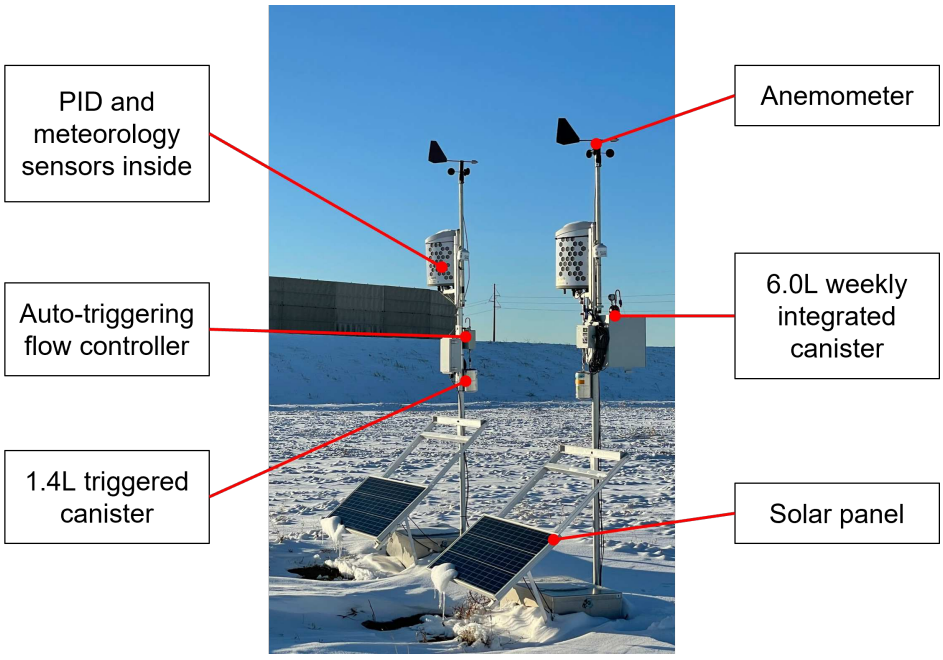

Figure 2.4: Co-located APIS real-time PID monitoring systems in Broomfield (Photo credit: Dr. Yong Zhou).

2.2 Tracers for Drilling Operations

Ku et al. (2024) analyzed four years of observations from 19 air monitoring sites in Broomfield and found that the use of a synthetic drilling mud caused significantly elevated concentrations of C_8-C_{10} n-alkanes (n-octane, n-nonane and n-decane) near well pads. To alleviate odor complaints, the operators switched from a petroleum hydrocarbon distillate-based drilling mud (Gibson D822) to a synthetic paraffin Neoflo 4633-based drilling mud (Neoflo 4633) after developing the first well in Livingston pad on 2019-07-11 (CDPHE, 2020). Concentrations of $C_8 - C_{10}$ n-alkanes observed near the well pad using the Neoflo 4633 drilling mud (Livingston pad, Figure 2.5 right panel) were significantly higher than those observed near the prior well pad drilled using the Gibson D822 drilling mud (Interchange B pad, Figure 2.5 left panel). Headspace analyses of the two drilling muds were conducted in the lab at the Department of Atmospheric Science, Colorado State University, and the results are shown in Figure 2.6. The results show that the Neoflo 4633 drilling mud emits more n-octane, n-nonane and n-decane than the Gibson D822 drilling mud by a factor of about 10, consistent with the enhanced concentrations of these species observed during drilling operations at the Livingston vs. the Interchange B pads.

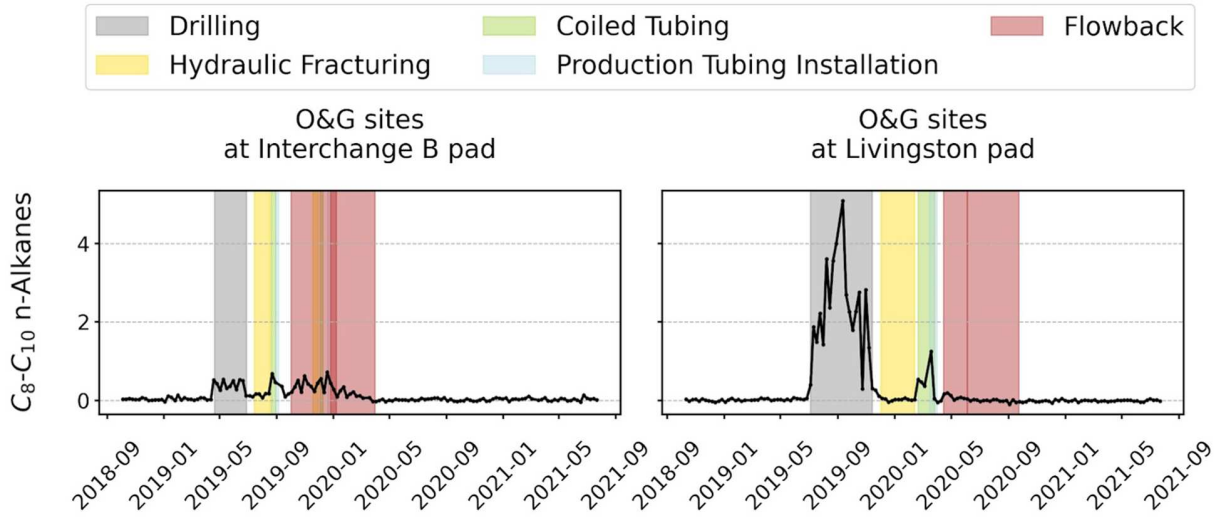

Figure 2.5: Time series of background-corrected $C_8 - C_{10}$ n-alkane concentrations (unit: ppbv) at monitoring sites near the Interchange B pad (left panel) and Livingston pad (right panel). Colored areas represent periods with different O&G operations. (Figure credit: Ku et al., 2024)

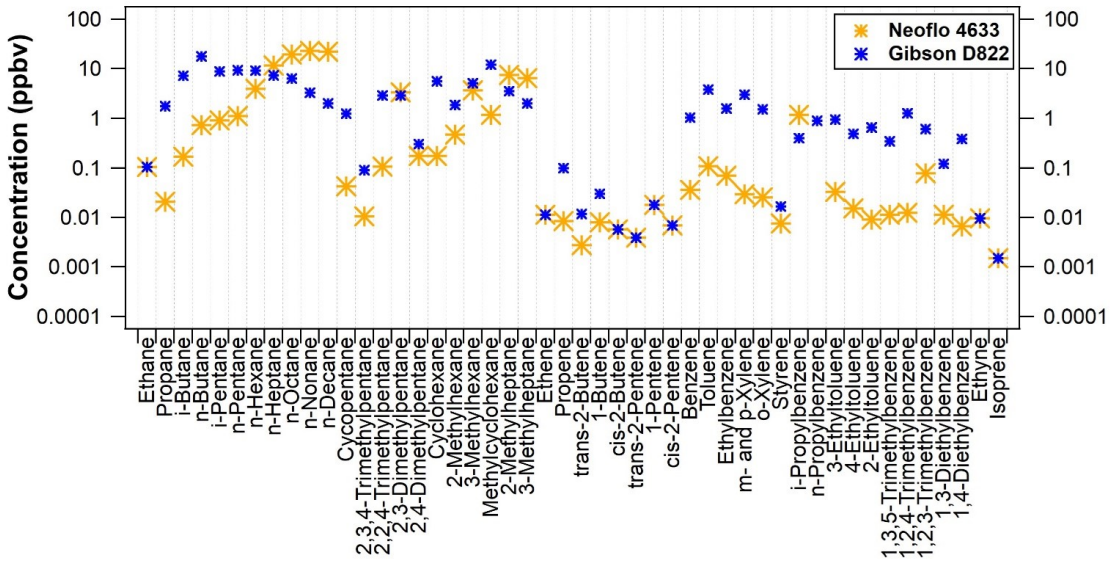

Figure 2.6: Comparison of VOC composition for Neoflo 4633 and Gibson D822 drilling muds from a laboratory headspace analysis. (Figure credit: Ku et al., 2024)

As discussed by Ku et al. (2024), the $C_8 - C_{10}$ n-alkanes are unique tracers for drilling operations using the Neoflo 4633 mud because emissions of $C_8 - C_{10}$ n-alkanes from the drilling mud are far higher than from other sources. Therefore, in this thesis, I use $C_8 - C_{10}$ n-alkanes to test if the inverse modeling is correctly identifying the location and timing of well pads that were drilled using the Neoflo 4633 mud. More specifically, I first quantify the emission rates of $C_8 - C_{10}$ n-alkanes from different well pads using the weekly and plume-triggered canister samples collected in Broomfield, and then I investigate if elevated $C_8 - C_{10}$ n-alkane emission periods are aligned with their drilling periods.

2.3 Dispersion Model

2.3.1 AERMOD Overview

The AMS and EPA Regulatory Model (AERMOD) is used to simulate the dispersion and concentration of VOCs from O&G operations in this thesis. AERMOD was developed by the American Meteorological Society (AMS) and EPA (EPA, 2023b). As a steady-state plume model, AERMOD treats vertical and horizontal concentration distributions to be Gaussian when in the

stable boundary layer. In the convective boundary layer, the horizontal distribution is also Gaussian while the vertical distribution is assumed to follow a bi-Gaussian probability density function, based on the model developed and demonstrated by Willis and Deardorff (1981) and Briggs (1993). AERMOD incorporates air dispersion based on planetary boundary layer turbulence structure and scaling concepts, including treatment of both surface and elevated sources and both simple and complex terrain (EPA, 2016).

Field measurements conducted in Wang et al. (2006) and Huang et al. (2023) with corresponding AERMOD simulations proved that AERMOD was effective for the simulation of odor's dispersion. The study of Perry et al. (2005) showed that AERMOD's performance is superior to that of the other applied dispersion models, including the Industrial Source Complex-Short Term, Version 3 model (ISCST3), the Complex Terrain Dispersion Model Plus Algorithms for Unstable Situations (CTDMPLUS), the Hybrid Plume Dispersion Model (HPDM), and the Rough Terrain Diffusion Model (RTDM).

Although the performance of AERMOD in terms of simulating hourly plume dispersion has been demonstrated, it may lack the capability of capturing short-term enhancements ($\sim$ minutes) observed by the real-time monitoring systems used in this study. As a steady-state model, AERMOD assumes Gaussian dispersion with the average meteorological condition of the hour (EPA, 2023c). In reality, the wind field can change dramatically within a short period of time; therefore, the actual pollutant plume may meander around. In such situations, the one-hour resolution of AERMOD simulations might be too coarse to capture some transient plumes. Section 2.4.2 addresses this issue by rotating the wind field to match observed short-term plumes.

As shown in Figure 2.7, the AERMOD dispersion modeling system consists of several preprocessors, the main AERMOD module, and AERPLOT. The preprocessors include AERMAP, AERMET, AERSURFACE, and AERMINUTE. In order to simulate an air pollutant's concentration and dispersion, AERMOD requires terrain and meteorological inputs, which are prepared by AERMAP and AERMET, respectively. AERPLOT reads the simulated concentration file from AERMOD and generates a corresponding dispersion map which can be opened in Google Earth.

AERMAP reads United States Geological Survey (USGS) terrain data and produces terrain base elevations for every source and receptor and a hill height scale value for each receptor, which are essential components of the AERMOD input file. The 1 arc-second DEM (digital elevation model) data are used in this thesis. More detailed information regarding AERMAP can be found in User's Guide for the AERMOD Terrain Preprocessor (AERMAP) (EPA, 2023b).

AERMET needs three input datasets: (1) low-frequency (hourly to twice daily) surface and upper air meteorological data; (2) high-frequency (1-min/5-min) Automated Surface Observing Stations (ASOS) wind data prepared by AERMINUTE as a supplement to low-frequency data; and (3) surface characteristics generated by AERSURFACE. AERSURFACE processes National Land Cover data from USGS and generates surface characteristic values that can be input into AERMET (EPA, 2020).

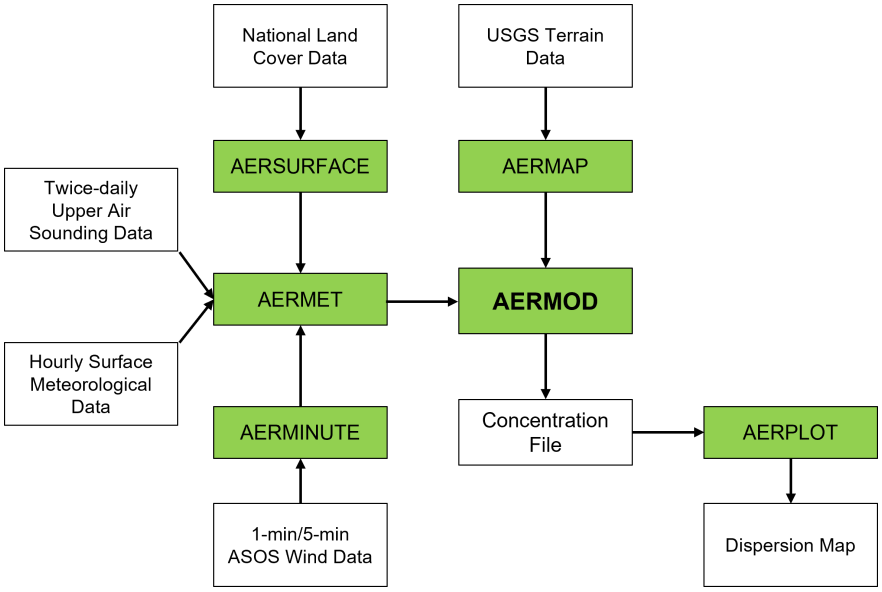

Figure 2.7: AERMOD dispersion modeling system modules (green boxes) and input/output datasets (white boxes).

2.3.2 Meteorological Data

EPA recommends using meteorological data from National Weather Service (NWS) stations. The closest station to the Broomfield area is at Denver International Airport (DIA). The DIA station

provides hourly surface and twice daily upper air meteorological data. However, the study areas are approximately 60 km away from DIA (Figure 2.8). Considering the influence of complex terrain that is much closer to Broomfield than to DIA and that the local wind field can change dramatically during a short period of time, the meteorological data from DIA station might not be representative for our study area. As an alternative to NWS station data, EPA also suggests using the prognostic meteorological data generated by the Weather Research and Forecasting (WRF) model (https://www2.mmm.ucar.edu/wrf/users/).

We obtained both meteorological data sets (DIA & WRF), with the WRF data provided by Lakes Environmental Consultants Inc. We found that even with the supplementary ASOS wind data prepared by AERMINUTE, there are still some missing values in the DIA data set. For example, as of May 2024, the DIA upper air sounding data after July 9, 2022, are not published. Using the WRF prognostic data set can avoid problems with such missing values. Moreover, the airport only provides twice-daily upper air sounding data which is extrapolated into hourly upper air data by AERMET while the WRF data provides a higher resolution for the upper air meteorology.

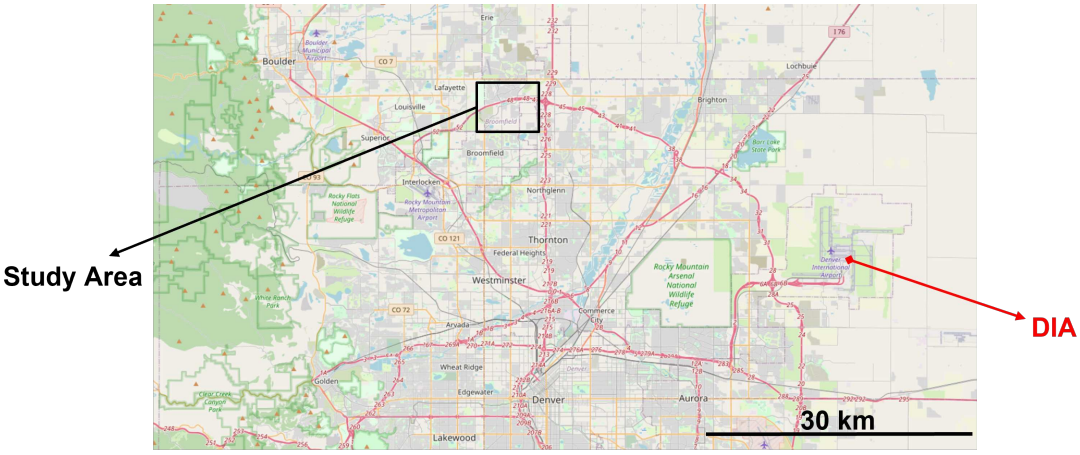

Figure 2.8: Maps of study area and Denver International Airport (DIA).

In-situ hourly winds collected at the Broomfield Soaring Eagle (BSE) site (39.98° N, 105.04° W) are compared with WRF and DIA wind data for the period from January to June 2022. The

site is close to all the monitoring sites (< 5 km). The in-situ wind data were measured at a height of 5.6 meters above the ground, whereas WRF and DIA wind data were reported at 10 meters. Therefore, I adjusted the in-situ WS to 10 meters using equation 2.1 (Stull, 1988), where z is the height of the wind (z_2 = 10m and z_1 = 5.6m); u is the wind speed (WS) at the given height; d is the displacement height; and z_0 is the surface roughness length. The log wind profile is valid for neutral conditions. I did not include the corrections for non-neutral conditions to avoid introducing additional uncertainties. Given that the measurement site is in a grassland, d $<<$ z_1 and z_2 and is ignored. The value of z_0 is obtained from the WRF meteorological data, taking into account the local terrain.

$$u(z_2) = u(z_1) \cdot \frac{ln(\frac{z_2-d}{z_0})}{ln(\frac{z_1-d}{z_0})} \tag{2.1}$$

Figure 2.9 presents the hourly averaged wind direction (WD) and WS from WRF and DIA compared with in-situ measurements, while Figure 2.10 shows daily averaged wind comparison. Wind directions (left panels in Figures 2.9 and 2.10) are colored by WS. Wind speeds (right panels in Figures 2.9 and 2.10) are compared with in-situ measurements using orthogonal distance regression (ODR). The comparisons include mean bias, mean error, normalized mean bias (NMB), and root square mean error (RSME) of both WRF and DIA wind data.

Analysis of Figures 2.9 and 2.10 reveals that DIA WD observations are more consistent with in-situ WD measurements than those of WRF. When low WS values (< 2 m/s) are excluded, the majority of DIA WD data points fall near the 1:1 line in relation to in-situ WD, while WRF WD data show greater scattering (Figures A.1 and A.2). Furthermore, DIA WD observations exhibit a smaller mean bias compared to WRF, reflecting the limitations in WRF's ability to simulate WD accurately. Conversely, the ODR slope between WRF WS and in-situ WS is closer to 1 than the slope between DIA WS and in-situ WS. WRF WS values show lower mean bias, mean error, RSME, and NMB than DIA WS measurements, indicating that DIA wind measurements likely underestimate WS.

To evaluate the impacts of WD on AERMOD simulations, I conduct simulations using both WRF data set and WRF-observation hybrid data set as inputs. Although WRF data set provides consistent and high resolution for both surface and upper air conditions, it has a large bias in WD. To minimize AERMOD simulation uncertainty stemming from WD errors, the WRF-observation hybrid data set combines in-situ WD and WRF WS as the inputs for AERMOD. When in-situ WD is unavailable, DIA WD is used as a substitute. The impacts of meteorological inputs are evaluated by comparing simulated and observed concentrations as described in Section 3.1.2.2.

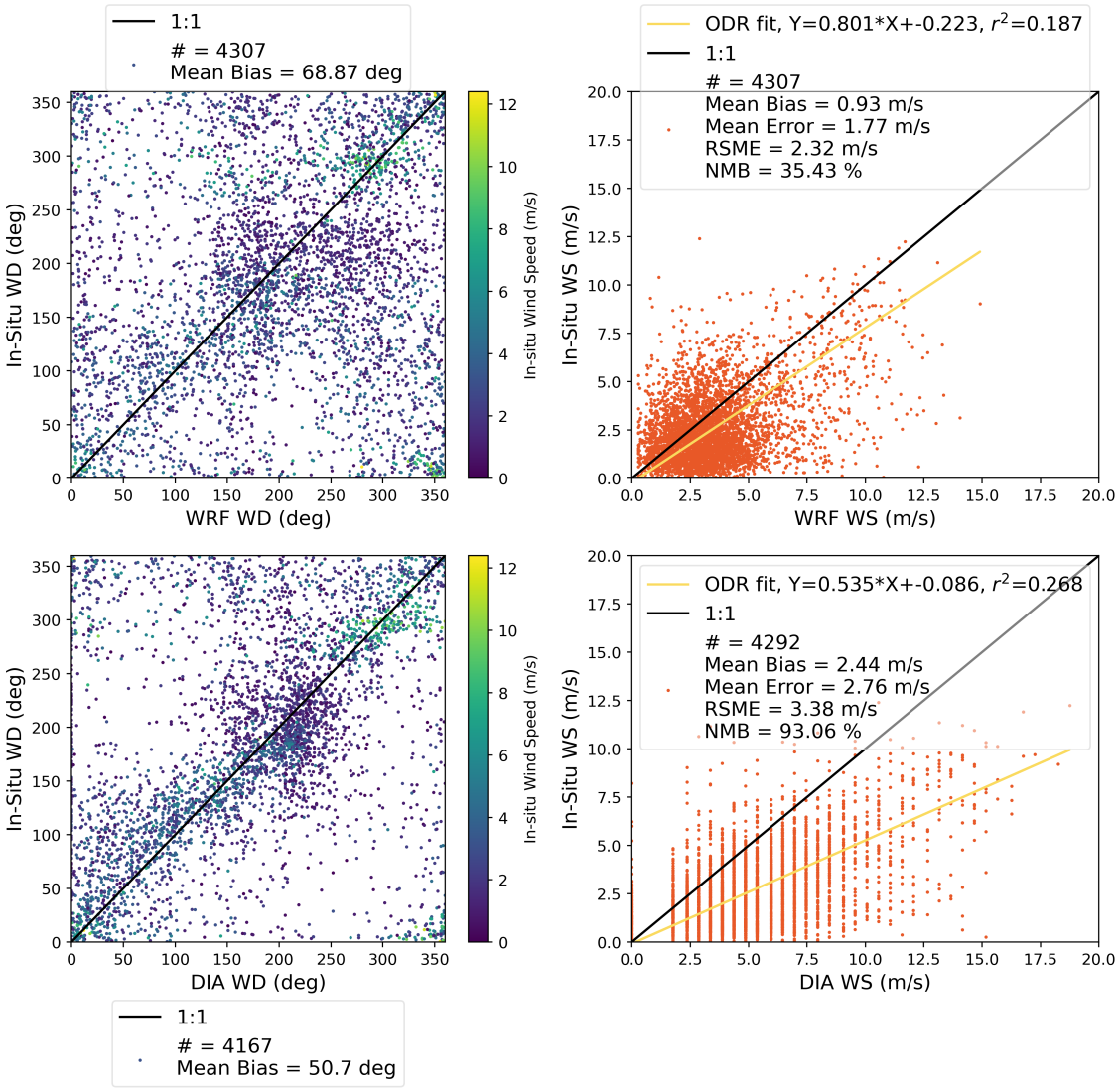

Figure 2.9: Hourly wind direction and wind speed comparison between in-situ observations and WRF (upper panels) & DIA (lower panels) for January to June 2022. Wind directions are colored by wind speed. Mean bias, mean error, normalized mean bias (NMB), and root square mean error (RSME) are calculated.

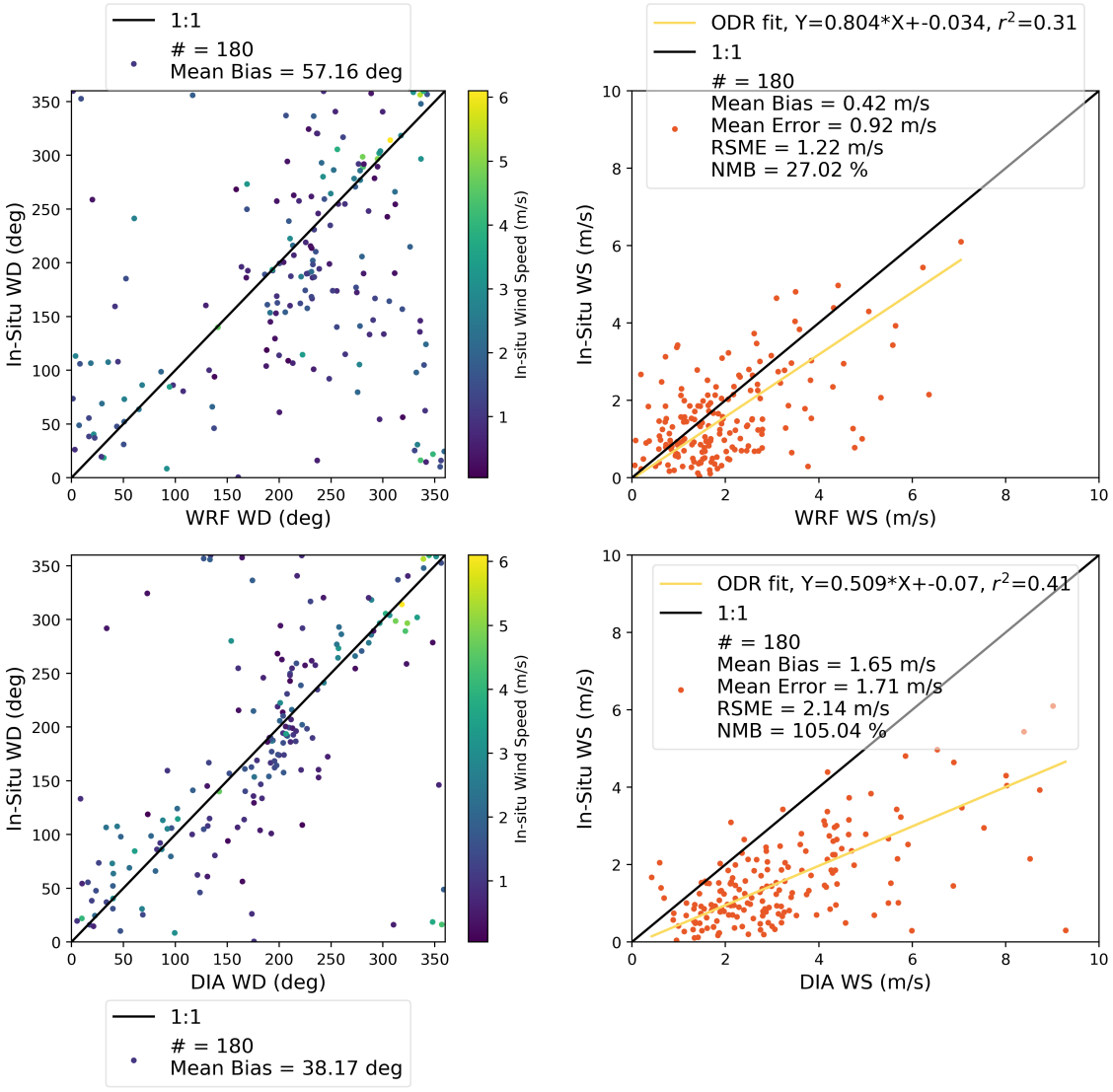

Figure 2.10: Daily wind direction and wind speed comparison between in-situ observations and WRF (upper panels) & DIA (lower panels) for January to June 2022. Wind directions are colored by wind speed. Mean bias, mean error, normalized mean bias (NMB), and root square mean error (RSME) are calculated.

2.4 Emission Inversion

Dispersion models have been widely used to infer site-level emissions based on in-situ measurements, a problem known as inverse modeling. Dispersion models generate the transfer function ($M_{i,j}$), describing the dispersion of emission plumes from a source j to a receptor i. Emission rates are then estimated using inversion methods that optimize the match between predicted and

observed concentrations. Previous studies differ mostly in their choices of dispersion model and inversion methods.

Both the analytical Gaussian dispersion model and AERMOD have been used to estimate methane emissions from landfills, O&G facilities, agricultural sources, and wastewater treatment facilities (Figueroa et al., 2009; Lan et al., 2015; Albertson et al., 2016; Caulton et al., 2019; Zhou et al., 2019; Golston et al., 2020; Olaguer et al., 2022; Moore et al., 2023). Due to its lower requirements for terrain and upper atmosphere data, the analytical Gaussian dispersion model has been used more frequently, especially with mobile observations. However, Lan et al. (2015) compared the simple analytical Gaussian dispersion model with AERMOD and found that AERMOD simulations might be more accurate when incorporating emission inversion method.

Several inversion techniques have been developed for emission estimation, including the integrated ratio (Lan et al., 2015; Albertson et al., 2016), Bayesian inference (Zhou et al, 2019; Moore et al., 2023), and regression (Figueroa et al., 2009; Olaguer et al., 2022) methods. The first two methods are often used with mobile observations with cross-plume transect observations. The integrated ratio method uses the ratio between cross-plume integrated observations and simulations to estimate emissions to minimize the uncertainty due to crosswind turbulent variability (Albertson et al., 2016). Bayesian inference incorporates uncertainties into the integrated ratio method when multiple transects are available (Zhou et al., 2019; Moore et al., 2023). The regression method is better suited for long-term stationary monitoring (Figueroa et al., 2009). When emissions from multiple sources are monitored at several locations, a multiple linear regression (MLR) approach is used. With one source and one receptor, the regression method reduces to a simple ratio method.

In this thesis, AERMOD simulations are used to infer VOC emission rates from O&G activities using the MLR method with weekly observations and the ratio method for plume-triggered samples. Together, the inverse modeling approach overcomes several limitations of existing methods discussed in section 1.5 and provides long-term emission characteristics.

2.4.1 Method for Weekly Canister Samples

The MLR for each week is based on the model expressed below:

$$\begin{pmatrix} C_1 \\ \vdots \\ C_n \end{pmatrix} = C_{bg} + \begin{pmatrix} M_{1,1} & \dots & M_{1,m} \\ \vdots & \ddots & \vdots \\ M_{n,1} & \dots & M_{n,m} \end{pmatrix} \cdot \begin{pmatrix} e_1 \\ \vdots \\ e_m \end{pmatrix} \tag{2.2}$$

In Equation 2.2, C_i (i = 1, ..., n) is the observed concentration at site i; C_{bg} is the background concentration in $\mu g/m^3$ inferred from MLR; $M_{i,j}$ (i = 1, ..., n; j = 1, ..., m) is the AERMOD transfer function simulated as the plume concentration ($\mu g/m^3$) at site i from source (O&G pad) j with a unit emission rate of 1 g/s; and e_j (j = 1, ..., m) is the emission rate for source (O&G pad) j in g/s inferred from the MLR. Both the number of active sampling monitoring sites (n) and the number of operating sources (O&G well pads, in our case) (m) can vary from week to week. For example, in a certain week when four monitoring sites collected valid weekly samples (n = 4) and three O&G well pads were operating (m = 3), the MLR matrix for that week would become the set of equations shown in Equation 2.3, where C_i (i = 1, 2, 3, 4) and $M_{i,j}$ (i = 1, 2, 3, 4; j = 1, 2, 3) are illustrated in Figure 2.11.

$$\begin{cases} C_1 = C_{bg} + M_{1,1} \cdot e_1 + M_{1,2} \cdot e_2 + M_{1,3} \cdot e_3 \\ C_2 = C_{bg} + M_{2,1} \cdot e_1 + M_{2,2} \cdot e_2 + M_{2,3} \cdot e_3 \\ C_3 = C_{bg} + M_{3,1} \cdot e_1 + M_{3,2} \cdot e_2 + M_{3,3} \cdot e_3 \\ C_4 = C_{bg} + M_{4,1} \cdot e_1 + M_{4,2} \cdot e_2 + M_{4,3} \cdot e_3 \end{cases} \tag{2.3}$$

Figure 2.11 illustrates the MLR inverse modeling method. In Figure 2.11, x and y axes represent the UTM Easting and UTM Northing in meters, respectively. The color bars indicate the concentrations (in $\mu g/m^3$), filled circles denote the locations of four monitoring sites, and black triangle, black star, and black plus signs represent the locations of three O&G pad (LS, NWB and ICB) sources, respectively. In panel (a), the color of each filled circle indicates the concentration of n-decane observed at each site (i.e., C_1, C_2, C_3, and C_4 in Equation 2.3). Panel (b) shows the

AERMOD simulated concentration from the LS pad with an assumed emission rate of 1 g/s. The simulated concentrations at the four monitoring sites are the transfer functions from the LS pad to the respective sites (i.e., $M_{i,1}$, i = 1, 2, 3, 4) in Equation 2.3. Similar to panel (b), panels (c) and (d) represent the AERMOD simulations of plumes from the NWB pad and the ICB pad with assumed emission rates of 1 g/s, respectively, which provides $M_{i,2}$ and $M_{i,3}$ (i = 1, 2, 3, 4) in Equation 2.3. With C_i and $M_{i,j}$ (i = 1, 2, 3, 4; j = 1, 2, 3) ready, the optimal emission rates for the three O&G pads (e_1, e_2 and e_3) and the background concentration (C_{bg}) can be inferred through the MLR.

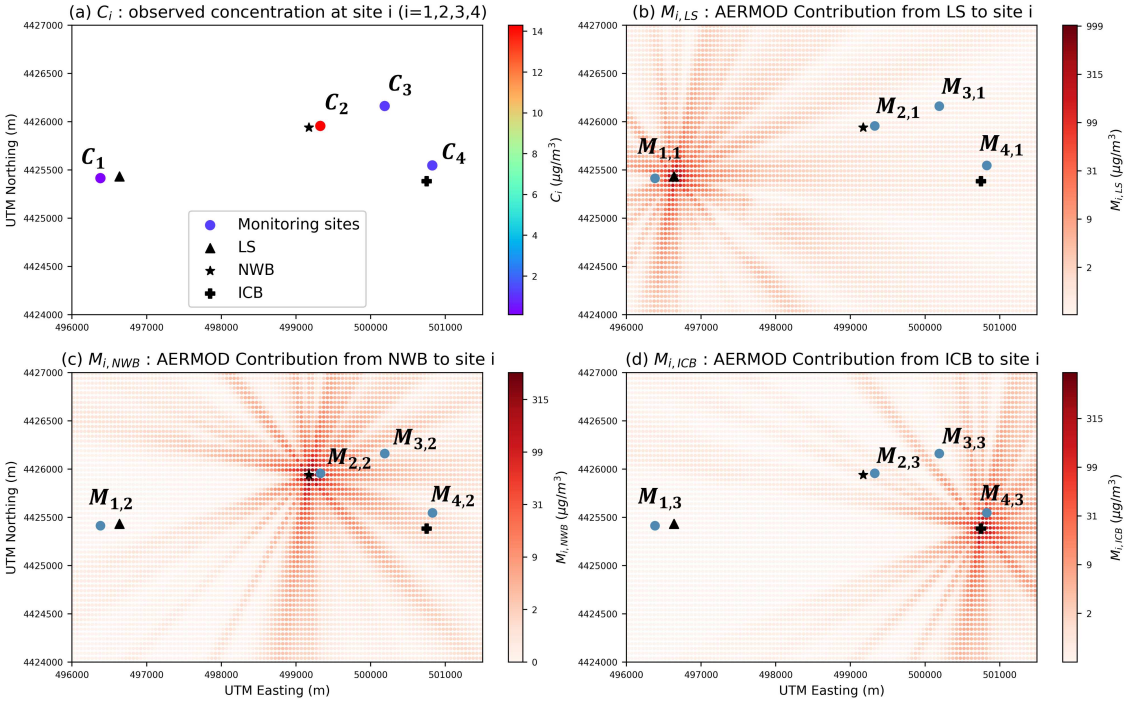

Figure 2.11: Diagrams of observed concentrations at four monitoring sites (panel (a)) and AERMOD simulated contributions from each of the three O&G well pads (panels (b) – (d)), corresponding to Equation 2.3.

For each week, the MLR method is applied to each of 51 measured VOCs to constrain the corresponding emission rates. However, the weekly sampling at each monitoring site was not always continuous (section 2.1). As a result, n is smaller than m + 1 (number of emission rates + constrained background concentration) for certain weeks, leading to an ill-defined equation set. Therefore, these weeks were removed from the MLR analysis. Additionally, the MLR coefficients are forced to be non-negative since the O&G sources can't be sinks of VOCs.

2.4.2 Method for Plume-Triggered Samples

The triggered canisters collect whole air samples in a very short period of time ($\sim$ 15 seconds) and their collection is determined by the detection of transient high-concentration plumes – not by a routine schedule like the weekly samples. The difference in the time scales of triggered samples and AERMOD simulations requires extrapolating the triggered samples to an hourly scale while uncertainties in instantaneous wind direction values in WRF simulations necessitate rotating AERMOD simulations to match the transport direction of transient plumes.

Triggered sample concentrations were extrapolated to 1-hour average concentrations (C_{1-hour}) based on the PID readings and VOC concentrations in the triggered canisters. The detailed description of this method can be found in Appendix E. Briefly, the composition of a plume is assumed to remain constant over an hour and the hourly average concentration is calculated by extrapolating the measured plume concentration above background using the time-varying elevation in the PID signal.

The difference in the sampling and simulation temporal scales also impacts dispersion characteristics. Transient plumes often last only several minutes (Ku et al., 2024) instead of hours and are impacted by cross-wind turbulence variability. Thus, short-term transport directions can differ dramatically from hourly-average wind directions. Consequently, the hourly AERMOD simulations might misplace transient plumes detected by the real-time PID monitoring system. Figure 2.12 shows an example. With the hourly averaged wind field, the AERMOD simulation indicates that the plume did not intercept the monitoring site. However, a triggered sample was collected at the monitoring site within that hour. Combining the in-situ measured wind direction, O&G operations schedule, and VOC composition signature in the triggered canister, it has been confirmed that this triggered sample came from the O&G source.

To address this issue, a wind rotation method is applied to the AERMOD simulated plume. The wind rotation method is to manually adjust the wind direction in AERMOD meteorological data, aligning it with the direction from the emission source to the monitoring site. After the wind rotation, the center of the plume (the maximum at a given distance) passes through the site, and

dispersed plumes of 1 g/s emission from AERMOD simulations are used as the transfer function (M_{center}). Since triggered canisters capture one plume from one source, a ratio method (Equation 2.4) is used to infer the VOC emission rates.

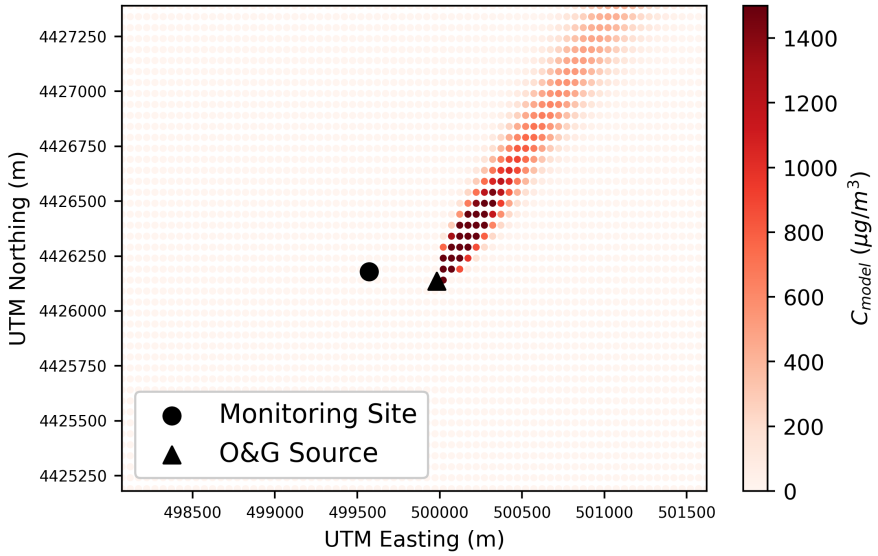

Figure 2.12: An example of AERMOD simulated plume. This plume doesn't pass through the monitoring site while one plume-triggered sample was collected at the monitoring site within that hour.

$$e = e_m \cdot (\frac{C_{1-hour} - C_{bg}}{M_{center}}) \tag{2.4}$$

In Equation 2.4, e is the inferred emission rate in g/s; e_m is the constant emission rate (1 g/s) when running AERMOD; M_{center} is the transfer function; C_{1-hour} is the extrapolated 1-hour VOC concentration for the triggered sample; and C_{bg} is the VOC background concentration (the VOC concentration at COM site in the corresponding weekly sample). However, by using the center concentration of the plume (M_{center}) as the transfer function, the inferred emission rate (e) might be biased low since the triggered samples might not always capture the maximum concentration of the plume. This means that our estimated emission rates from triggered canister samples should be considered a lower bound on actual emission rates.

Chapter 3

Results and Discussion

3.1 Emission Rates Based on Weekly Canister Samples

This section presents the constrained VOCs emission rates from weekly samples using the quantification method I developed aiming at (1) examining the performance of this method – MLR using long-term weekly observations and dispersion model simulations and (2) providing insights into different VOC emission rates during different UOGD operational phases.

In the following subsections, the development timelines of six O&G well pads in Broomfield and constrained emission rates for drilling tracers are presented in Sections 3.1.1 and 3.1.2, respectively. Section 3.1.3 provides the emission rates of select VOCs during all operations and compares those values with previously published emission rates (EPA Emission Tool and Hecobian et al., 2019).

3.1.1 O&G Development Timeline

In Broomfield, Colorado, six O&G well pads (ICB, LS, NWA, NWB, UT, and ICA) were developed between 2019 and 2022. The pre-production development timelines of each O&G well pad are shown in Figure 3.1 including drilling, hydraulic fracturing, coiled tubing/millout, production tubing installation and flowback. After flowback, production begins. For the six O&G well pads in Broomfield, the pre-production developments included here spanned 192 weeks (from 2019-04-18 to 2022-12-29).

As discussed in Section 2.2, n-octane, n-nonane and n-decane ($C_8 - C_{10}$ n-alkanes) are useful tracers for drilling operations using synthetic Neoflo drilling mud; therefore, I first quantify the emission rates of the three tracers during drilling phases using the MLR method to assess whether the MLR emission constraint method assigns drilling emissions to the right pads during the correct times. Among the 192-week period, the drilling periods for each O&G well pad are listed below:

(1) 2019-04-20 – 2019-06-28, ICB drilling.

(2) 2019-07-05 – 2019-11-14, LS drilling.

(3) 2019-11-09 – 2020-01-10, NWA drilling.

(4) 2021-09-14 – 2021-10-10, NWB drilling.

(5) 2021-10-14 – 2021-11-17, UT drilling.

(6) 2021-11-24 – 2022-01-04, UT drilling.

(7) 2022-01-11 – 2022-02-26, ICA drilling.

(8) 2022-03-01 – 2022-04-17, ICA drilling.

These eight drilling periods contain 66 weeks, with 11 weeks removed to avoid an ill-defined MLR equation set, as discussed in Section 2.4.1. From 2022-04-21 to 2022-05-24, ICB had its second drilling operation (drilling of additional, new wells on the completed pad) whose emissions can't readily be distinguished from the emissions of simultaneous production phases. Therefore, this period is not included in the analyses of drilling operations.

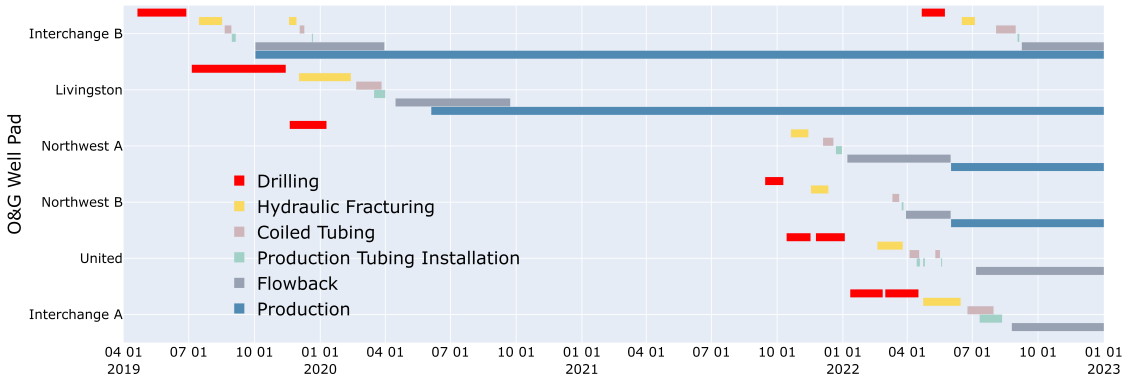

Figure 3.1: Development timelines of six O&G well pads in Broomfield.

For different weeks, the number of weekly samples can change due to the sampling schedule (Figure 2.2). During each drilling week, there was only one pad undergoing drilling operations

while other pads might be undergoing different operations (Figure 3.1), which leads to the number of active O&G well pads varying from 1 to 6 for different drilling weeks.

3.1.2 Drilling Tracers

This section provides constrained emission rates for drilling tracers, $C_8 - C_{10}$ n-alkanes, during drilling operations. In the following sections, the concentrations and emission rates of $C_8 - C_{10}$ n-alkanes are the sums of concentrations and emission rates of n-octane, n-nonane and n-decane.

Observed Concentration

The weekly average concentration time series of $C_8 - C_{10}$ n-alkanes at six monitoring sites (ITC01, LS01, NWP02, NWP03, UT02, and COM) in Broomfield are shown in Figure 3.2, where colored areas represent the drilling periods for different O&G well pads and the gap in the x-axis represents a shutdown of pre-production activities due to the COVID-19 pandemic and a financial reorganization of the operator when no O&G well pad was in drilling operation. For the monitoring sites in Broomfield, ITC01 is near ICB & ICA, LS01 is near LS, NWP02 is near NWA, NWP03 is near NWB, and UT02 is near UT (Figure 2.1). The colors of the lines match the colored areas that indicate drilling periods at the closest pad.

Figure 3.2 depicts variations of $C_8 - C_{10}$ n-alkane concentrations at different monitoring sites during different drilling periods. Except for the drilling at ICB, significantly elevated $C_8 - C_{10}$ n-alkane concentrations were observed at monitoring sites near the corresponding drilling well pad while the concentrations at other sites were relatively low. Once the drilling operations were completed, the concentrations at the site near the drilling pad dropped to background levels. This can be attributed to the use of Neoflo 4633 drilling mud as discussed in Section 2.2. For example, when the LS pad was being drilled (red area in Figure 3.2), LS01 observed high concentrations of $C_8 - C_{10}$ n-alkanes, and the concentrations dropped to low levels when the drilling finished at the pad. Concentration enhancements were much less at ITC01 during the first drilling at ICB in 2019 than observed near other drilling pads because of the use of Gibson D822 drilling mud at ICB before odor complaints led to the operator implementing use of Neoflo drilling mud.

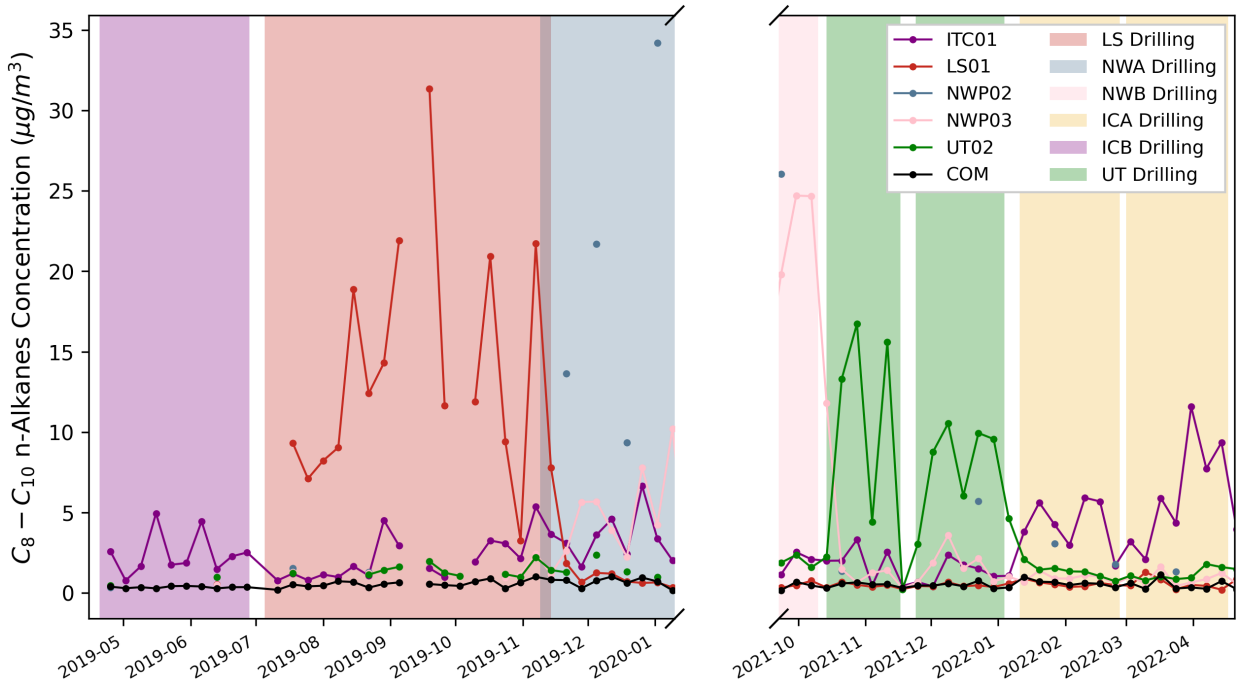

Figure 3.2: Observed weekly $C_8 - C_{10}$ n-alkane concentrations at 6 monitoring sites in Broomfield. Colored areas represent the drilling phases of different O&G well pads.

AERMOD Simulation and Model Evaluation

I obtained simulated plume concentrations from different O&G sources for every monitoring site. AERMOD simulations were conducted for every active well pad with a unit emission rate (1 g/s). Two sets of meteorological inputs were used to investigate the impacts of WD uncertainties (Section 2.3.2). Emission rates of $C_8 - C_{10}$ n-alkanes are estimated for O&G well pads with active operations using the MLR method (Equation 2.2) with these simulations. As drilling tracers, background concentrations of $C_8 - C_{10}$ n-alkanes are low and have clear sources, making them ideal for model evaluation.

The performance of weekly AERMOD simulations with inversed emission rates is evaluated by comparing the predicted and observed concentrations of $C_8 - C_{10}$ n-alkanes. In Figure 3.3, the predicted concentrations are the AERMOD simulation results with the MLR constrained emission rates. Adjacent monitoring sites are grouped into single categories; for instance, ITC01, ITC02, and ITC03 are combined into ITC. The mean observed concentrations and mean bias (MB) of predicted concentrations are included in the legend.

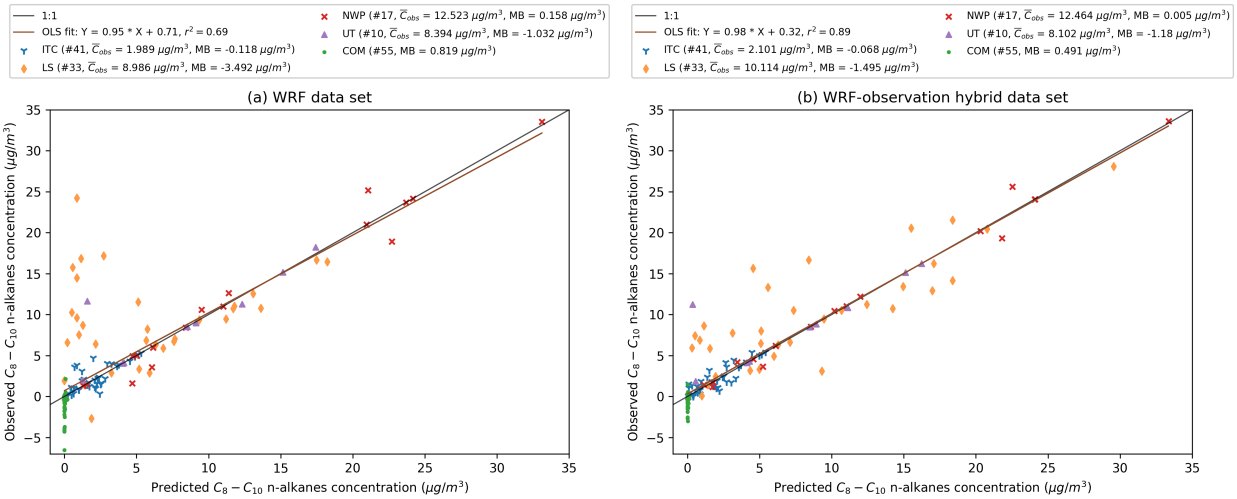

Figure 3.3: Observed $C_8 - C_{10}$ n-alkane concentrations vs. MLR predicted $C_8 - C_{10}$ n-alkane concentrations for drilling operations only. Both concentrations are the results after subtracting regression constants. ITC is the combination of ITC01, ITC02, and ITC03. LS is the combination of LS01 and LS02. NWP is the combination of NWP02 and NWP03. UT is the combination of UT02 and UT03. In the legend, # represents the number of weekly concentrations; $\overline{C}_{obs}$ is the mean observed concentrations; and MB is the mean bias of predicted concentration.

With the WRF data set as inputs, AERMOD simulations miss several plumes observed at LS sites and substantially underestimate $C_8 - C_{10}$ n-alkanes (Figure 3.3a). In contrast, the WRF-observation hybrid data set has lower WD errors and significantly improves the performance of AERMOD simulations (Figure 3.3b). For example, with the hybrid data set, the regression slope, r^2 value, and overall mean bias between predicted and observed concentrations are 0.98, 0.89, and -0.2363 $\mu g/m^3$, respectively. When using WRF data set alone, these values are 0.95, 0.69, and -0.5397 $\mu g/m^3$, respectively. Therefore, simulations with the hybrid data set and corresponding constrained emission rates are reported and discussed in the following sections. A detailed discussion of model performance for other operations and select VOCs are provided in Appendix B.

The AERMOD simulated weekly averaged (synchronized with weekly air samples with the WRF-observation hybrid inputs) plume contributions from different O&G sources at ten monitoring sites ($M_{i,j}$ in Equation 2.2) are provided in Figures C.1 and C.2. For the background site – COM, the contributions from the six O&G well pads are negligible since COM is far ($\sim$ 5 km) from the six O&G well pads. At the sites near well pads, the plumes with highest concentrations

originate from the nearest O&G well pad while the contributions from other pads are generally small, as expected.

Constrained Emission Rates

By conducting the MLR with the hybrid meteorological inputs for the 192 weeks (39 weeks were excluded based on the criteria in Section 2.4.1), I obtain a total of 309 constrained emission rates for different UOGD operations in which 55 emission rates are for drilling operations.

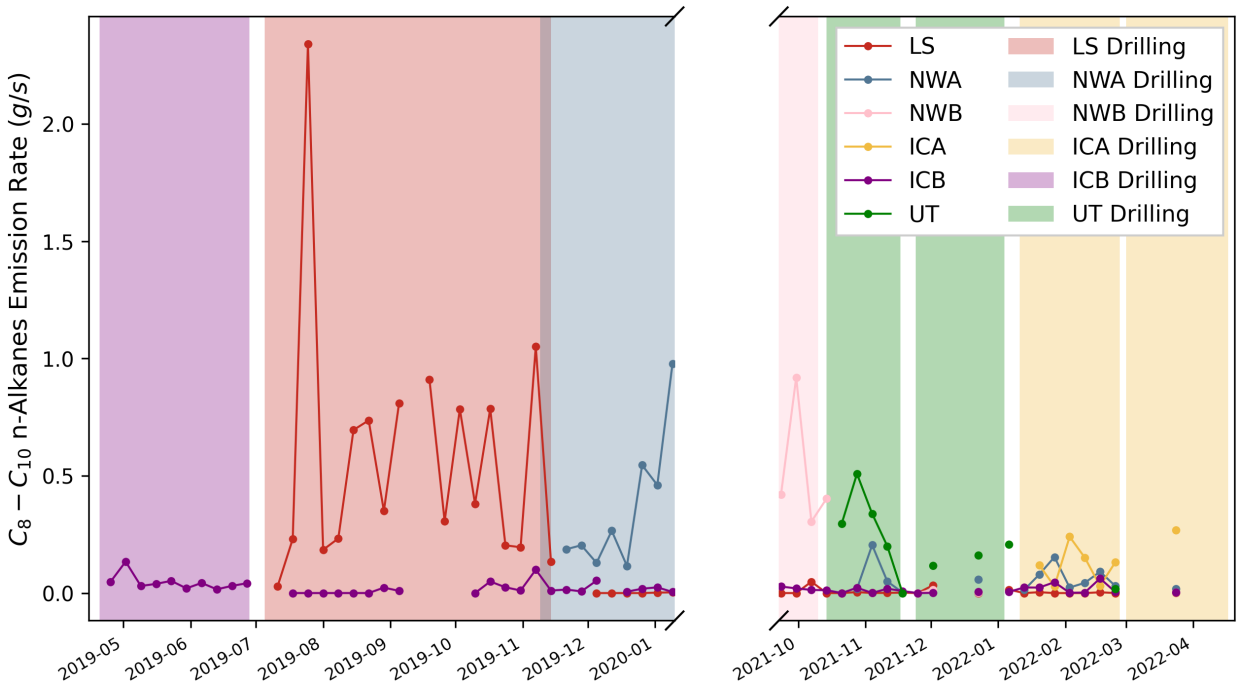

Figure 3.4: Constrained $C_8 - C_{10}$ n-alkane emission rates for six O&G well pads. Colored areas represent the drilling phases of different O&G well pads.

The constrained emission rates of $C_8 - C_{10}$ n-alkanes (the sum of emission rates of n-octane, n-nonane, and n-decane) for periods with drilling operations are shown in Figure 3.4. From 2020-01-10 to 2021-09-14, there was no drilling operation. After 2022-04-20, there was no single drilling operation at one well pad. Therefore, these two periods are not shown in the figure. Solid lines and colored areas represent the emission rates and drilling periods of different O&G well pads, respectively. The emissions of $C_8 - C_{10}$ n-alkanes vary by operation types and emission sources. As

previously mentioned, during each drilling period, there could be multiple active O&G well pads being developed but only one with active drilling. The MLR method successfully distinguishes the well pads being drilled from other active well pads and assigns the highest emission rates of $C_8 - C_{10}$ n-alkanes to the corresponding drilling locations. For instance, for the period of 2021-10-14 to 2022-01-01, the UT pad was in drilling operations while the other five well pads were otherwise being developed or in production at the same time. The MLR method is still able to infer the emission rates for different operations.

The emission rates for the ICB drilling period (purple area) are the lowest among all drilling emission rates, consistent with much lower $C_8 - C_{10}$ n-alkane concentrations in the headspace analysis of the Gibson D822 drilling mud used in ICB drilling operations. The constrained $C_8 - C_{10}$ n-alkane emission rates clearly show the capability of the MLR method to properly assign emissions to appropriate locations at appropriate times when used with weekly observation samples and AERMOD simulations.

3.1.3 Select VOCs During All Operations

This section presents constrained emission rates for select VOCs using the MLR method with weekly samples and dispersion model simulations and compares them with previous studies. The EPA Emission Tool (Eastern Research Group, Inc., 2022) provides emission factors for several pre-production activities; however, only those for drilling mud degassing, fracking engine emissions, and flowback green completion are applicable to the well pad development activities conducted in Broomfield. In addition, the EPA Emission Tool only offers emission factors for methane, BTEX, and non-methane VOC (NMVOC) without detailed speciation. Furthermore, the EPA Emission Tool estimates that flowback green completion practices produce no emissions. Hecobian et al. (2019) quantified emission rates of 46 VOCs plus methane and ethane during drilling, fracking, flowback, and production operations in the Denver-Julesburg (DJ, a mixed oil and gas play) and Piceance (primarily natural gas) basins in Colorado using a tracer ratio method.

Emission rates are examined here for Broomfield O&G operations for methane, ethane, propane, ethyne, $C_8 - C_{10}$ n-alkanes, benzene, toluene, ethylbenzene, xylenes (m-p-xylene + o-xylene), and NMVOC. Methane, the primary component of natural gas and a potent greenhouse gas, has a high background concentration ($\sim$ 2 ppm) compared to other VOCs in Broomfield. Ethane, a major constituent of crude oil and natural gas and a dominant non-methane VOC in urban areas (Thompson et al., 2014; Abeleira et al., 2017; Ku et al., 2024), has such a high regional background concentration in Broomfield that enhancements in ethane concentrations at monitoring sites near O&G pads are not always readily apparent, as reported by Ku et al. (2024). Propane is also a predominant byproduct in O&G production (Gilman et al., 2013; Thompson et al., 2014; Ku et al., 2024). Ethyne (acetylene), primarily derived from combustion and typically absent from non-combustion O&G emissions (Borbon et al., 2001; Baker et al., 2008; Gilman et al., 2013; Hecobian et al., 2019; Ku et al., 2024), serves as a combustion tracer. $C_8 - C_{10}$ n-alkanes are selected since they have proven to be good tracers for some drilling operations as discussed above. BTEX are of special interest because they are HAPs that can cause adverse health impacts (EPA, 2015b). Sources of BTEX include combustion and O&G activities (Ho et al., 2004; Khoder 2007; Miller et al., 2012; Bolden et al., 2015; Halliday et al., 2016; EPA, 2023d). The emission rates of NMVOC are calculated as the sum of emission rates of 50 measured VOCs.

Table 3.1 lists the number of constrained weekly emission rates for select VOCs during each O&G operation phase. The emission rates for production tubing installation are difficult to quantify/distinguish due to its short duration and/or multiple operations at the same time, resulting in only two constrained emission rates. Due to the limited number of observations, the emission rates for production tubing installation are not included in the analyses but are provided in Figure C.7. As mentioned in Section 2.4.1, the MLR coefficients are constrained to be non-negative. Using the emission rates of $C_8 - C_{10}$ n-alkanes as an example, it was found that without employing such constraint, approximately 41% of emission rates were negative values, ranging from -0.1 to -0.00001 g/s. Notably, 77% of these negative emission rates were from production operations, which has been identified as having significantly lower emissions compared to pre-production operations (Ku

et al., 2024). After applying this constraint, all the negative emission rates, ranging from -0.1 to -0.00001 g/s, were adjusted to 0 g/s. These negative values typically represented low-emission operations, thus it's reasonable to treat them as emission rates of 0 g/s rather than negative values, especially considering that O&G well pads are unlikely to be sinks for VOCs.

Table 3.1: Number of constrained emission rates for different UOGD operations using weekly samples. Numbers in parentheses are the numbers of emission rates of methane where they differ from other VOCs.

Operation	Drilling-Gibson mud	Drilling-Neoflo mud	Hydraulic Fracturing	Coiled Tubing	Production Tubing Installation	Flowback	Production
# of emission rates	11	44 (41)	25 (23)	7	2	29	191 (189)

Figure 3.5 shows the operation-composite emissions rate of ethane, propane, $C_8 - C_{10}$ n-alkanes, BTEX, ethyne, and NMVOC during different UOGD operations while Figure 3.6 presents the corresponding box plots for methane. In the panels, the boxes and whiskers represent the 5^{th}, 25^{th}, 75^{th}, and 95^{th} percentiles while orange lines and green triangles show the median and mean values, respectively. The red solid lines indicate the emission rates calculated based on the EPA Emission Tool, which provides emission factors of drilling mud degassing (for methane and NMVOC), fracking engines (for methane, BTEX, and NMVOC), and flowback green completion (for all VOCs). The brown crosses represent the median emission rates reported in Hecobian et al. (2019) for all species except ethyne, which was released as the study tracer. The columns colored in gray represent values (both emission rates and EPA Emission Tool emission factors) multiplied by 10 for better illustration.

Large variations in Broomfield O&G alkane emission rates are observed between different operation phases in Figure 3.5. The highest median emission rates of ethane and propane are from coiled tubing/millout, followed by drilling, flowback, and production. Hydraulic fracturing has the lowest median emission rates of ethane and propane. Although the observed concentrations of ethane are higher than those of propane at all monitoring sites, the constrained emission rates of ethane are still in the same magnitude as those of propane. This is because the MLR method

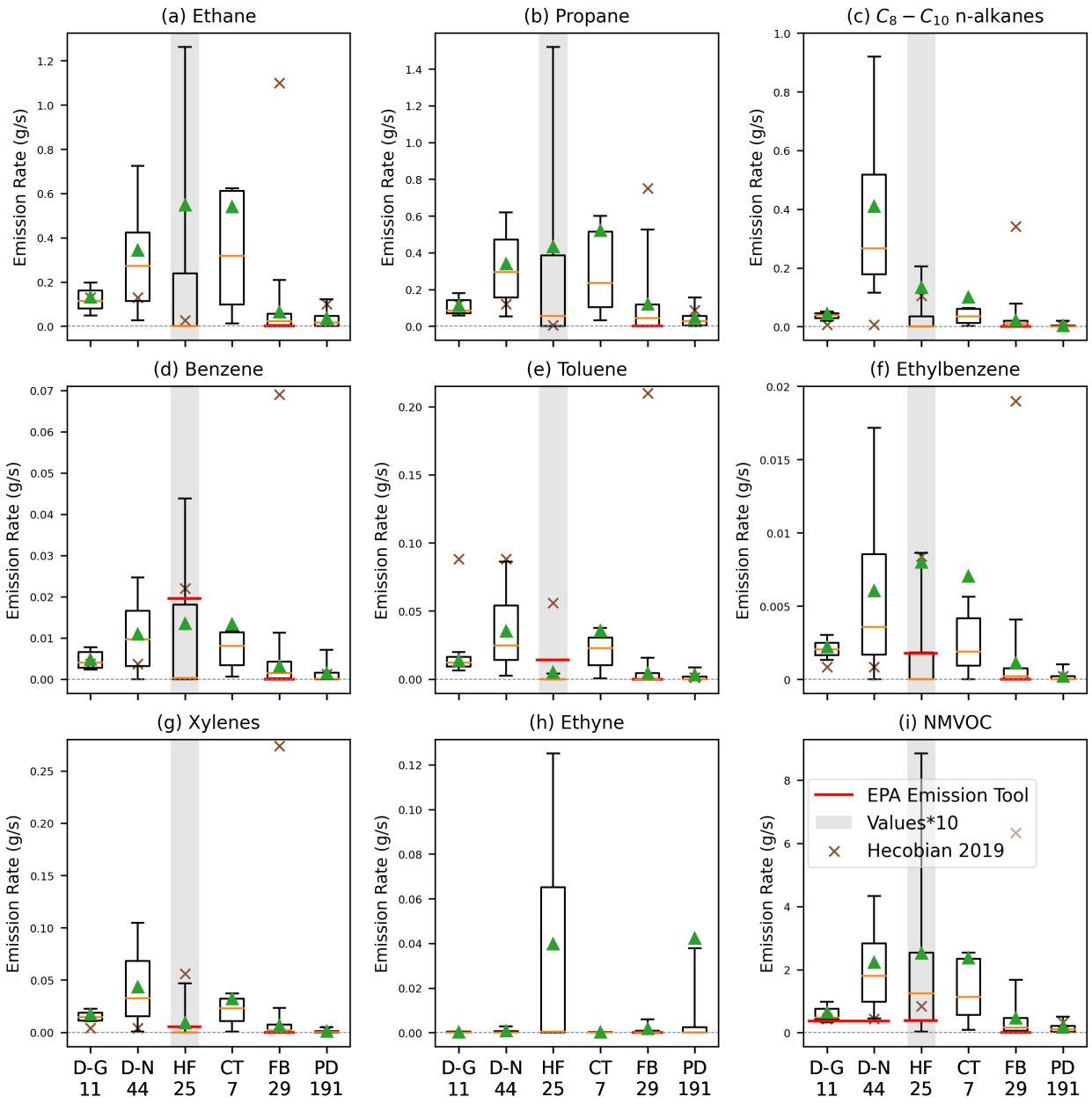

Figure 3.5: Box plots for emission rates of ethane, propane, $C_8 - C_{10}$ n-alkanes, benzene, toluene, ethylbenzene, xylenes (m-p-xylene + o-xylene), ethyne, and NMVOC during drilling-Gibson (D-G), drilling-Neoflo (D-N), hydraulic fracturing (HF), coiled tubing/millout (CT), flowback (FB) and production (PD) operations using weekly samples. The boxes and whiskers represent the 5^{th}, 25^{th}, 75^{th}, and 95^{th} percentiles, respectively. Orange line and green triangle represent the median and mean, respectively. The red solid lines represent the emission factors from the EPA Emission Tool. The brown cross sign represents the median emission rate reported in Hecobian et al. (2019). The columns colored in gray indicate the values are multiplied by 10 for better illustration. The numbers under the x axes represent the number of emission rates for different operations.

incorporates background contributions, demonstrating that the MLR method is able to optimize emission rates when incorporating background observations from the Commons (COM) site. Consistent with the prior discussion on drilling mud emissions, the highest median emission rates of $C_8 - C_{10}$ n-alkanes are from drilling with Neoflo mud while drilling with Gibson mud leads to the second highest. Coiled tubing/millout also shows high $C_8 - C_{10}$ n-alkane emission rates, in accordance with the elevated $C_8 - C_{10}$ n-alkane concentrations during coiled tubing/millout operations reported in Ku et al. (2024). The $C_8 - C_{10}$ n-alkane emission rates during flowback and production are about one to two orders of magnitude lower than those of drilling with Neoflo mud.

For BTEX, the median Broomfield emission rates during drilling with Neoflo mud, drilling with Gibson mud, and coiled tubing/millout are higher than those of other operations. Hydraulic fracturing and production exhibit the lowest and second lowest median BTEX emission rates, respectively. The emission rates of benzene, toluene, and xylenes show smaller variabilities between different operations compared to ethylbenzene.

For the combustion tracer, ethyne, the highest median emission rates are from hydraulic fracturing, an expected result because fracking is powered by diesel engines. The mean emission rate during production is high due to sporadic high emission rates. Periodic maintenance and truck emissions (EPA, 2019; Lachenmayer 2022; Ku et al., 2024) could account for some of these sporadic high emission rates during the production phase; however, Ku et al. (2024) also report an unknown (likely combustion) source that led to significant local increases in ethyne concentrations during some periods at the Livingston pad. However, all other operations exhibit low ethyne emission rates, as many operations were electrified in Broomfield and closed loop systems were used to move fluids off-pad, helping limit truck traffic (Ku et al., 2024). As for NMVOC, two drilling operations and coiled tubing have the highest emission rates, while flowback, hydraulic fracturing, and production show relatively low emission rates.

Figure 3.6 presents the emission rates of methane along with the emission rates from EPA Emission Tool and Hecobian et al. (2019). The variations of methane median emission rates across different operations are approximately within one order of magnitude. Drilling with Neoflo mud

and coiled tubing/millout again show the highest and second highest emission rates. Production exhibits the third highest median emission rate of methane.

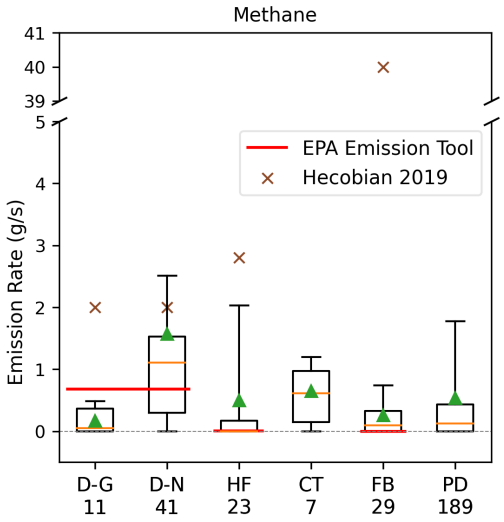

Figure 3.6: Box plots for emission rates of methane during drilling-Gibson (D-G), drilling-Neoflo (D-N), hydraulic fracturing (HF), coiled tubing/millout (CT), flowback (FB) and production (PD) operations using weekly samples. The boxes and whiskers represent the 5^{th}, 25^{th}, 75^{th}, and 95^{th} percentiles, respectively. Orange line and green triangle represent the median and mean, respectively. The red solid lines represent the emission factors from the EPA Emission Tool. The brown cross sign represents the median emission rate reported in Hecobian et al. (2019). The numbers under the x axis represent the number of emission rates for different operations.

The emission rates of individual VOCs can vary significantly between operations. Drilling and coiled tubing/millout operations typically exhibit higher VOC emission rates. During these operations hydrocarbons can be released from rock formations, drilling mud, and drilling debris, leading to emissions into the atmosphere. During hydraulic fracturing, VOC emission rates are generally the lowest among pre-production and production activities, consistent with the fact that material is generally being pushed downhole during fracking, limiting opportunities for emission of subsurface hydrocarbons. One exception is ethyne that has elevated emissions due to combustion in powerful engines used to generate the substantial power needed for fracking operations. Emission rates within a particular operation type can also vary substantially. For example, drilling operations include several phases for each well, including rig setup/movement, vertical drilling, horizontal drilling through the hydrocarbon "payzone", pipe tripping (pulling of pipe out of the wellbore),

and cementing/casing, and each of these activities can feature different opportunities for emissions. Recycling of drilling mud can lead to VOC volatilization of drilling mud components, for example, but can also lead to emission of entrained subsurface hydrocarbons while drilling through the payzone. Emissions during cementing operations, for example, are more likely dominated by combustion of engines on the surface used during this operation. Changing emissions across such sub-operations, however, are likely difficult to discern using weeklong observations. We also lack detailed drilling logs spelling out the exact timing of these operations in Broomfield O&G well development.

Although median VOC emission rates during the production phase are much lower than those seen during many pre-production operations, the extended duration of production means that emissions continue over years to decades and total emissions can climb over these extended production operations (Swarthout et al., 2013; Wilde et al., 2021).

Thinking beyond Broomfield, differences in VOC emissions during both pre-production and production operations can also vary substantially. Different operators and subcontractors often employ different practices, while even the same operator might use different best management practices at different locations. For example, the use of grid-powered, electrified drill rigs, closed loop, tankless fluid handling systems, and synthetic drilling mud in Broomfield are not common practices at every location and differences in these practices certainly can alter emissions. Moreover, different O&G reservoirs have distinct oil and gas compositions, which may also affect the composition of emissions from a well pad (Gilman et al., 2013; Lachenmayer, 2022).

A comparison of VOC emission rates from Broomfield O&G development with previously published values can help evaluate (1) the appropriateness of these prior values for describing emissions associated with present-day operations and (2) the effectiveness of recently adopted management practices in the O&G industry in reducing VOC emissions. Evaluating the applicability of values published in the EPA Emission tool is particularly valuable given the strong reliance on these values by industry and government for assessing O&G contributions to emissions inventories utilized for modeling ozone pollution and addressing other air quality impacts. Tables 3.2 - 3.5

compare the median and mean emission rates of select VOCs during drilling, hydraulic fracturing, flowback and production operations with these previously values. In the Tables, "NA" denotes no available value.

In the drilling phase, as illustrated in Table 3.2, Figure 3.5, and Figure 3.6, the median emission rates estimated for methane using Gibson mud (0.05 g/s) and Neoflo mud (1.11 g/s) are lower than the values from Hecobian et al. (2019) (2.0 g/s), while the median value for Neoflo mud is higher than the value reported by the EPA emission tool (0.68 g/s). However, In the case of NMVOC, median emissions rates for drilling operations using synthetic-based Neoflo mud (1.8 g/s) and petroleum-based Gibson mud (0.48 g/s) in Broomfield are higher than the value provided for drilling mud volatilization in the EPA Emission Tool (0.36 g/s) for synthetic-based or oil-based drilling mud. The EPA Emission Tool only includes methane and four VOCs (ethane, propane, butane, and pentane) when estimating the emission factors of total hydrocarbons, compared to 50 VOCs included here. However, even when considering only four VOCs (ethane, propane, butane, and pentane), as included in the EPA Emission Tool, the median emission rate of NMVOC from Broomfield drilling with Neoflo mud remains higher than the EPA Emission Tool.

The median emission rates of $C_8 - C_{10}$ n-alkanes, ethylbenzene and xylenes are significantly higher than values published by Hecobian et al. (2019) for drilling operations in Piceance Basin. The higher $C_8 - C_{10}$ n-alkane emission rates in Broomfield are consistent with their emission from Neoflo-based drilling mud, as discussed above. Hecobian et al. (2019); however, reported higher emission rates of toluene. The drilling operations studied by Hecobian et al. did not use electrified drill rigs, so the higher emission rates of toluene, a combustion product, are not surprising. Median emission rates of light alkanes and benzene in Broomfield are broadly similar to values reported by Hecobian et al. The median drilling emission rates for NMVOC in Broomfield are higher than Hecobian et al. reported for Piceance Basin drilling (0.43 g/s), despite the lack of combustion-based drilling rigs in Broomfield. The difference appears largely attributable to increased emissions of heavier alkanes and may reflect increased volatilization of these compounds from synthetic

drilling mud in Broomfield and the larger oil content of the Broomfield hydrocarbon resource relative to the drier gas production in the Piceance Basin.

In Table 3.3 the EPA Emission Tool emission rates of methane, BTEX and NMVOC from 700 horsepower (hp) and 1500 hp fracking engines are provided in separate columns. 700 hp is the default option in the EPA Emission Tool, while 1500 hp is a more realistic assumption based on Nieuwenburg et al., (2023). The median emission rate of methane (0.0 g/s) determined from the Broomfield observations is consistent with the small values included in the EPA Emission Tool (0.003 and 0.007 for the 700 hp and 1500 hp engine sizes). The median NMVOC emission rate (0.12 g/s) determined from the Broomfield observations is higher than both values for NMVOC emissions from the two engine sizes in the EPA Emission Tool (0.04 and 0.08 g/s). The EPA Emission Tool only includes engine emissions during fracking, overlooking potential contributions from other sources such as truck traffic. These are likely small relative to the fracking engine emissions and the consistency between the EPA Emission Tool and Broomfield values is reassuring. Emissions of NMVOC reported by Hecobian et al. (2019) are also consistent with these values, with a median reported value of 0.08 g/s.

During flowback (Table 3.4 and Figure 3.5), the median emission rates of all select VOCs are significantly lower compared to values reported by Hecobian et al. (2019) for DJ Basin. The median emission rate of NMVOC (0.15 g/s) is approximately 42 times lower than the median value reported by Hecobian et al. (6.33 g/s). The EPA Emission Tool reports that the green completion techniques produce no emissions, implying all VOC emission rates of 0 g/s. Green completion practices were used for flowback operations in Broomfield and Hecobian et al. (2019); however, both studies show non-zero median VOC emission rates, indicating the significant underestimation of EPA Emission Tool for flowback green completion techniques.

Hecobian et al. (2019) observed that pre-production emission rates of most VOCs were highest during flowback phases. The operations studied by Hecobian et al. between 2014 and 2016 were green completion systems, with separators included to reduce emissions; however, they featured on-site flowback fluid storage in vented tanks, allowing substantial VOC emissions. The

substantial reduction of flowback VOC emissions in Broomfield indicates the success of improved management practices utilized in Broomfield, including the use of closed loop systems to handle fracking fluids and produced water returned to the surface (Lachenmayer 2022; Ku et al., 2024). The median flowback NMVOC and benzene emission rates in Broomfield represent reductions of 98% each from the earlier DJ Basin flowback values reported by Hecobian et al. (2019).

During production at the Broomfield O&G well pads (Table 3.5), the median emission rate of NMVOC (0.10 g/s) is also lower than the median value (0.33 g/s) reported by Hecobian et al. (2019). The production facilities studied by Hecobian et al. included a mix of older and newer operations such that the nearly 70% lower values observed for the new production operations in Broomfield are not surprising.

Table 3.2: Median and mean emission rates of select VOCs for drilling operations: this study (weekly samples) vs. EPA Emission Tool vs. Hecobian et al. (2019).

VOC	This study drilling Gibson mud median (mean) emission rates (g/s)	This study drilling Neoflo mud median (mean) emission rates (g/s)	EPA Emission Tool oil-based or synthetic-based drilling mud degassing emission rate (g/s)	Hecobian et al. drilling median emission rate (g/s) – Piceance basin
Methane	0.05 (0.17)	1.11 (1.57)	0.68	2*
Ethane	0.11 (0.13)	0.27 (0.34)	NA	0.13
Propane	0.08 (0.11)	0.29 (0.34)	NA	0.12
$C_8 - C_{10}$ n-alkanes	0.04 (0.044)	0.27 (0.41)	NA	0.007
Benzene	0.004 (0.005)	0.0096 (0.0109)	NA	0.004
Toluene	0.012 (0.014)	0.025 (0.035)	NA	0.088
Ethylbenzene	0.002 (0.002)	0.0036 (0.0061)	NA	0.0009
Xylenes	0.014 (0.017)	0.0326 (0.0434)	NA	0.004
Ethyne	0.0001 (0.0003)	0.0 (0.0009)	NA	NA
NMVOC	0.48 (0.65)	1.8 (2.23)	0.36	0.43

* This emission rate is from Collett et al. (2016), which used the same dataset as Hecobian et al. (2019).

Table 3.3: Median and mean emission rates of select VOCs for fracking operations: this study (weekly samples) vs. EPA Emission Tool vs. Hecobian et al. (2019).

VOC	This study fracking median (mean) emission rates (g/s)	EPA Emission Tool fracking 700 hp engine emission rate (g/s)	EPA Emission Tool fracking 1500 hp engine emission rate (g/s)	Hecobian et al. fracking median emission rate (g/s) – DJ basin
Methane	0.0 (0.5)	0.003	0.007	2.8*
Ethane	0.0 (0.055)	NA	NA	0.0026
Propane	0.006 (0.043)	NA	NA	0.0005
$C_8 - C_{10}$ n-alkanes	0.0 (0.0134)	NA	NA	0.0105
Benzene	0.00003 (0.0014)	0.002	0.0042	0.0022
Toluene	0.0 (0.0005)	0.0014	0.003	0.0056
Ethylbenzene	0.0 (0.0008)	0.0002	0.0004	0.0008
Xylenes	0.0 (0.0009)	0.0005	0.0011	0.0056
Ethyne	0.0005 (0.04)	NA	NA	NA
NMVOC	0.12 (0.25)	0.04	0.08	0.08

* This emission rate is from Collett et al. (2016), which used the same dataset as Hecobian et al. (2019).

Table 3.4: Median and mean emission rates of select VOCs for flowback operations: this study (weekly samples) vs. EPA Emission Tool vs. Hecobian et al. (2019).

VOC	This study flowback median (mean) emission rates (g/s)	EPA Emission Tool flowback green-completion emission rate (g/s)	Hecobian et al. flowback median emission rate (g/s) – DJ basin
Methane	0.095 (0.257)	0	40*
Ethane	0.023 (0.064)	0	1.1
Propane	0.044 (0.121)	0	0.75
$C_8 - C_{10}$ n-alkanes	0.012 (0.022)	0	0.342
Benzene	0.0014 (0.0032)	0	0.069
Toluene	0.0 (0.0043)	0	0.21
Ethylbenzene	0.0002 (0.0011)	0	0.019
Xylenes	0.002 (0.006)	0	0.274
Ethyne	0.00004 (0.0018)	0	NA
NMVOC	0.15 (0.46)	0	6.33

* This emission rate is from Collett et al. (2016), which used the same dataset as Hecobian et al. (2019).

Table 3.5: Median and mean emission rates of select VOCs for production operations: this study (weekly samples) vs. Hecobian et al. (2019).

VOC	This study production median (mean) emission rates (g/s)	Hecobian et al. production median emission rate (g/s) – DJ basin
Methane	0.13 (0.54)	NA
Ethane	0.017 (0.037)	0.1
Propane	0.027 (0.047)	0.088
$C_8 - C_{10}$ n-alkanes	0.001 (0.004)	0.0021
Benzene	0.00007 (0.0014)	0.0013
Toluene	0.0 (0.0032)	0.0011
Ethylbenzene	0.0 (0.0002)	0.0002
Xylenes	0.00006 (0.00097)	0.0016
Ethyne	0.0001 (0.04)	NA
NMVOC	0.10 (0.20)	0.33

3.2 Emission Rates Based on Plume-Triggered Samples

This section presents VOC emission rates constrained using plume-triggered canister sample observations. The primary objectives are (1) providing quantitative characteristics (emission rates) for transient high-concentration plumes, and (2) comparing emission rates for these short-term events with longer-term emission rates obtained using weekly samples. Sections 3.2.1 and 3.2.2 discuss the emission rates of drilling tracers and the emission rates of select VOCs during drilling, coiled tubing/millout, and flowback operations, respectively.

3.2.1 Drilling Tracers

34 plume-triggered canisters collected in Broomfield from 2021-09-16 to 2021-11-05 are used to constrain emission rates for drilling operations using Neoflo mud. Information regarding triggered sample collection times, sampling sites, and O&G sources for these samples is provided in Table D.1. These triggered canisters sampled elevated VOC concentration plumes attributed to O&G drilling operations using the following approach: (1) comparing the in-situ wind direction during the triggered sample time to ensure the plume originated from an O&G well pad undergoing drilling, and (2) calculating concentration ratios of i-pentane to n-pentane in the triggered sample to verify that the ratio was less than 1.0, indicating strong influence of O&G emissions (Gilman et al., 2013; Hecobian et al., 2019; Ku et al., 2024).

Observation and AERMOD Simulation

VOC concentrations in the triggered canister samples were extrapolated to 1-hour average concentrations based on the corresponding PID readings. Additionally, a wind rotation method was used to better represent transport of the transient VOC plume to the receptor location.

Figure 3.7 shows C_8-C_{10} n-alkane concentrations measured in triggered samples (red line), the corresponding 1-hour extrapolated concentrations (blue line), and the background concentrations (yellow line) for each triggered event. Background concentrations are observed concentrations from the corresponding weekly canisters at the regional background site (COM). Concentrations in triggered samples generally, as expected, exceed the background level except for two triggered

events which appear to represent false trigger events when the PID response was influenced by something (e.g., high humidity) other than elevated VOC concentrations.

One-hour extrapolated concentrations are generally lower than the concentrations measured directly in the triggered canisters, indicating that most triggered samples captured a higher concentration portion of transient plumes intercepting the monitoring site (see Figure 3.7). However, several triggered canisters were collected at the onset of plumes where concentrations continued to rise, and their corresponding 1-hour extrapolated concentrations are higher than those of the triggered samples. Figure 3.8 shows an example of such an event. Scenarios like this point to the value of PID monitors having the ability to trigger multiple canisters, something that was not incorporated in the APIS PID systems in Broomfield.

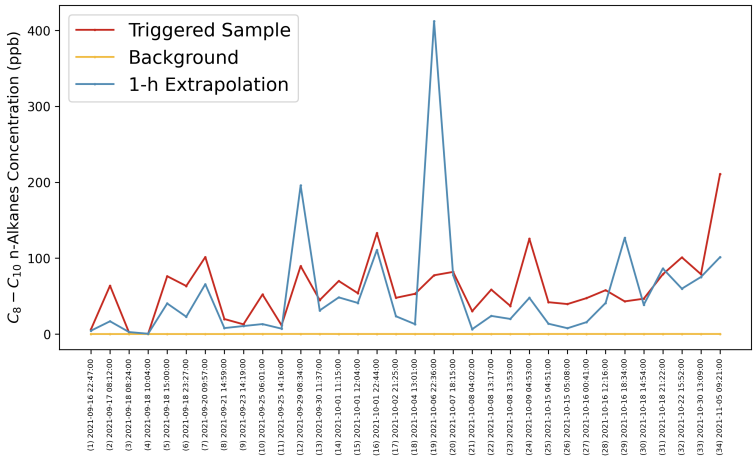

Figure 3.7: $C_8 - C_{10}$ n-alkanes observed, background, and 1-hour extrapolated concentrations for triggered events during drilling operations using Neoflo mud. X axis is the triggered time of each sample.

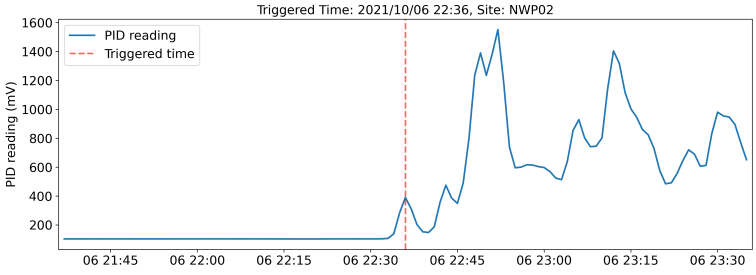

Figure 3.8: PID readings for the 2021-10-06 22:36 triggered event at NWP02. Blue solid line is the PID reading. Red dashed line represents the triggered time.

Constrained Emission Rates

Figure 3.9 illustrates the constrained $C_8 - C_{10}$ n-alkane emission rates (red solid line) for the 34 triggered events. The mean (black solid line), median, and standard deviation (black dashed line) of these 34 emission rates are 6.2, 0.8, and 12.2 g/s, respectively. The 1^{st} to 5^{th} highest emission rates (with the corresponding triggered times) are 47.5 g/s (2021-10-22 15:52), 38.0 g/s (2021-10-30 13:09), 35.2 g/s (2021-10-18 14:54), 32.9 g/s (2021-10-16 12:16), and 12.8 g/s (2021-11-05 09:21), respectively. The four highest values are 5 to 10 times higher than the majority. These episodes are further considered below. If we exclude these 4 highest emission rates, the mean (blue solid line), median and standard deviation (blue dashed line) for the remaining 30 events are 1.9, 0.7 and 2.7 g/s respectively.

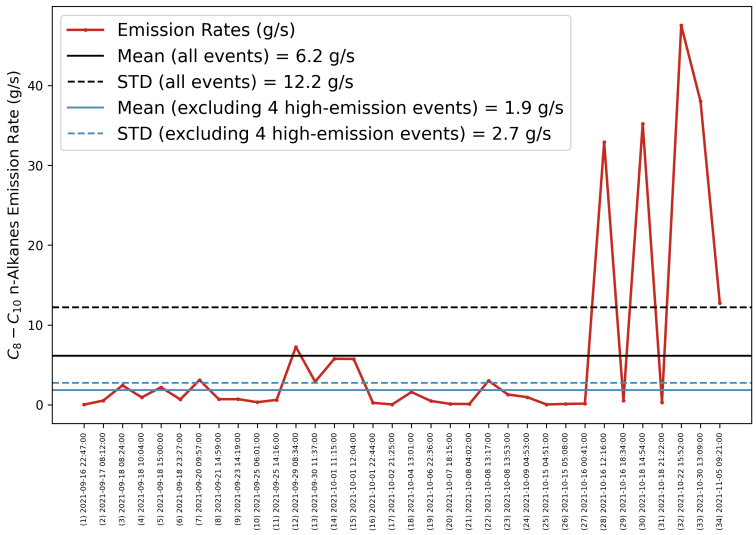

Figure 3.9: Constrained emission rates for $C_8 - C_{10}$ n-alkanes using drilling plume-triggered samples (red solid line). Black solid and dashed lines are the mean and standard deviations of the total 34 emission rates. Blue solid and dashed lines are the mean and standard deviation of the 30 emission rates excluding four highest emission rates.

High Emission Event Analyses

When quantifying VOC emission rates using triggered samples, uncertainties may arise from the 1-hour extrapolated concentrations (C_{1-hour}) and/or the AERMOD simulated concentrations using wind rotation method (M_{center}). Based on Equation 2.4, the constrained emission rate can be

exceptionally high if C_{1-hour} is highly elevated or if the AERMOD simulation does not properly represent the turbulent nature of transient plumes, leading to a low M_{center}. To investigate the four highest emission rates obtained for our triggered canister analysis of drilling emissions, Figure 3.10 presents the C_{1-hour} and M_{center} along with the constrained emission rates for all triggered events. The emission rates are on the left y-axis while the two right y-axes represent the M_{center} and C_{1-hour}, respectively. For the 4 high emission estimates, the 1-hour extrapolated concentrations are similar to other triggered events suggesting the high emission events are more likely driven by factors associated with the dispersion simulation. Indeed, the corresponding AERMOD center concentrations are exceptionally low compared to other triggered events, leading to very high emission rate estimates.

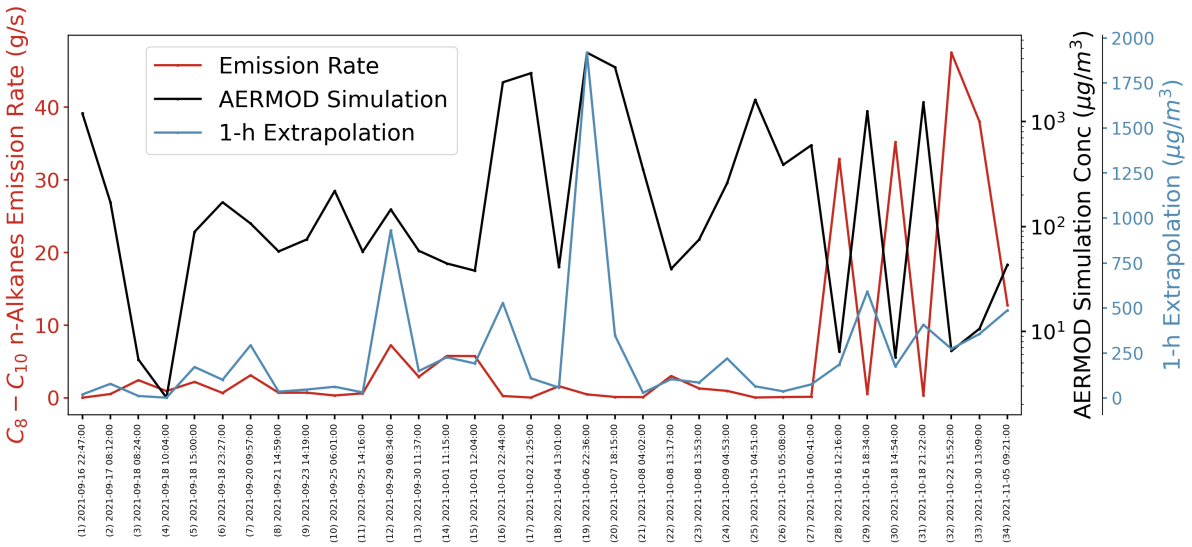

Figure 3.10: Constrained emission rates of $C_8 - C_{10}$ n-alkanes (red), AERMOD simulated plume center concentrations (black), and extrapolated 1-hour concentrations of $C_8 - C_{10}$ n-alkanes (blue) for each triggered event.

Although the M_{center} denotes the plume center concentration (maximum concentration within a specific distance), the M_{center} for the four high emission events remain very low, indicating that the simulations of AERMOD for these four events differ from those of other triggered events. Upon a thorough investigation of AERMOD concentration dispersion maps for all triggered events, a distinct difference in dispersion patterns was identified between the four high emission events and

the remaining thirty triggered events. Figure 3.11 visually illustrates this contrast, presenting typical dispersion maps for the four high emission events in panel (a) and for the other triggered events in panel (b). Specifically, the 4 high emission events have stronger cross-wind dispersions (horizontally wider) plumes than other triggered events, and show rapidly decreasing simulated concentrations with distance. Consequently, the transfer functions remain low even after rotating the dispersed plumes to the center at the monitoring sites for these four cases. These high emission estimates highlight that the accuracy of AERMOD simulations can be compromised due to its inherent limitations of hourly averaged meteorological data input and the absence of higher-resolution meteorological information.

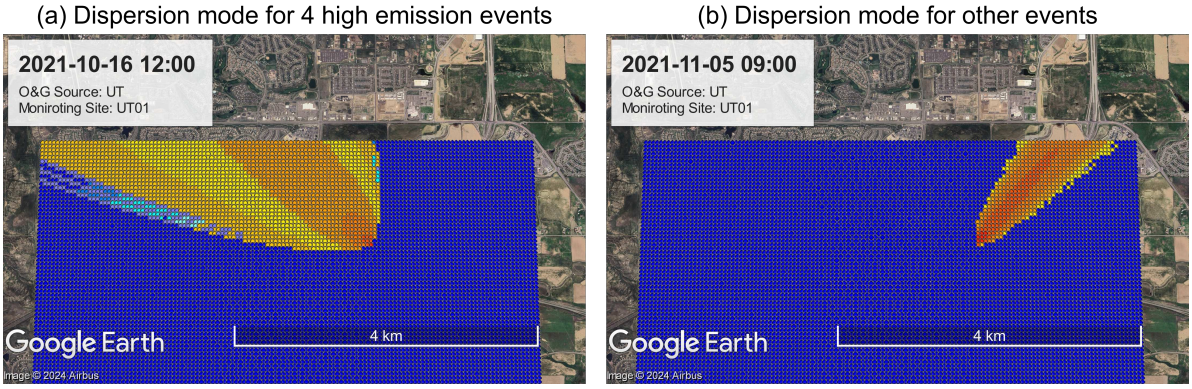

Figure 3.11: Typical AERMOD simulated plume dispersion modes for the 4 high emission events (panel (a)) and other triggered events (panel (b)).

3.2.2 Select VOCs During Different Operations

This section presents constrained emission rates of select VOCs during drilling with Neoflo mud, coiled tubing/millout and flowback operations using plume-triggered samples and compares VOC short and longer duration emission rate estimates constrained using triggered vs. weekly canister observations. Despite potential uncertainties in estimating 1-hour emission rates from triggered sample data, stemming especially from uncertainties in short-term AERMOD simulations, quantifying emissions at this time scale is especially important for assessing emissions associated with short-duration activity (e.g., emptying of sand cans during flowback).

Table 3.6 lists the number of select plume-triggered canister samples for different UOGD operations. In addition to the 34 triggered samples for drilling operations using Neoflo mud discussed above, 6 and 14 triggered samples were attributed to emissions from coiled tubing/millout and flowback operations, respectively (corresponding information is provided in Table D.2 and Table D.3). These samples are used to estimate the 1-hour emission rates for the same select list of VOCs discussed in section 3.1.3.

Table 3.6: Number of select plume-triggered samples for drilling with Neoflo mud, coiled tubing/millout and flowback operations.

Operation	Drilling with Neoflo mud	Coiled tubing/millout	Flowback
# of plume-triggered samples	34	6	14

Figure 3.12 presents estimated 1-hour emission rates for ethane, propane, $C_8 - C_{10}$ n-alkanes, BTEX, ethyne and NMVOC during drilling with Neoflo mud, coiled tubing/millout, and flowback operations using plume-triggered samples, and Figure 3.13 shows emission rates of methane. The purple triangles and crosses show the mean and median emission rates using weekly samples for comparative analysis. Table 3.7 lists the median and mean 1-hour emission rates of select VOCs during drilling with Neoflo mud, coiled tubing/millout, and flowback operations. Notably, as mentioned in section 2.4.2, the 1-hour estimated emission rates should be considered a lower bound on actual emissions since the triggered canister samples may not always capture the maximum concentration of plumes.

The emission rates of ethane and propane for each operation type are generally similar in magnitude to each other. Median values for both species are higher for drilling and coiled tubing/millout operations than for flowback. The highest emission rates of $C_8 - C_{10}$ n-alkanes are for drilling, consistent with the use of Neoflo-based drilling mud which is known to contain enhanced concentrations of these compounds. These emissions during drilling are actually of similar magnitude to those for ethane and propane which are generally considered the major components emitted

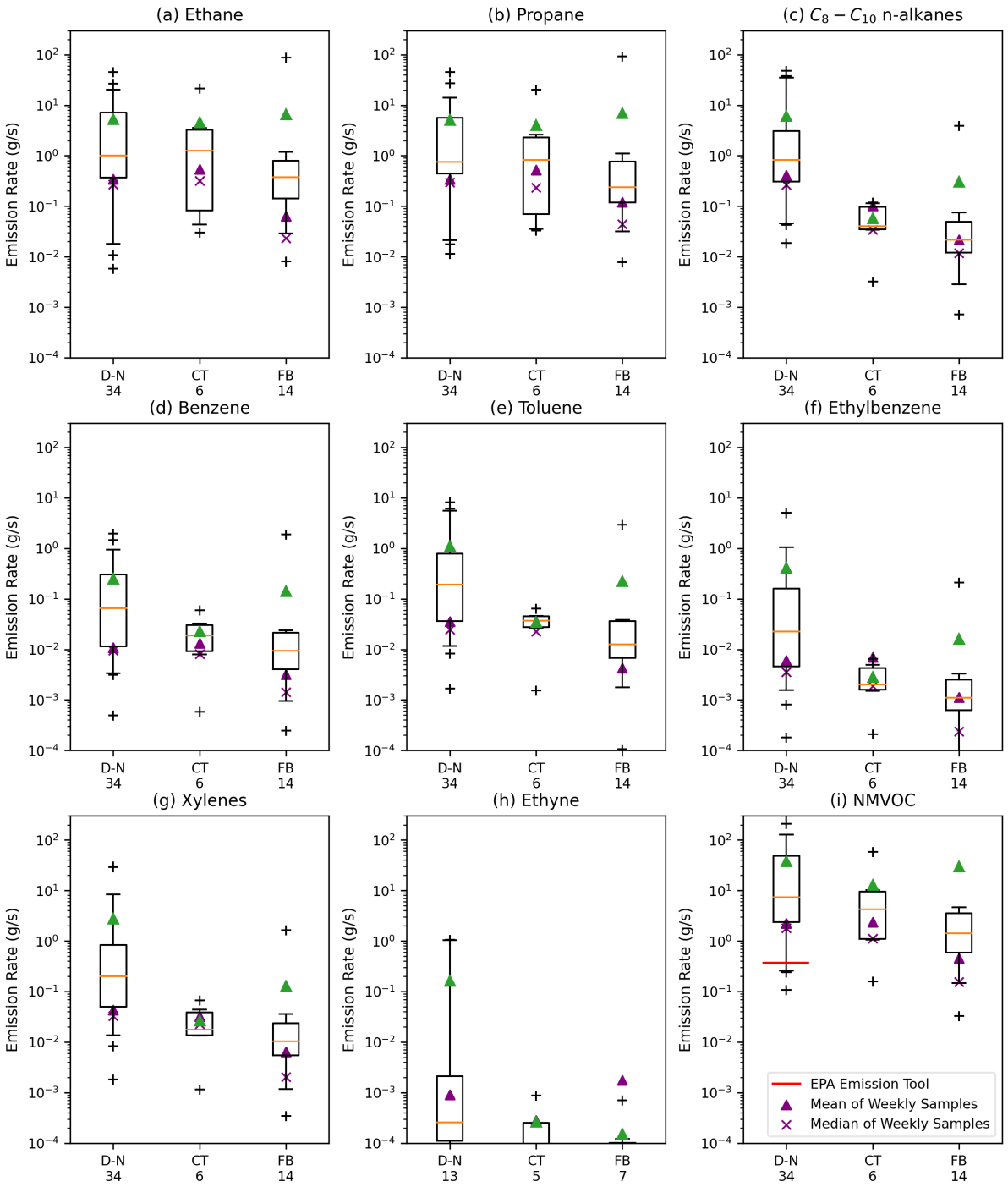

Figure 3.12: Box plots for emission rates of ethane, propane, $C_8 - C_{10}$ n-alkanes, benzene, toluene, ethylbenzene, xylenes (m-p-xylene + o-xylene), ethyne, and NMVOC during drilling-Neoflo (D-N), coiled tubing/millout (CT), and flowback (FB) using plume-triggered samples. The boxes and whiskers represent the 5^{th}, 25^{th}, 75^{th}, and 95^{th} percentiles, respectively. Orange line and green triangle represent the median and mean, respectively. The red solid line represents the emission factor from EPA Emission Tool. The EPA emission factors for flowback green completion (0 g/s) are not shown here. The purple arrow and cross sign represent the mean and median of emission rates from weekly samples. The numbers under the x axes represent the number of emission rates for different operations.

during O&G operations. Increased emission of these heavier alkanes is of interest because of their potential air quality and health effects. Reactivities of these compounds with hydroxyl radical are much higher than values for light alkanes, raising concerns about potential increased contribution of drilling emissions to ozone formation. Nonane has also been identified as an air toxic, raising potential concerns about increased exposure for residents living close to drilling operations. Both median and mean emission rates are also highest during drilling operations for BTEX which are also hazardous air pollutants.

Emission rates of ethyne are relatively low compared to other VOCs, consistent with results from weekly samples and with expectations for these three operation types which had limited combustion sources on-pad. Fracking operations involve the use of large diesel engines that are expected to be larger contributors to ethyne emissions, but the study captured only 1 triggered sample during fracking operations. This is likely because emissions of subsurface hydrocarbons tend to be limited during fracking operations when material is being pushed down the well bore. The median 1-hour NMVOC emission rates constrained by plume-triggered samples are highest for drilling operations and lowest for flowback, following the patterns seen for major VOC components ethane, propane, and $C_8 - C_{10}$ n-alkanes.

As for methane (Figure 3.13 and Table 3.7), the highest median 1-hour emission rates are seen during drilling (3.11 g/s) and coiled tubing/millout operations (3.08 g/s), a same pattern as seen for the VOCs in the weekly emission estimates. The higher values in coiled tubing/millout might reflect direct venting of subsurface gas during millout of the plugs installed to isolate well sections during hydraulic fracturing. During these three operations, the 1-hour median methane emission rates are significantly higher than weekly estimates, indicating processes characterized by periods of shorter-term, higher emissions.

The median NMVOC 1-hour emission rates, constrained by triggered samples, are higher than the weekly average emission rates by factors of about 5 and 10 for drilling and flowback operations, respectively. Again, this is suggestive of processes with intermittent emission of more concentrated VOC plumes. Similar patterns are observed for many of the individual VOCs included in Figure

3.12. During drilling and flowback, certain short-term activities, such as horizontal drilling and emptying sand cans, emit significantly more VOCs than other activities, leading to the large gaps between 1-hour and weekly emission rates. Somewhat smaller differences are observed for some individual VOCs between 1-hour and weekly emission rates for coiled tubing/millout operations consistent with what are expected to be more consistent activity patterns. The median 1-hour emission rates for NMVOC are approximately 20 times higher than the drilling mud degassing emission factor from the EPA Emission Tool (0.36 g/s).

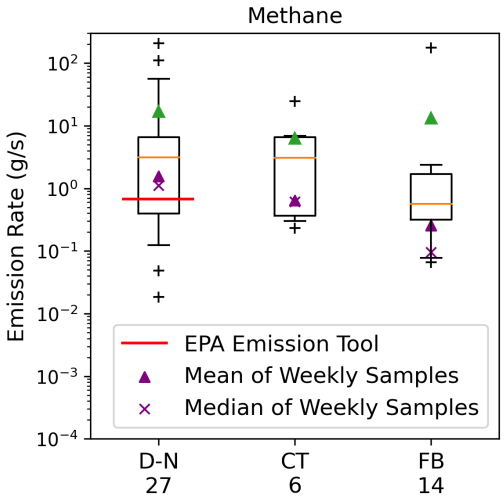

Figure 3.13: Box plots for methane during drilling-Neoflo (D-N), coiled tubing/millout (CT), and flowback (FB) using plume-triggered samples. The boxes and whiskers represent the 5^{th}, 25^{th}, 75^{th}, and 95^{th} percentiles, respectively. Orange line and green triangle represent the median and mean, respectively. The red solid line represents the emission factor from EPA Emission Tool. The EPA emission factors for flowback green completion (0 g/s) are not shown here. The purple arrow and cross sign represent the mean and median of emission rates from weekly samples. The numbers under the x axis represent the number of emission rates for different operations.

Table 3.7: Median and mean emission rates of select VOCs for drilling with Neoflo mud, coiled tubing/millout, and flowback operations using plume-triggered samples.

VOC	Drilling with Neoflo mud median (mean) emission rate (g/s)	Coiled tubing/millout median (mean) emission rate (g/s)	Flowback median (mean) emission rate (g/s)
Methane	3.11 (16.97)	3.08 (6.36)	0.57 (13.41)
Ethane	1.01 (5.33)	1.27 (4.57)	0.38 (6.67)
Propane	0.75 (5.10)	0.83 (4.08)	0.24 (6.95)
$C_8 - C_{10}$ n-alkanes	0.82 (6.16)	0.04 (0.06)	0.02 (0.31)
Benzene	0.07 (0.25)	0.02 (0.02)	0.01 (0.14)
Toluene	0.19 (1.12)	0.04 (0.04)	0.01 (0.23)
Ethylbenzene	0.02 (0.42)	0.002 (0.003)	0.001 (0.02)
Xylenes	0.20 (2.80)	0.02 (0.03)	0.01 (0.13)
Ethyne	0.0003 (0.16)	0.0001 (0.0003)	0.00007 (0.00015)
NMVOC	7.43 (38.17)	4.25 (13.02)	1.42 (30.19)

Data Availability

Dataset URL: https://doi.org/10.5061/dryad.g1jwstqzs

Chapter 4

Conclusions and Recommendations for Future Work

4.1 Conclusions

Aided by unconventional extraction techniques and greatly accelerated in the past two decades, U.S. oil and gas (O&G) development has raised concerns among the public. Activity-specific emission factors/rates of emissions of air toxics and other VOCs from O&G development are limited. In this thesis I quantify VOC emission rates during different UOGD operations, using spatially and temporally resolved observations (weekly and plume-triggered VOC canister samples) and dispersion model simulations, through emission inversion methods (MLR and ratio methods).

The MLR method is validated by examining weekly sample-constrained emission rates of drilling-specific chemical tracers ($C_8 - C_{10}$ n-alkanes enriched in emissions of synthetic Neoflo-based drilling mud). The MLR method was found to be capable of correctly assigning emissions of these tracers to locations where and when drilling operations were underway.

Significant variations in VOC emission rates across different operation types are observed. Drilling and coiled tubing/millout have the highest median VOC emission rates while hydraulic fracturing exhibits the lowest except for ethyne. During drilling and coiled tubing/millout operations, hydrocarbons can be released from rock formations, drilling mud, and drilling debris causing emissions into the atmosphere. Conversely, hydraulic fracturing, which involves pumping fluids down into the well, reduces the likelihood of subsurface hydrocarbon emissions to the atmosphere. Elevated emission rates of ethyne during fracking reflect the intensive use of large, diesel-powered engines during this operation. Although O&G production typically exhibits lower VOC emission rates than pre-production activities, its much longer duration means these emissions still deserve special attention. Considerable variability in emission rates for a single operation type often reflects variations in specific activities during those operations. For example, drilling operations consist of a series of sub-operations, including rig setup, vertical drilling, horizontal drilling through the

hydrocarbon payzone, and cementing/casing operations. More generally, there can also be substantial differences in O&G pre-production practices between operators, subcontractors, and O&G basins.

During drilling operations, the median emission rates of NMVOC are 0.48 g/s for petroleum-based Gibson mud and 1.8 g/s for synthetic-based Neoflo mud, as determined by weekly canister samples. These median emission rates are higher than those reported by the EPA Emission Tool for drilling mud degassing (0.36 g/s for NMVOC) and by Hecobian et al. (2019) (median NMVOC emission rate of 0.43 g/s).

In the case of hydraulic fracturing, the mean emission rate of NMVOC (0.12 g/s) is higher than the rates from the EPA Emission Tool for fracking engine emissions, which are 0.04 g/s for a 700 hp engine and 0.08 g/s for a 1500 hp engine.

During flowback, the median emission rates of VOCs are significantly lower than those reported in Hecobian et al. (2019), suggesting that improved management practices utilized in Broomfield flowback operations (e.g., employing a closed-loop system to handle fracking fluids and produced water returned to the surface and limiting fluid storage on-pad) have greatly reduced emissions compared to previous practices (e.g., storing flowback fluids in open tanks). Comparison of the median values from the two studies, both of which employed green completion techniques, suggest average emissions reductions of 98% for both NMVOC and benzene. However, EPA Emission Tool estimates that the green completion techniques produce no emissions.

For shorter-term temporal variability in O&G emissions, I utilize plume-triggered canister samples to estimate 1-hour emission rates for drilling, coiled tubing/millout and flowback operations, respectively. Too few triggered canisters were captured during fracking operations to support such analysis. The median emission rates from triggered samples are typically approximately 5 to 10 times higher than the average emission rates obtained using weekly samples for drilling and flowback operations, during which certain short-term activities (e.g., horizontal drilling and emptying sand cans) can emit significantly more VOCs than other operations. In the context of flowback operations, this suggests that while average flowback emissions of air toxics and other VOCs have

been greatly reduced by improvement in techniques used to handle flowback fluids, the periodic emptying of sand canisters, required to capture fracking sand brought back up the well bore during flowback, remains a weak point in terms of emission control.

While the extensive ambient air monitoring observations collected in Broomfield over time and space during well pad development provides an exceptional opportunity to help constrain O&G VOC emission rates for specific well drilling and completion activities, there are uncertainties that arise from the inversion techniques used. In particular, inaccuracies in local meteorological fields that are input to AERMOD dispersion simulations can send an emitted plume in the wrong direction and/or lead to inaccurate rates of pollutant dispersion. These problems are generally larger when looking at individual hours and can be mitigated by conducting inversions over longer time periods. The MLR method combined with long-term observations (e.g., weekly samples) is, therefore, likely to yield a more accurate solution. When sub-daily data (e.g., plume-triggered samples) are used, adjustments such as wind rotation might be needed.

Despite these limitations, however, the findings in this thesis fill a crucial knowledge gap concerning VOC emission rates during different UOGD phases. Accurate knowledge of these emission rates, across a range of industry practices that are evolving over time, is needed to properly assess health risks associated with air toxics exposure for individuals living, working, or playing near O&G operations and to improve our understanding of how these O&G operations contribute to the formation of ozone and regional haze.

4.2 Recommendations for Future Work

This work focuses on quantifying the emission rates of VOCs during different UOGD phases, comparing findings with previous studies, evaluating the validity of current estimations, and providing suggestions regarding quantification methods. With the 4-year spatially dense record of VOC observations from Broomfield, we are able to estimate emission rates of a wide range of VOCs for specific development phases and operational practices. Despite this important progress,

additional research is needed to further enhance understanding of this complex environmental issue. The following recommendations outline potential directions for future work.

- **Quantifying VOC emission rates using high-time resolution data.** Apart from weekly and plume-triggered samples, there are 1-minute methane concentration data, 1-minute BTEX data from a PTR-MS, and mobile sampling data available. The 1-minute methane was provided by the Picarro G-2401 at one monitoring site in Broomfield, operated by Boulder Air, for monitoring the impacts of a leaking pipeline, which persisted for at least 6 months. With the available corresponding high-time resolution wind data, the wind-rotation method can be applied in conjunction with AERMOD to simulate concentrations at a higher time resolution and thus, quantify the emission rate of methane. A similar approach could be taken using more than two years of data from an Ionicon PTR-MS, measuring benzene, toluene, and several other compounds, operated by our CSU team in a residential neighborhood near the Livingston well pad. Additionally, mobile sampling was conducted periodically in Broomfield. The mobile laboratory is a hybrid SUV "plume tracker" equipped with fast mobile measurement of methane and ethyne, BTEX, and grab samples for VOC speciation. Concentrations of methane and ethyne are measured at 2 Hz, BTEX at 6-min time resolution, and other VOCs in grab samples, along with route coordinates (Ku et al., 2024). By using AERMOD simulations for sampling trajectories with observed concentrations, the emission rates can be quantified.

- **Improving AERMOD simulations.** It may be possible to further improve AERMOD simulations by refining the meteorological inputs. If every monitoring site is equipped with a weather station measuring meteorological parameters required by AERMOD, such as wind field, surface heat flux, and convective velocity scale, in future monitoring programs, the model simulations could be greatly improved, especially for the simulation of transient plumes.

- **Apply these approaches to quantify emissions for additional operations.** Another UOGD air monitoring project in the DJ Basin, sponsored by the Health Effects Institute – Energy program (HEI), commenced in the summer of 2022. This project also focuses on monitoring increased VOC concentrations near O&G facilities during different development phases. Even better operational information (e.g., hourly drilling records) is available for some of the operations monitored in this study. This HEI-funded study also included monitoring operations from three different O&G operators, vs. the single operator who developed the 6 Broomfield well pads. Quantifying VOC emission rates for this new project and comparing them with results reported here can help provide a more robust dataset of emission rates and new insights into how different management practices influence those rates. Such information would improve stakeholder ability to design effective strategies to mitigate emissions of air toxics and ozone precursors from UOGD.

- **Health impact assessment via forward modeling.** The UOGD activity-specific VOC emission rates reported in this study can be used to drive dispersion simulations under a variety of meteorological conditions to estimate both acute and chronic exposure potential to individual air toxics at a range of distances (and directions) from UOGD operations. The emission rates measured by Hecobian et al. (2019) were used in just this way by a Colorado state-sponsored health risk assessment for UOGD in the Piecance and DJ Basins (Holder et al., 2019). This analysis, which found potential for acute exposures for benzene and some other air toxics to exceed health guideline values at distances as far as 2000 feet, was an important finding that contributed to a decision by the Colorado Oil and Gas Conservation Commission to increase the setback distance for new wells to 2,000 feet in Colorado. An update to this analysis, using emission rates characteristic of current operations, would be timely. It would also be helpful to examine exposure potential at distances beyond 2000 feet, the farthest distance examined by Holder et al. (2019).

References

Abeleira, A., Pollack, I.B., Sive, B., Zhou, Y., Fischer, E.V., Farmer, D.K., 2017. Source characterization of volatile organic compounds in the Colorado Northern Front Range Metropolitan Area during spring and summer 2015. Journal of Geophysical Research: Atmospheres 122, 3595–3613. https://doi.org/10.1002/2016JD026227

Ajax Analytics, 2022. Estimating High-Resolution VOC Concentrations from PID Sensor Signals and Triggered Canister Sample Results. https://drive.google.com/file/d/1eyf7OTHKrvYKJHQlSwkSNwk-8rpsgJrK/view

Albertson, John.D., Harvey, T., Foderaro, G., Zhu, P., Zhou, X., Ferrari, S., Amin, M.S., Modrak, M., Brantley, H., Thoma, E.D., 2016. A Mobile Sensing Approach for Regional Surveillance of Fugitive Methane Emissions in Oil and Gas Production. Environ. Sci. Technol. 50, 2487–2497. https://doi.org/10.1021/acs.est.5b05059

Allen, D.T., 2016. Emissions from oil and gas operations in the United States and their air quality implications. Journal of the Air & Waste Management Association 66, 549–575. https://doi.org/10.1080/10962247.2016.1171263

Allen, D.T., Pacsi, A.P., Sullivan, D.W., Zavala-Araiza, D., Harrison, M., Keen, K., Fraser, M.P., Daniel Hill, A., Sawyer, R.F., Seinfeld, J.H., 2015. Methane Emissions from Process Equipment at Natural Gas Production Sites in the United States: Pneumatic Controllers. Environ. Sci. Technol. 49, 633–640. https://doi.org/10.1021/es5040156

Alvarez, R.A., Zavala-Araiza, D., Lyon, D.R., Allen, D.T., Barkley, Z.R., Brandt, A.R., Davis, K.J., Herndon, S.C., Jacob, D.J., Karion, A., Kort, E.A., Lamb, B.K., Lauvaux, T., Maasakkers, J.D., Marchese, A.J., Omara, M., Pacala, S.W., Peischl, J., Robinson, A.L., Shepson, P.B., Sweeney, C., Townsend-Small, A., Wofsy, S.C., Hamburg, S.P., 2018. Assessment of methane emissions from the U.S. oil and gas supply chain. Science 361, 186–188. doi: 10.1126/science.aar7204

Atkinson, R., Arey, J., 2003. Atmospheric Degradation of Volatile Organic Compounds. Chem. Rev. 103, 4605–4638. https://doi.org/10.1021/cr0206420

Baker, A.K., Beyersdorf, A.J., Doezema, L.A., Katzenstein, A., Meinardi, S., Simpson, I.J., Blake, D.R., Sherwood Rowland, F., 2008. Measurements of nonmethane hydrocarbons in 28 United States cities. Atmospheric Environment 42, 170–182. doi: 10.1016/j.atmosenv.2007.09.007

Bergamaschi, P., Segers, A., Brunner, D., Haussaire, J.-M., Henne, S., Ramonet, M., Arnold, T., Biermann, T., Chen, H., Conil, S., Delmotte, M., Forster, G., Frumau, A., Kubistin, D., Lan, X., Leuenberger, M., Lindauer, M., Lopez, M., Manca, G., Müller-Williams, J., O'Doherty, S., Scheeren, B., Steinbacher, M., Trisolino, P., Vítková, G., Yver Kwok, C., 2022. High-resolution inverse modelling of European CH4 emissions using the novel FLEXPART-COSMO TM5 4DVAR inverse modelling system. Atmospheric Chemistry and Physics 22, 13243–13268.

Bolden, A.L., Kwiatkowski, C.F., Colborn, T., 2015. New Look at BTEX: Are Ambient Levels a Problem? Environ. Sci. Technol. 49, 5261–5276. https://doi.org/10.1021/es505316f

Borbon, A., Fontaine, H., Veillerot, M., Locoge, N., Galloo, J.C., Guillermo, R., 2001. An investigation into the traffic-related fraction of isoprene at an urban location. Atmospheric Environment 35, 3749–3760. https://doi.org/10.1016/S1352-2310(01)00170-4

Brantley, H.L., Thoma, E.D., Eisele, A.P., 2015. Assessment of volatile organic compound and hazardous air pollutant emissions from oil and natural gas well pads using mobile remote and on-site direct measurements. Journal of the Air & Waste Management Association 65, 1072–1082. https://doi.org/10.1080/10962247.2015.1056888

Brantley, H.L., Thoma, E.D., Squier, W.C., Guven, B.B., Lyon, D., 2014. Assessment of Methane Emissions from Oil and Gas Production Pads using Mobile Measurements. Environ. Sci. Technol. 48, 14508–14515. https://doi.org/10.1021/es503070q

Broomfield Air Quality Monitoring Program (AQM), n.d. https://www.broomfield.org/3004/Air-Quality-Monitoring

Briggs, G.A., 1993. Plume Dispersion in the Convective Boundary Layer. Part II: Analyses of CONDORS Field Experiment Data. Journal of Applied Meteorology and Climatology 32, 1388–1425.

Buzcu, B., Fraser, M.P., 2006. Source identification and apportionment of volatile organic compounds in Houston, TX. Atmospheric Environment 40, 2385–2400. doi: 10.1016/j.atmosenv.2005.12.020

Byers, A., Fedak, M., Freeman, P., Gibson, B., Hopkins, M., Mann, S., Pearson, R., Quinn, P., Reynolds, S., Silvers, T., Speec, S., n.d. Oil & Gas Comprehensive Plan for the City and County of Broomfield. https://www.broomfield.org/2273/Comprehensive-Plan

CalEPA, 2011. Final Guidance for the Evaluation and Mitigation of Subsurface Vapor Intrusion to Indoor Air (Vapor Intrusion Guidance).

Campbell, L., Toolen, J., Grubert, D., Napp, G., 2021. Compendium of Greenhouse Gas Emissions Methodologies for the Natural Gas and Oil Industry.

Caulton, D.R., Lu, J.M., Lane, H.M., Buchholz, B., Fitts, J.P., Golston, L.M., Guo, X., Li, Q., McSpiritt, J., Pan, D., Wendt, L., Bou-Zeid, E., Zondlo, M.A., 2019. Importance of Superemitter Natural Gas Well Pads in the Marcellus Shale. Environ. Sci. Technol. 53, 4747–4754. https://doi.org/10.1021/acs.est.8b06965

CDPHE, 2020. Investigation of Reported Health Concerns Near Livingston Oil and Gas Site in Broomfield. https://cdphe.colorado.gov/oil-and-gas-and-your-health/oil-and-gas-community-investigations

Cheadle, L.C., Oltmans, S.J., Pétron, G., Schnell, R.C., Mattson, E.J., Herndon, S.C., Thompson, A.M., Blake, D.R., McClure-Begley, A., 2017. Surface ozone in the Colorado northern Front Range and the influence of oil and gas development during FRAPPE/DISCOVER-AQ in summer 2014. Elementa: Science of the Anthropocene 5, 61. https://doi.org/10.1525/elementa.254

Cheng, X., Hao, Z., Zang, Z., Liu, Z., Xu, X., Wang, S., Liu, Y., Hu, Y., Ma, X., 2021. A new inverse modeling approach for emission sources based on the DDM-3D and 3DVAR techniques:

an application to air quality forecasts in the Beijing–Tianjin–Hebei region. Atmospheric Chemistry and Physics 21, 13747–13761. https://doi.org/10.5194/acp-21-13747-2021

Collett, J., Hecobian, A., Ham, J., Pierce, J., Clements, A., Shonkwiler, K., Zhou, Y., Desyaterik, Y., MacDonald, L., Wells, B., Hilliard, N., 2016. Characterizing emissions from natural gas drilling and well completion operations in Garfield County, CO. Colorado State University. http://dx.doi.org/10.25675/10217/172972

De Gouw, J., Jimenez, J.L., 2009. Organic Aerosols in the Earth's Atmosphere. Environ. Sci. Technol. 43, 7614–7618. https://doi.org/10.1021/es9006004

Deguillaume, L., Beekmann, M., Menut, L., 2007. Bayesian Monte Carlo analysis applied to regional-scale inverse emission modeling for reactive trace gases. Journal of Geophysical Research: Atmospheres 112. https://doi.org/10.1029/2006JD007518

Eastern Research Group, Inc., 2022. 2020 Nonpoint Oil and Gas Emission Estimation Tool Version 1.3.

Edie, R., Robertson, A.M., Field, R.A., Soltis, J., Snare, D.A., Zimmerle, D., Bell, C.S., Vaughn, T.L., Murphy, S.M., 2020. Constraining the accuracy of flux estimates using OTM 33A. Atmospheric Measurement Techniques 13, 341–353. https://doi.org/10.5194/amt-13-341-2020

Eklund, B., 1992. Practical Guidance for Flux Chamber Measurements of Fugitive Volatile Organic Emission Rates. Journal of the Air & Waste Management Association 42, 1583–1591. https://doi.org/10.1080/10473289.1992.10467102

Energy Resources Co, Inc., 1977. Atmospheric Emissions from Offshore Oil and Gas Development and Production.

EPA, 2023a. Basic Information about Oil and Natural Gas Air Pollution Standards. https://www.epa.gov/controlling-air-pollution-oil-and-natural-gas-operations/basic-information-about-oil-and-natural

EPA, 2023b. User's Guide for the AERMOD Meteorological Preprocessor (AERMET).

EPA, 2023c. AERMOD Model Formulation.

EPA, 2023d. Locating and Estimating (L&E) Documents. https://www.epa.gov/air-emissions-factors-and-quantification/locating-and-estimating-le-documents

EPA, 2020. User's Guide for AERSURFACE Tool.

EPA, 2019. Management of Oil and Gas Exploration, Development and Production Wastes: Factors Informing a Decision on the Need for Regulatory Action.

EPA, 2016. Air Quality Dispersion Modeling - Preferred and Recommended Models. https://www.epa.gov/scram/air-quality-dispersion-modeling-preferred-and-recommended-models

EPA, 2015a. What are Hazardous Air Pollutants? https://www.epa.gov/haps/what-are-hazardous-air-pollutants

EPA, 2015b. Initial List of Hazardous Air Pollutants with Modifications. https://www.epa.gov/haps/initial-list-hazardous-air-pollutants-modifications

EPA, 2014. Draft Other Test Method 33A: Geospatial Measurement of Air Pollution, Remote Emissions Quantification - Direct Assessment (GMAP-REQ-DA). https://www.epa.gov/emc/emc-other-test-methods

EPA, 1986. Measurement of Gaseous Emission Rates from Land Surfaces Using an Emission Isolation Flux Chamber. User's Guide.

Figueroa, V.K., Mackie, K.R., Guarriello, N., Cooper, C.D., 2009. A Robust Method for Estimating Landfill Methane Emissions. Journal of the Air & Waste Management Association 59, 925–935. https://doi.org/10.3155/1047-3289.59.8.925

Francoeur, C.B., McDonald, B.C., Gilman, J.B., Zarzana, K.J., Dix, B., Brown, S.S., de Gouw, J.A., Frost, G.J., Li, M., McKeen, S.A., Peischl, J., Pollack, I.B., Ryerson, T.B., Thompson, C., Warneke, C., Trainer, M., 2021. Quantifying Methane and Ozone Precursor Emissions from Oil and Gas Production Regions across the Contiguous US. Environ. Sci. Technol. 55, 9129–9139. https://doi.org/10.1021/acs.est.0c07352

Gilman, J.B., Kuster, W.C., Goldan, P.D., Herndon, S.C., Zahniser, M.S., Tucker, S.C., Brewer, W.A., Lerner, B.M., Williams, E.J., Harley, R.A., Fehsenfeld, F.C., Warneke, C., de Gouw, J.A., 2009. Measurements of volatile organic compounds during the 2006 TexAQS/GoMACCS campaign: Industrial influences, regional characteristics, and diurnal dependencies of the OH reactivity. Journal of Geophysical Research: Atmospheres 114. https://doi.org/10.1029/2008JD011525

Gilman, J.B., Lerner, B.M., Kuster, W.C., de Gouw, J.A., 2013. Source Signature of Volatile Organic Compounds from Oil and Natural Gas Operations in Northeastern Colorado. Environ. Sci. Technol. 47, 1297–1305. https://doi.org/10.1021/es304119a

Gkatzelis, G.I., Coggon, M.M., McDonald, B.C., Peischl, J., Aikin, K.C., Gilman, J.B., Trainer, M., Warneke, C., 2021. Identifying Volatile Chemical Product Tracer Compounds in U.S. Cities. Environ. Sci. Technol. 55, 188–199. https://doi.org/10.1021/acs.est.0c05467

Golston, L.M., Pan, D., Sun, K., Tao, L., Zondlo, M.A., Eilerman, S.J., Peischl, J., Neuman, J.A., Floerchinger, C., 2020. Variability of Ammonia and Methane Emissions from Animal Feeding Operations in Northeastern Colorado. Environ. Sci. Technol. 54, 11015–11024.

Gu, S., Guenther, A., Faiola, C., 2021. Effects of Anthropogenic and Biogenic Volatile Organic Compounds on Los Angeles Air Quality. Environ. Sci. Technol. 55, 12191–12201. https://doi.org/10.1021/acs.est.1c01481

Halliday, H.S., Thompson, A.M., Wisthaler, A., Blake, D.R., Hornbrook, R.S., Mikoviny, T., Müller, M., Eichler, P., Apel, E.C., Hills, A.J., 2016. Atmospheric benzene observations from oil and gas production in the Denver-Julesburg Basin in July and August 2014. Journal of Geophysical Research: Atmospheres 121, 11,055-11,074. https://doi.org/10.1002/2016JD025327

Hecobian, A., Clements, A.L., Shonkwiler, K.B., Zhou, Y., MacDonald, L.P., Hilliard, N., Wells, B.L., Bibeau, B., Ham, J.M., Pierce, J.R., Collett, J.L.Jr., 2019. Air Toxics and Other Volatile

Organic Compound Emissions from Unconventional Oil and Gas Development. Environ. Sci. Technol. Lett. 6, 720–726. https://doi.org/10.1021/acs.estlett.9b00591

Ho, K.F., Lee, S.C., Guo, H., Tsai, W.Y., 2004. Seasonal and diurnal variations of volatile organic compounds (VOCs) in the atmosphere of Hong Kong. Science of The Total Environment 322, 155–166. https://doi.org/10.1016/j.scitotenv.2003.10.004

Holder, C., Hader, J., Avanasi, R., Hong, T., Carr, E., Mendez, B., Wignall, J., Glen, G., Guelden, B., Wei, Y., 2019. Evaluating potential human health risks from modeled inhalation exposures to volatile organic compounds emitted from oil and gas operations. Journal of the Air & Waste Management Association 69, 1503–1524. https://doi.org/10.1080/10962247.2019.1680459

Howard, T., Lamb, B.K., Bamesberger, W.L., Zimmerman, P.R., 1992. Measurement of Hydrocarbon Emissions Fluxes from Refinery Wastewater Impoundments Using Atmospheric Tracer Techniques. Journal of the Air & Waste Management Association 42, 1336–1344.

Huang, D., Guo, H., 2023. Performance of AERMOD for predicting livestock odour dispersion under Canadian Prairies climate and flat terrain. Biosystems Engineering 226, 223–237. https://doi.org/10.1016/j.biosystemseng.2023.01.015

Karion, A., Sweeney, C., Kort, E.A., Shepson, P.B., Brewer, A., Cambaliza, M., Conley, S.A., Davis, K., Deng, A., Hardesty, M., Herndon, S.C., Lauvaux, T., Lavoie, T., Lyon, D., Newberger, T., Pétron, G., Rella, C., Smith, M., Wolter, S., Yacovitch, T.I., Tans, P., 2015. Aircraft-Based Estimate of Total Methane Emissions from the Barnett Shale Region. Environ. Sci. Technol. 49, 8124–8131. https://doi.org/10.1021/acs.est.5b00217

Karion, A., Sweeney, C., Pétron, G., Frost, G., Michael Hardesty, R., Kofler, J., Miller, B.R., Newberger, T., Wolter, S., Banta, R., Brewer, A., Dlugokencky, E., Lang, P., Montzka, S.A., Schnell, R., Tans, P., Trainer, M., Zamora, R., Conley, S., 2013. Methane emissions estimate from airborne measurements over a western United States natural gas field. Geophysical Research Letters 40, 4393–4397. https://doi.org/10.1002/grl.50811

Khoder, M.I., 2007. Ambient levels of volatile organic compounds in the atmosphere of Greater Cairo. Atmospheric Environment 41, 554–566. https://doi.org/10.1016/j.atmosenv.2006.08.051

Koblitz, M., 2020. API Comments on EPA's Updates under Consideration for the 2021 GHGI: Mud Degassing and Produced Water Emissions (EPA memos, September 2020).

Ku, I.-T., Zhou, Y., Hecobian, A., Benedict, K., Buck, B., Lachenmayer, E., Terry, B., Frazier, M., Zhang, J., Pan, D., Low, L., Sullivan, A., Collett, J.L., 2024. Air quality impacts from the development of unconventional oil and gas well pads: Air toxics and other volatile organic compounds. Atmospheric Environment 317, 120187. https://doi.org/10.1016/j.atmosenv.2023.120187

Lachenmayer, E., 2022. Impacts of Oil and Natural Gas Development and Other Sources on Volatile Organic Compound Concentrations in Broomfield, Colorado. Colorado State University.

Lamb, B.K., McManus, J.B., Shorter, J.H., Kolb, C.E., Mosher, Byard., Harriss, R.C., Allwine, Eugene., Blaha, Denise., Howard, Touche., Guenther, Alex., Lott, R.A., Siverson, Robert., Westburg, Hal., Zimmerman, Pat., 1995. Development of Atmospheric Tracer Methods To Measure

Methane Emissions from Natural Gas Facilities and Urban Areas. Environ. Sci. Technol. 29, 1468–1479. https://doi.org/10.1021/es00006a007

Lan, X., Talbot, R., Laine, P., Torres, A., 2015. Characterizing Fugitive Methane Emissions in the Barnett Shale Area Using a Mobile Laboratory. Environ. Sci. Technol. 49, 8139–8146. https://doi.org/10.1021/es5063055

Leuchner, M., Rappenglück, B., 2010. VOC source–receptor relationships in Houston during TexAQS-II. Atmospheric Environment 44, 4056–4067.

Ma, J., McHugh, T., Eklund, B., 2020. Flux Chamber Measurements Should Play a More Important Role in Contaminated Site Management. Environ. Sci. Technol. 54, 11645–11647. https://doi.org/10.1021/acs.est.0c04078

MacDonald, L.P., 2015. Estimating emission rates of volatile organic compounds from oil and natural gas operations in the Piceance Basin. Colorado State University.

McKenzie, L.M., Blair, B., Hughes, J., Allshouse, W.B., Blake, N.J., Helmig, D., Milmoe, P., Halliday, H., Blake, D.R., Adgate, J.L., 2018. Ambient Nonmethane Hydrocarbon Levels Along Colorado's Northern Front Range: Acute and Chronic Health Risks. Environ. Sci. Technol. 52, 4514–4525. https://doi.org/10.1021/acs.est.7b05983

Miller, L., Xu, X., Grgicak-Mannion, A., Brook, J., Wheeler, A., 2012. Multi-season, multi-year concentrations and correlations amongst the BTEX group of VOCs in an urbanized industrial city. Atmospheric Environment 61, 305–315. https://doi.org/10.1016/j.atmosenv.2012.07.041

Mochizuki, T., Miyazaki, Y., Ono, K., Wada, R., Takahashi, Y., Saigusa, N., Kawamura, K., Tani, A., 2015. Emissions of biogenic volatile organic compounds and subsequent formation of secondary organic aerosols in a Larix kaempferi forest. Atmospheric Chemistry and Physics 15, 12029–12041. https://doi.org/10.5194/acp-15-12029-2015

Moore, D.P., Li, N.P., Wendt, L.P., Castañeda, S.R., Falinski, M.M., Zhu, J.-J., Song, C., Ren, Z.J., Zondlo, M.A., 2023. Underestimation of Sector-Wide Methane Emissions from United States Wastewater Treatment. Environ. Sci. Technol. 57, 4082–4090. doi: 10.1021/acs.est.2c05373

Nieuwenburg, W., Nix, A.C., Fu, D., Yeung, T., Zemlak, W., Wells, N., 2023. Analysis of Emissions Profiles of Hydraulic Fracturing Engine Technologies. Energy and Power Engineering 15, 1–34. https://doi.org/10.4236/epe.2023.151001

Olaguer, E.P., Jeltema, S., Gauthier, T., Jermalowicz, D., Ostaszewski, A., Batterman, S., Xia, T., Raneses, J., Kovalchick, M., Miller, S., Acevedo, J., Lamb, J., Benya, J., Wendling, A., Zhu, J., 2022. Landfill Emissions of Methane Inferred from Unmanned Aerial Vehicle and Mobile Ground Measurements. Atmosphere 13, 983. https://doi.org/10.3390/atmos13060983

Omara, M., Zimmerman, N., Sullivan, M.R., Li, X., Ellis, A., Cesa, R., Subramanian, R., Presto, A.A., Robinson, A.L., 2018. Methane Emissions from Natural Gas Production Sites in the United States: Data Synthesis and National Estimate. Environ. Sci. Technol. 52, 12915–12925.

Orak, N.H., Reeder, M., Pekney, N.J., 2021. Identifying and quantifying source contributions of air quality contaminants during unconventional shale gas extraction. Atmospheric Chemistry and Physics 21, 4729–4739. https://doi.org/10.5194/acp-21-4729-2021

Peischl, J., Eilerman, S.J., Neuman, J.A., Aikin, K.C., de Gouw, J., Gilman, J.B., Herndon, S.C., Nadkarni, R., Trainer, M., Warneke, C., Ryerson, T.B., 2018. Quantifying Methane and Ethane Emissions to the Atmosphere From Central and Western U.S. Oil and Natural Gas Production Regions. Journal of Geophysical Research: Atmospheres 123, 7725–7740.

Peischl, J., Karion, A., Sweeney, C., Kort, E.A., Smith, M.L., Brandt, A.R., Yeskoo, T., Aikin, K.C., Conley, S.A., Gvakharia, A., Trainer, M., Wolter, S., Ryerson, T.B., 2016. Quantifying atmospheric methane emissions from oil and natural gas production in the Bakken shale region of North Dakota. Journal of Geophysical Research: Atmospheres 121, 6101–6111.

Peischl, J., Ryerson, T.B., Aikin, K.C., de Gouw, J.A., Gilman, J.B., Holloway, J.S., Lerner, B.M., Nadkarni, R., Neuman, J.A., Nowak, J.B., Trainer, M., Warneke, C., Parrish, D.D., 2015. Quantifying atmospheric methane emissions from the Haynesville, Fayetteville, and northeastern Marcellus shale gas production regions. Journal of Geophysical Research: Atmospheres 120, 2119–2139. https://doi.org/10.1002/2014JD022697

Perry, S.G., Cimorelli, A.J., Paine, R.J., Brode, R.W., Weil, J.C., Venkatram, A., Wilson, R.B., Lee, R.F., Peters, W.D., 2005. AERMOD: A Dispersion Model for Industrial Source Applications. Part II: Model Performance against 17 Field Study Databases. Journal of Applied Meteorology and Climatology 44, 694–708. https://doi.org/10.1175/JAM2228.1

Pétron, G., Frost, G., Miller, B.R., Hirsch, A.I., Montzka, S.A., Karion, A., Trainer, M., Sweeney, C., Andrews, A.E., Miller, L., Kofler, J., Bar-Ilan, A., Dlugokencky, E.J., Patrick, L., Moore Jr., C.T., Ryerson, T.B., Siso, C., Kolodzey, W., Lang, P.M., Conway, T., Novelli, P., Masarie, K., Hall, B., Guenther, D., Kitzis, D., Miller, J., Welsh, D., Wolfe, D., Neff, W., Tans, P., 2012. Hydrocarbon emissions characterization in the Colorado Front Range: A pilot study. Journal of Geophysical Research: Atmospheres 117. https://doi.org/10.1029/2011JD016360

Pétron, G., Karion, A., Sweeney, C., Miller, B.R., Montzka, S.A., Frost, G.J., Trainer, M., Tans, P., Andrews, A., Kofler, J., Helmig, D., Guenther, D., Dlugokencky, E., Lang, P., Newberger, T., Wolter, S., Hall, B., Novelli, P., Brewer, A., Conley, S., Hardesty, M., Banta, R., White, A., Noone, D., Wolfe, D., Schnell, R., 2014. A new look at methane and nonmethane hydrocarbon emissions from oil and natural gas operations in the Colorado Denver-Julesburg Basin. Journal of Geophysical Research: Atmospheres 119, 6836–6852. https://doi.org/10.1002/2013JD021272

Pollack, I.B., Helmig, D., O'Dell, K., Fischer, E.V., 2021. Seasonality and Source Apportionment of Nonmethane Volatile Organic Compounds at Boulder Reservoir, Colorado, Between 2017 and 2019. Journal of Geophysical Research: Atmospheres 126, e2020JD034234.

Prenni, A.J., Day, D.E., Evanoski-Cole, A.R., Sive, B.C., Hecobian, A., Zhou, Y., Gebhart, K.A., Hand, J.L., Sullivan, A.P., Li, Y., Schurman, M.I., Desyaterik, Y., Malm, W.C., Collett Jr., J.L., Schichtel, B.A., 2016. Oil and gas impacts on air quality in federal lands in the Bakken region: an overview of the Bakken Air Quality Study and first results. Atmospheric Chemistry and Physics 16, 1401–1416. https://doi.org/10.5194/acp-16-1401-2016

Reimann, S., Lewis, A.C., 2007. Anthropogenic VOCs, in: Volatile Organic Compounds in the Atmosphere. John Wiley & Sons, Ltd, pp. 33–81. https://doi.org/10.1002/9780470988657.ch2

Robertson, A.M., Edie, R., Snare, D., Soltis, J., Field, R.A., Burkhart, M.D., Bell, C.S., Zimmerle, D., Murphy, S.M., 2017. Variation in Methane Emission Rates from Well Pads in Four Oil and Gas Basins with Contrasting Production Volumes and Compositions. Environ. Sci. Technol. 51, 8832–8840. https://doi.org/10.1021/acs.est.7b00571

Roest, G.S., Schade, G.W., 2020. Air quality measurements in the western Eagle Ford Shale. Elementa: Science of the Anthropocene 8, 18. https://doi.org/10.1525/elementa.414

Rutter, A.P., Griffin, R.J., Cevik, B.K., Shakya, K.M., Gong, L., Kim, S., Flynn, J.H., Lefer, B.L., 2015. Sources of air pollution in a region of oil and gas exploration downwind of a large city. Atmospheric Environment 120, 89–99. https://doi.org/10.1016/j.atmosenv.2015.08.073

ShaleXP, n.d. Colorado Oil and Gas Data Summary. https://www.shalexp.com/colorado (accessed on 7 April 2024).

Stevenson, D.S., Young, P.J., Naik, V., Lamarque, J.-F., Shindell, D.T., Voulgarakis, A., Skeie, R.B., Dalsoren, S.B., Myhre, G., Berntsen, T.K., Folberth, G.A., Rumbold, S.T., Collins, W.J., MacKenzie, I.A., Doherty, R.M., Zeng, G., van Noije, T.P.C., Strunk, A., Bergmann, D., Cameron-Smith, P., Plummer, D.A., Strode, S.A., Horowitz, L., Lee, Y.H., Szopa, S., Sudo, K., Nagashima, T., Josse, B., Cionni, I., Righi, M., Eyring, V., Conley, A., Bowman, K.W., Wild, O., Archibald, A., 2013. Tropospheric ozone changes, radiative forcing and attribution to emissions in the Atmospheric Chemistry and Climate Model Intercomparison Project (ACCMIP). Atmospheric Chemistry and Physics 13, 3063–3085. https://doi.org/10.5194/acp-13-3063-2013

Stull, R.B. (Ed.), 1988. An Introduction to Boundary Layer Meteorology. Springer Netherlands, Dordrecht. https://doi.org/10.1007/978-94-009-3027-8

Swarthout, R.F., Russo, R.S., Zhou, Y., Hart, A.H., Sive, B.C., 2013. Volatile organic compound distributions during the NACHTT campaign at the Boulder Atmospheric Observatory: Influence of urban and natural gas sources. Journal of Geophysical Research: Atmospheres 118, 10,614-10,637. https://doi.org/10.1002/jgrd.50722

Taylor, D.M., Chow, F.K., Delkash, M., Imhoff, P.T., 2016. Numerical simulations to assess the tracer dilution method for measurement of landfill methane emissions. Waste Management 56, 298–309. https://doi.org/10.1016/j.wasman.2016.06.040

Thoma, E. and B. Squier., 2014. OTM 33 Geospatial Measurement of Air Pollution, Remote Emissions Quantification (GMAP-REQ) and OTM33A Geospatial Measurement of Air Pollution-Remote Emissions Quantification-Direct Assessment (GMAP-REQ-DA).

Thompson, C.R., Hueber, J., Helmig, D., 2014. Influence of oil and gas emissions on ambient atmospheric non-methane hydrocarbons in residential areas of Northeastern Colorado. Elementa: Science of the Anthropocene 3, 000035. https://doi.org/10.12952/journal.elementa.000035

Wang, L., Parker, D.B., Parnell, C.B., Lacey, R.E., Shaw, B.W., 2006. Comparison of CALPUFF and ISCST3 models for predicting downwind odor and source emission rates. Atmospheric Environment 40, 4663–4669. https://doi.org/10.1016/j.atmosenv.2006.04.043

Weber, D.T., 2018. Volatile Organic Compound Concentrations and the Impacts of Future Oil and Natural Gas Development in the Colorado Northern Front Range. Colorado State University.

White, W.H., Anderson, J.A., Blumenthal, D.L., Husar, R.B., Gillani, N.V., Husar, J.D., Wilson, W.E., 1976. Formation and Transport of Secondary Air Pollutants: Ozone and Aerosols in the St. Louis Urban Plume. Science 194, 187–189. https://doi.org/10.1126/science.959846

Wilde, S.E., Dominutti, P.A., Allen, G., Andrews, S.J., Bateson, P., Bauguitte, S.J.-B., Burton, R.R., Colfescu, I., France, J., Hopkins, J.R., Huang, L., Jones, A.E., Lachlan-Cope, T., Lee, J.D., Lewis, A.C., Mobbs, S.D., Weiss, A., Young, S., Purvis, R.M., 2021. Speciation of VOC emissions related to offshore North Sea oil and gas production. Atmospheric Chemistry and Physics 21, 3741–3762. https://doi.org/10.5194/acp-21-3741-2021

Willis, G.E., Deardorff, J.W., 1981. A laboratory study of dispersion from a source in the middle of the convectively mixed layer. Atmospheric Environment (1967) 15, 109–117.

Wilson, D., Billings, R., Oommen, R., Chang, R., 2007. Year 2005 Gulfwide Emission Inventory.

Zavala-Araiza, D., Allen, D.T., Harrison, M., George, F.C., Jersey, G.R., 2015. Allocating Methane Emissions to Natural Gas and Oil Production from Shale Formations. ACS Sustainable Chem. Eng. 3, 492–498. https://doi.org/10.1021/sc500730x

Zhou, X., Passow, F.H., Rudek, J., von Fisher, J.C., Hamburg, S.P., Albertson, J.D., 2019. Estimation of methane emissions from the U.S. ammonia fertilizer industry using a mobile sensing approach. Elementa: Science of the Anthropocene 7, 19. https://doi.org/10.1525/elementa.358

Appendix A

Supplementary for Wind Data

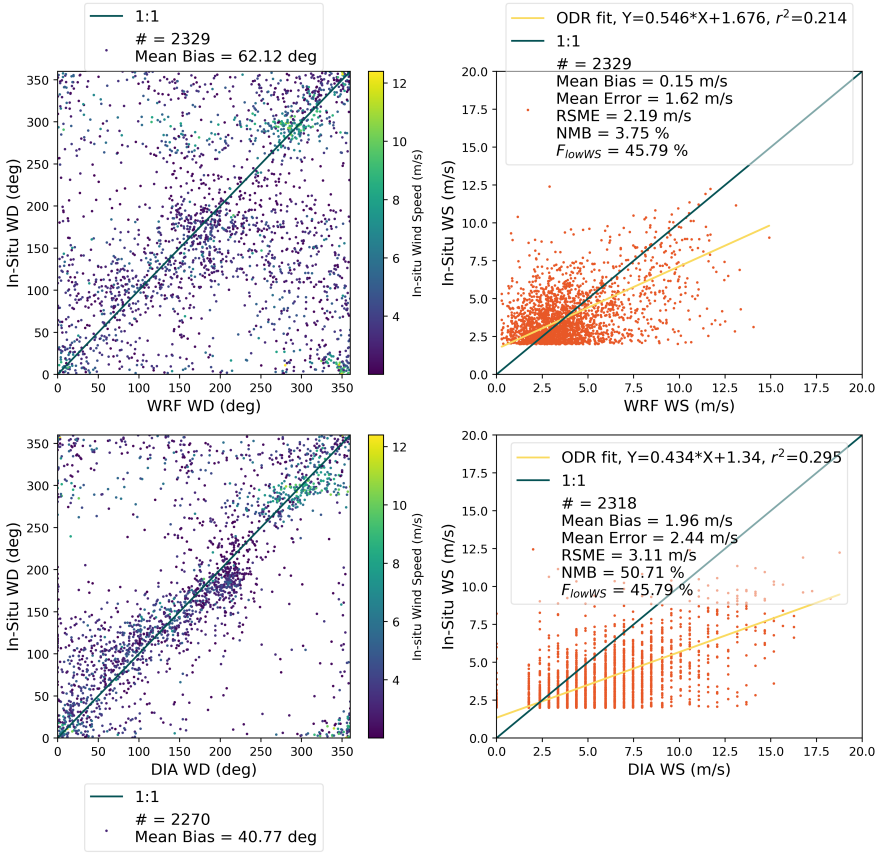

Figure A.1: Hourly wind direction and wind speed comparison between in-situ observations and WRF & DIA for January to June 2022 after removing low wind speed (< 2m/s). Wind directions are colored by wind speed. F_{lowWS} is the fraction of WS smaller than 2 m/s.

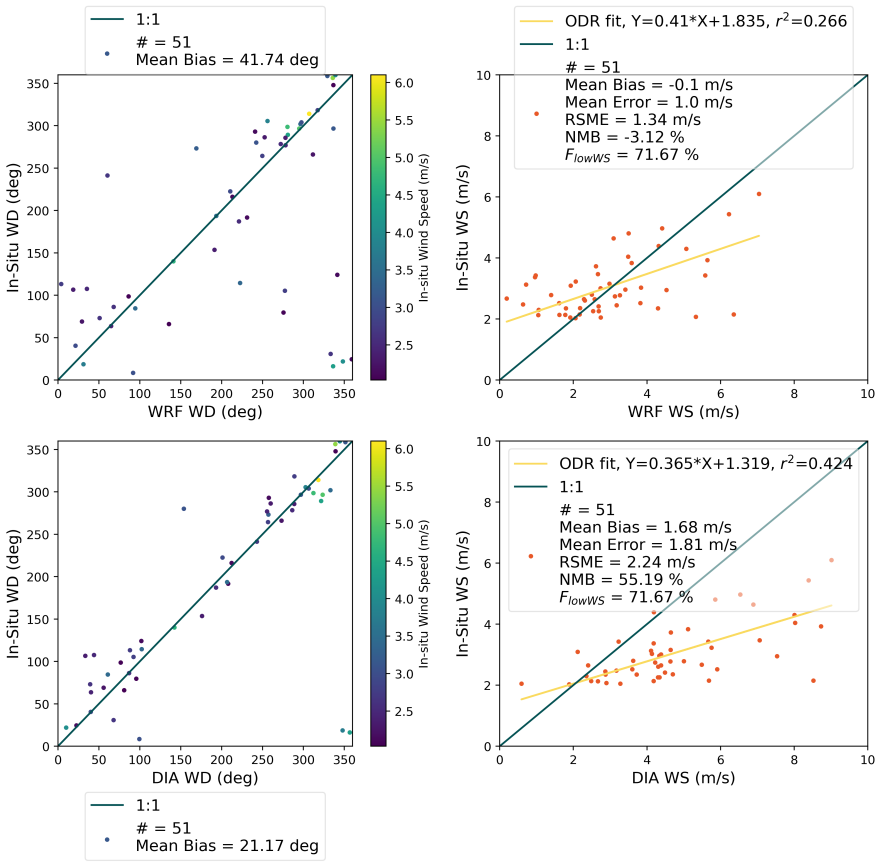

Figure A.2: Daily wind direction and wind speed comparison between in-situ observations and WRF & DIA for January to June 2022 after removing low wind speed (< 2m/s). Wind directions are colored by wind speed. F_{lowWS} is the fraction of WS smaller than 2 m/s.

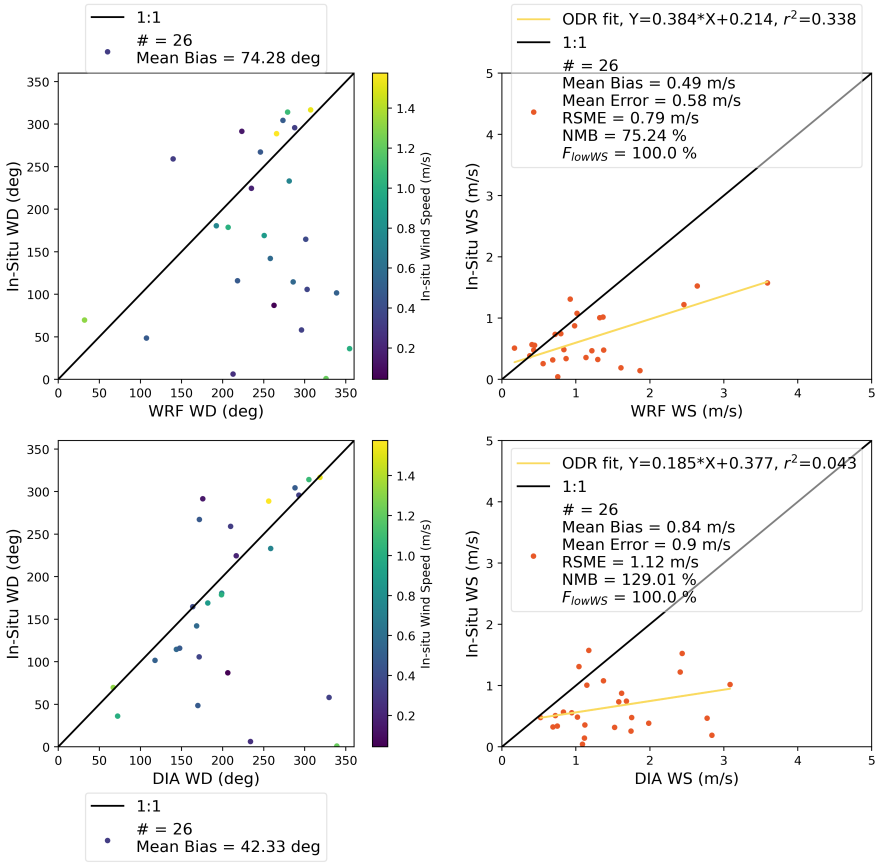

Figure A.3: Weekly wind direction and wind speed comparison between in-situ observations and WRF & DIA for January to June 2022. Wind directions are colored by wind speed. F_{lowWS} is the fraction of WS smaller than 2 m/s.

Appendix B

Supplementary for Model Evaluation

According to Figure 3.3, the MLR method incorporating AERMOD simulations and observations is able to predict VOC concentrations with low mean bias and a small amount of scatter. The mean bias for ITC, LS, NWP, UT, and COM are -0.068, -1.495, 0.005, -1.18, and 0.491 $\mu g/m^3$, respectively. The overall mean bias is -0.2363 $\mu g/m^3$. Most points are situated close to the 1:1 line, indicating the capability of AERMOD in capturing the emission contributions from different sources. Points below the 1:1 line (predicted > observed) may be due to the plume not being adequately diluted caused by underpredicted atmospheric instability in AERMOD. Conversely, if AERMOD overpredicts atmospheric instability, the simulated plume would be more diluted. Points above the 1:1 line (observed > predicted) may result from inaccurate wind direction used in AERMOD, causing pollutant plume not reaching the monitoring sites as it should be. However, we used the optimal wind direction data available to run AERMOD as discussed in section 2.3.2.

Without strong bias, AERMOD can be used to simulate weekly-averaged VOC concentration dispersions and, moreover, to constrain VOC emission rates for different sources when used with MLR and weekly averaged observations, as demonstrated in this thesis.

In addition to AERMOD's simulation performance for drilling tracers during drilling operations, Figures B.1, B.2, B.3, B.4, and B.5 present the observed concentration vs. predicted concentrations during all operations for methane, ethane, $C_8 - C_{10}$ n-alkanes, benzene, and NMVOC, respectively.

In general, the mean bias for ethane, $C_8 - C_{10}$ n-alkanes, benzene, and NMVOC are small. The overall mean bias for methane, ethane, $C_8 - C_{10}$ n-alkanes, and benzene are -2.6e-14, -1.44e-17, -4.7e-17, and 8.4e-18 $\mu g/m^3$, respectively. As for NMVOC, the mean bias for ITC, LS, NWP, UT, and COM are -1.665, 1.798, 0.563, -2.162, and 1.875 $\mu g/m^3$, respectively. The overall mean bias for NMVOC is 0.055 $\mu g/m^3$. Therefore, AERMOD is able to simulate the dispersion plumes for different VOCs during all UOGD operations with low bias.

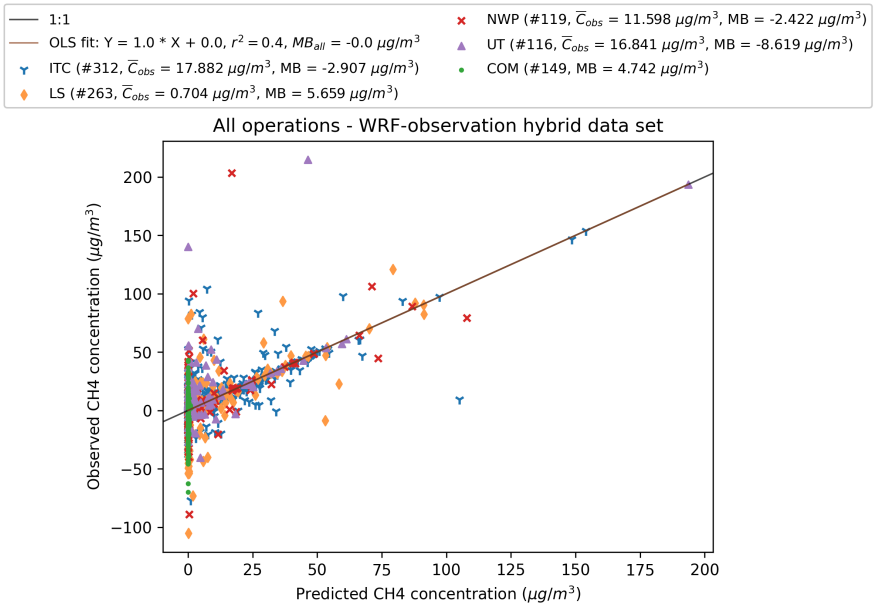

Figure B.1: Observed methane concentrations vs. MLR predicted methane concentrations for all operations. ITC01, ITC02, and ITC03 are all labeled as ITC. LS01 and LS02 are all labeled as LS. NWP02 and NWP03 are all labeled as NWP. UT02 and UT03 are all labeled as UT. In the legend, # represents the number of weekly concentrations; $\overline{C}_{obs}$ is the mean observed concentrations; and MB is the mean bias of predicted concentration.

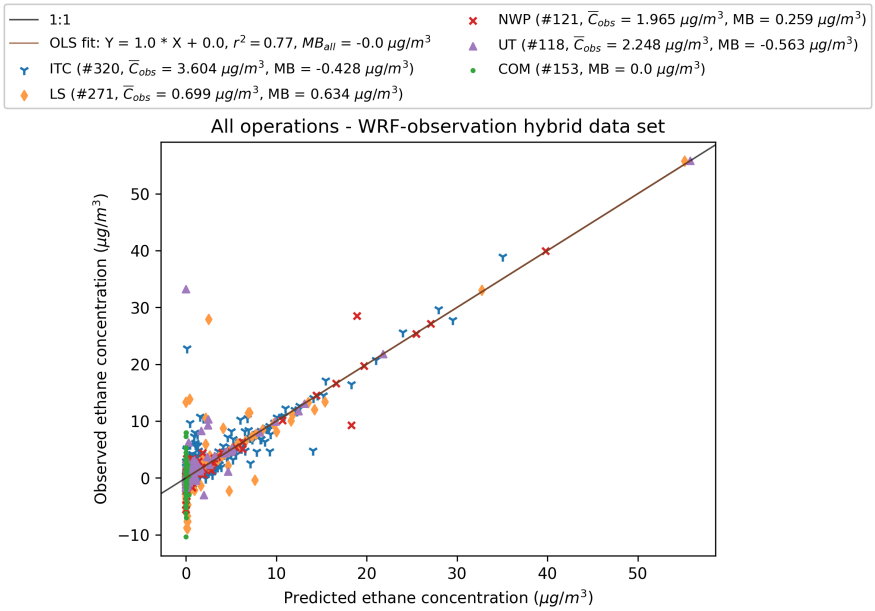

Figure B.2: Observed ethane concentrations vs. MLR predicted ethane concentrations for all operations. ITC01, ITC02, and ITC03 are all labeled as ITC. LS01 and LS02 are all labeled as LS. NWP02 and NWP03 are all labeled as NWP. UT02 and UT03 are all labeled as UT. In the legend, # represents the number of weekly concentrations; $\overline{C}_{obs}$ is the mean observed concentrations; and MB is the mean bias of predicted concentration.

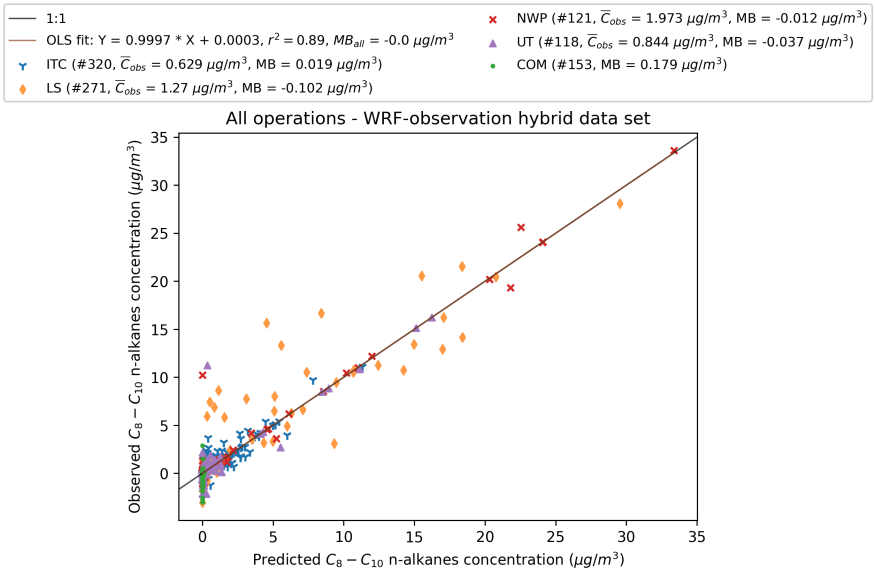

Figure B.3: Observed $C_8 - C_{10}$ n-alkane concentrations vs. MLR predicted $C_8 - C_{10}$ n-alkane concentrations for all operations. ITC01, ITC02, and ITC03 are all labeled as ITC. LS01 and LS02 are all labeled as LS. NWP02 and NWP03 are all labeled as NWP. UT02 and UT03 are all labeled as UT. In the legend, # represents the number of weekly concentrations; $\overline{C}_{obs}$ is the mean observed concentrations; and MB is the mean bias of predicted concentration.

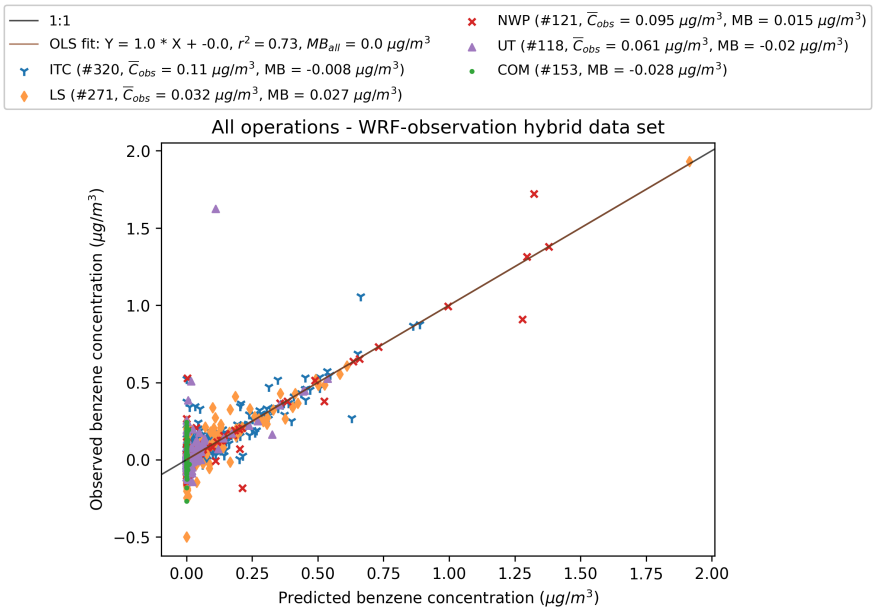

Figure B.4: Observed benzene concentrations vs. MLR predicted benzene concentrations for all operations. ITC01, ITC02, and ITC03 are all labeled as ITC. LS01 and LS02 are all labeled as LS. NWP02 and NWP03 are all labeled as NWP. UT02 and UT03 are all labeled as UT. In the legend, # represents the number of weekly concentrations; $\overline{C}_{obs}$ is the mean observed concentrations; and MB is the mean bias of predicted concentration.

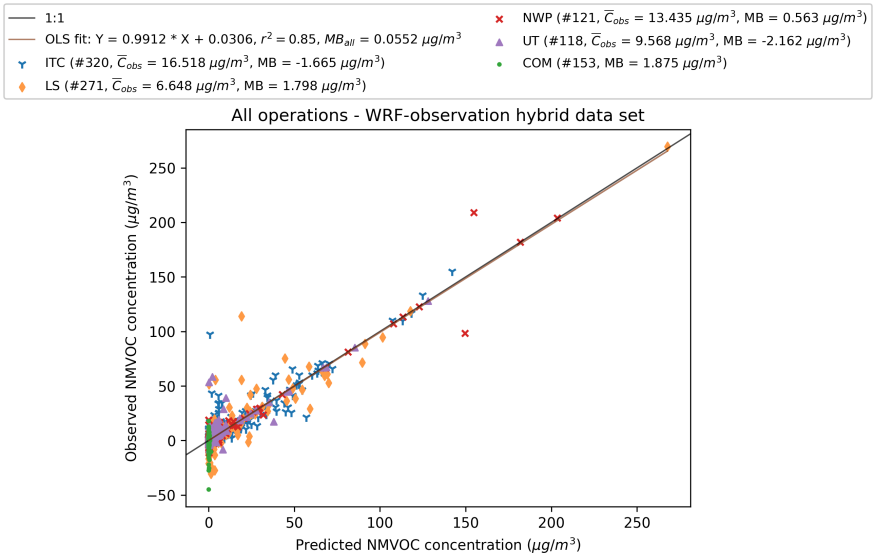

Figure B.5: Observed NMVOC concentrations vs. MLR predicted NMVOC concentrations for all operations. ITC01, ITC02, and ITC03 are all labeled as ITC. LS01 and LS02 are all labeled as LS. NWP02 and NWP03 are all labeled as NWP. UT02 and UT03 are all labeled as UT. In the legend, # represents the number of weekly concentrations; $\overline{C}_{obs}$ is the mean observed concentrations; and MB is the mean bias of predicted concentration.

Appendix C

Supplementary for Weekly Canister Samples

Figure C.1: AERMOD simulated weekly plume concentrations at five monitoring sites (COM, ITC01, LS01, NWP02, and UT01) from six O&G well pads (LS, NWA, NWB, ICA, ICA, and ICB) with unit emission rate of 1 g/s, respectively.

Figure C.2: AERMOD simulated weekly plume concentrations at five monitoring sites (ITC02, ITC03, LS02, NWP03, and UT02) from six O&G well pads (LS, NWA, NWB, ICA, ICA, and ICB) with unit emission rate of 1 g/s, respectively.

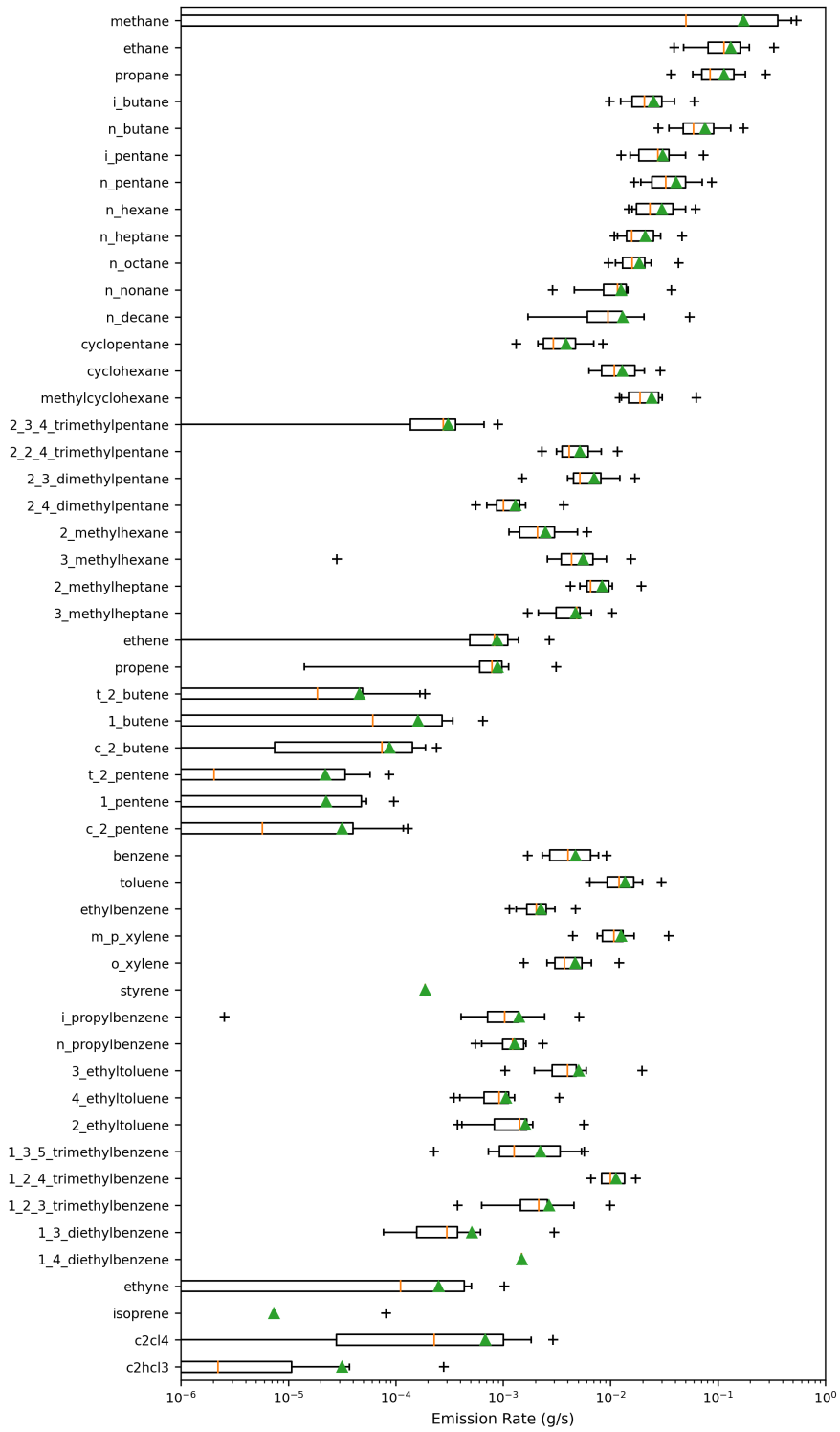

Figure C.3: Emission rates of 51 VOCs using weekly canister samples during drilling operations using Gibson mud. Green triangles and orange lines are mean and median values, respectively. Boxes and whiskers are 5^{th}, 25^{th}, 75^{th}, and 95^{th} percentiles.

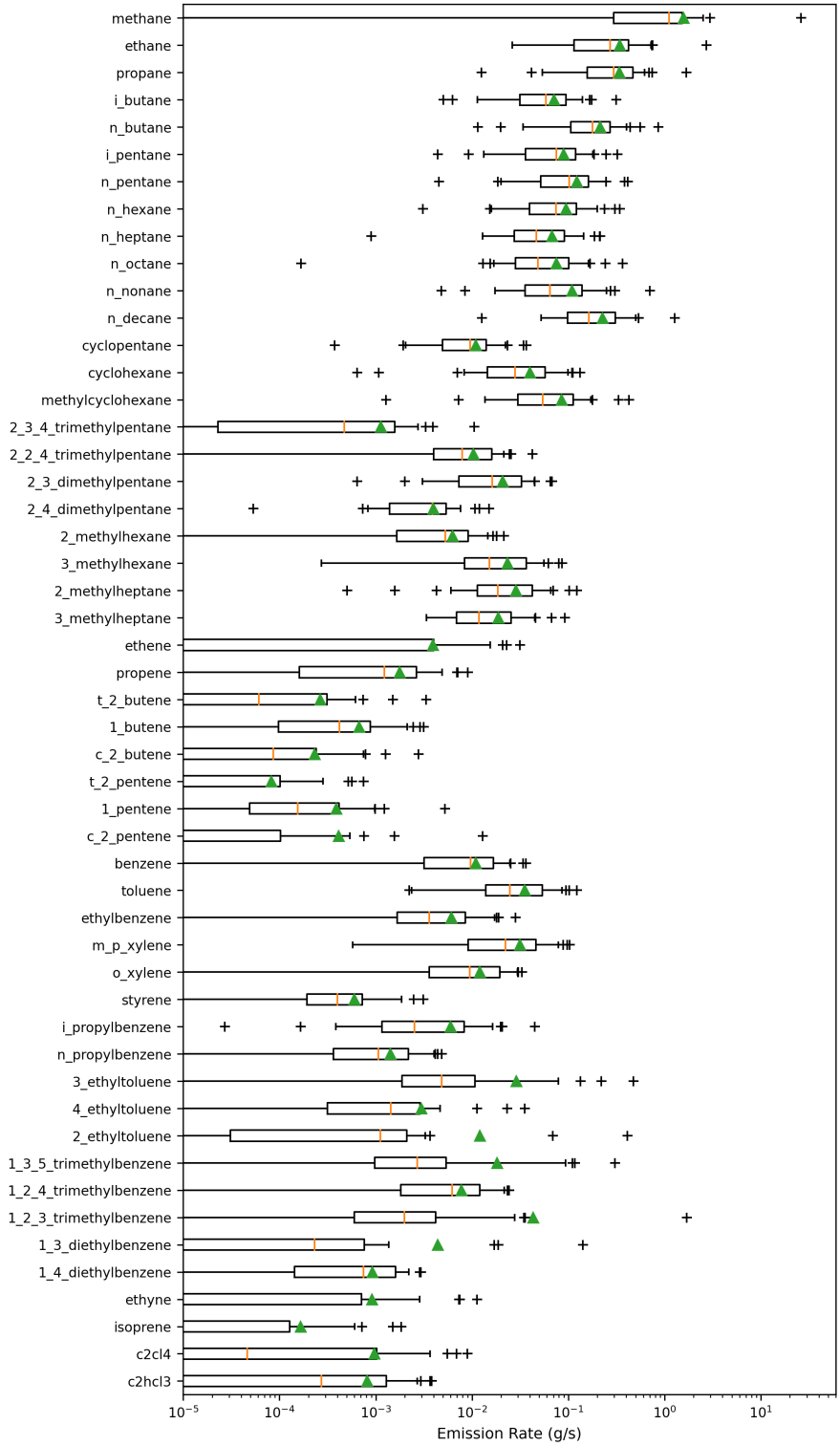

Figure C.4: Emission rates of 51 VOCs using weekly canister samples during drilling operations using Neoflo mud. Green triangles and orange lines are mean and median values, respectively. Boxes and whiskers are 5^{th}, 25^{th}, 75^{th}, and 95^{th} percentiles.

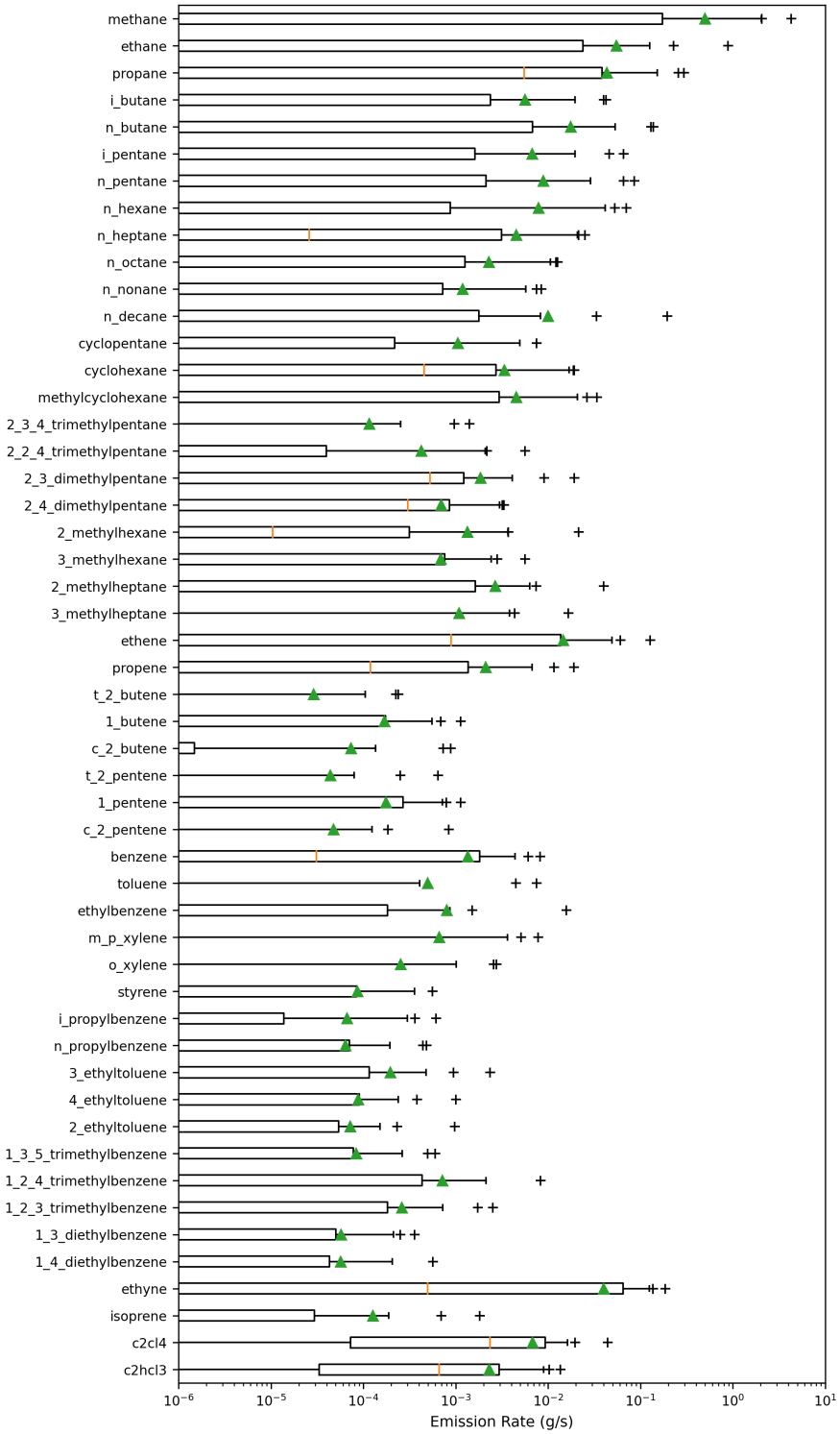

Figure C.5: Emission rates of 51 VOCs using weekly canister samples during hydraulic fracturing operations. Green triangles and orange lines are mean and median values, respectively. Boxes and whiskers are 5^{th}, 25^{th}, 75^{th}, and 95^{th} percentiles.

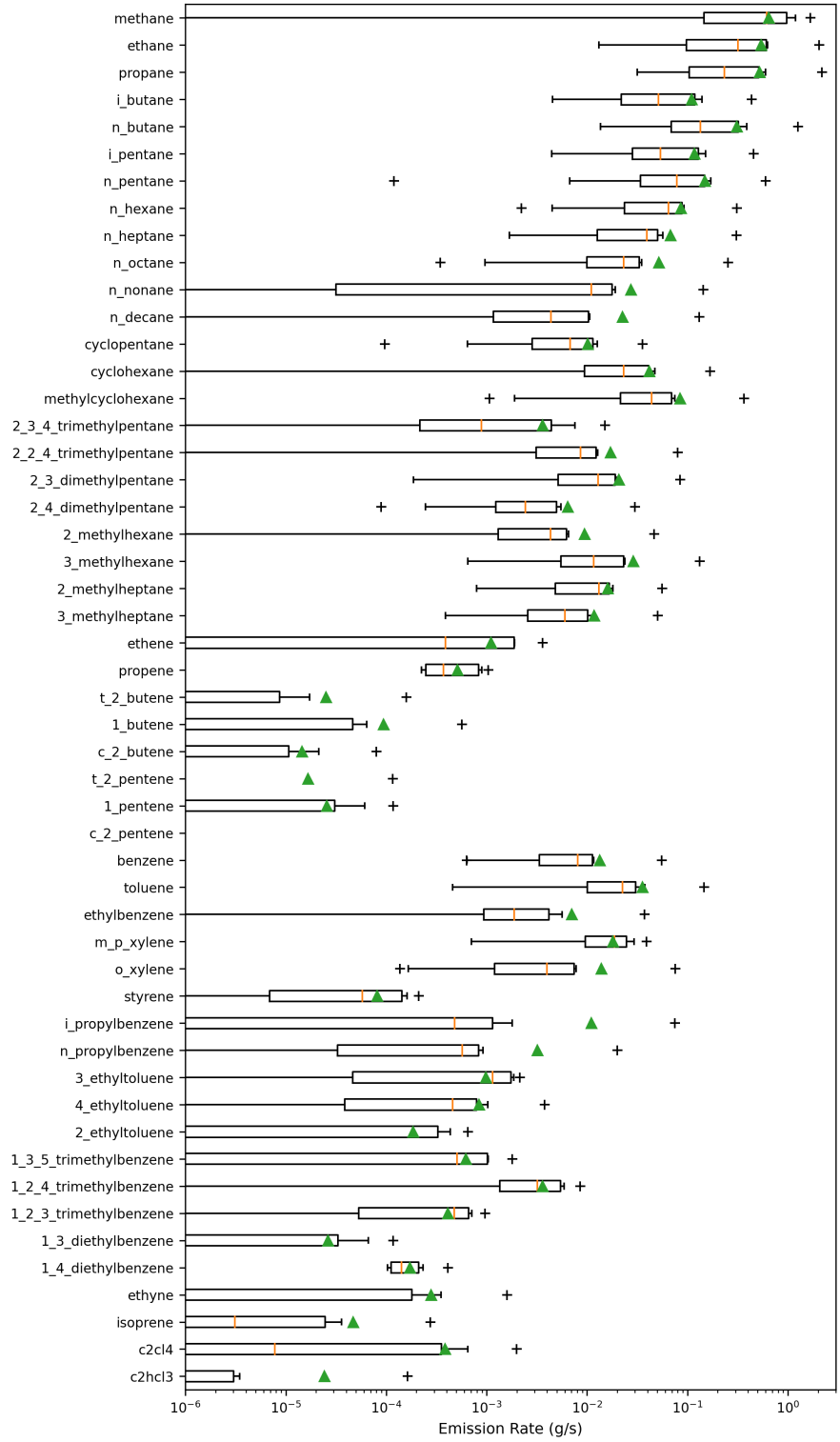

Figure C.6: Emission rates of 51 VOCs using weekly canister samples during coiled tubing/millout operations. Green triangles and orange lines are mean and median values, respectively. Boxes and whiskers are 5^{th}, 25^{th}, 75^{th}, and 95^{th} percentiles.

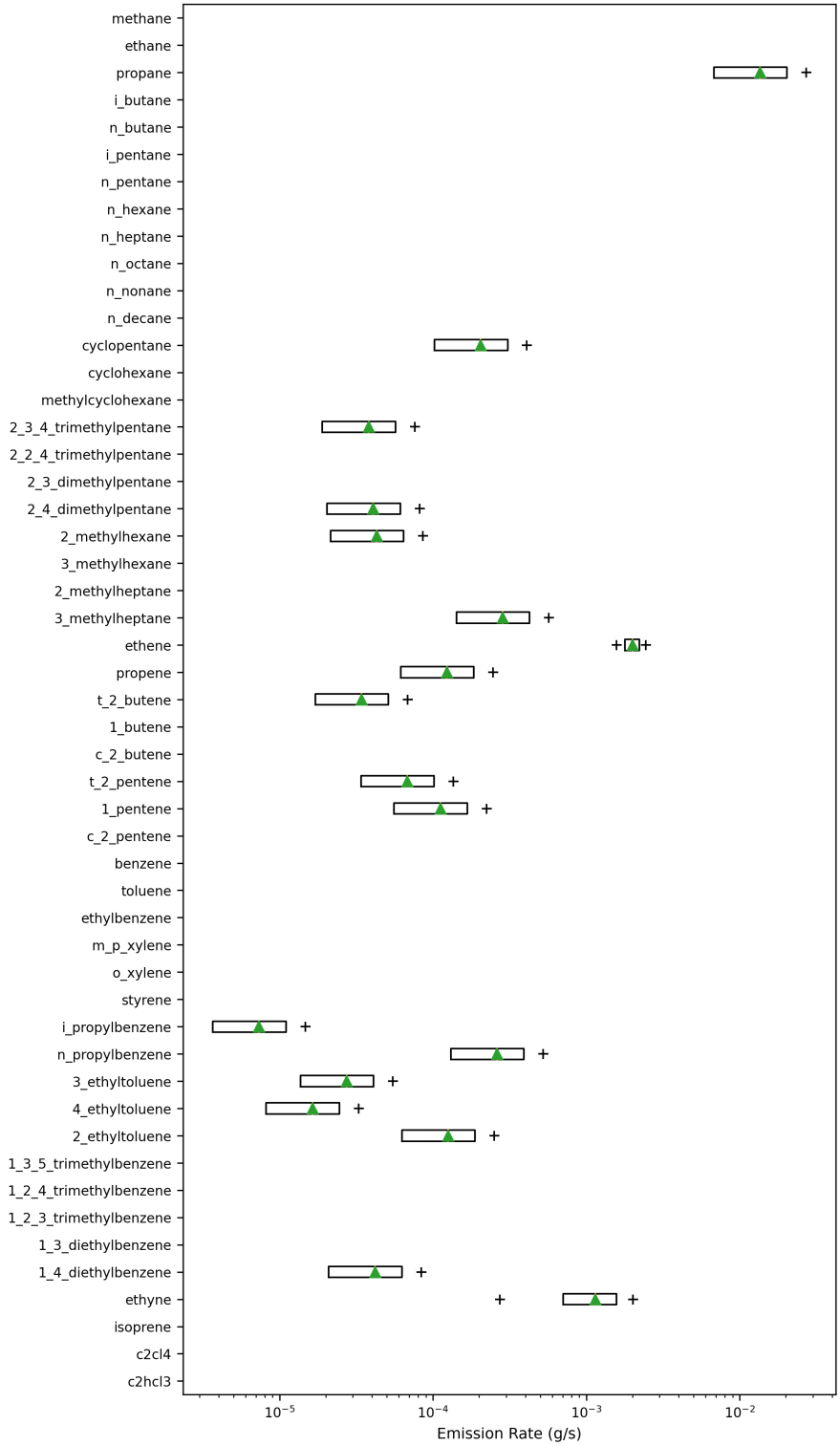

Figure C.7: Emission rates of 51 VOCs using weekly canister samples during production tubing installation operations. Green triangles and orange lines are mean and median values, respectively. Boxes and whiskers are 5^{th}, 25^{th}, 75^{th}, and 95^{th} percentiles.

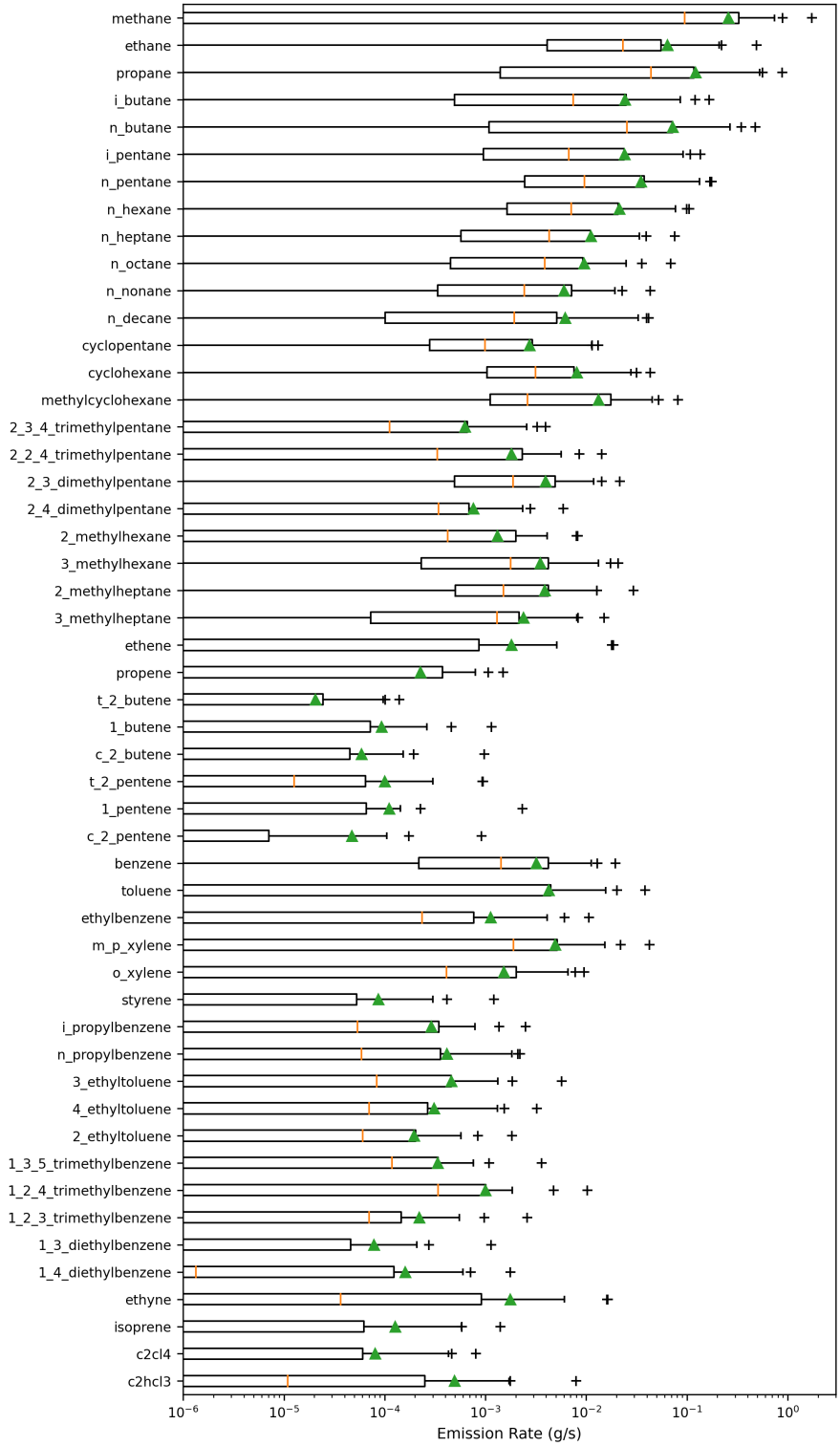

Figure C.8: Emission rates of 51 VOCs using weekly canister samples during flowback operations. Green triangles and orange lines are mean and median values, respectively. Boxes and whiskers are 5^{th}, 25^{th}, 75^{th}, and 95^{th} percentiles.

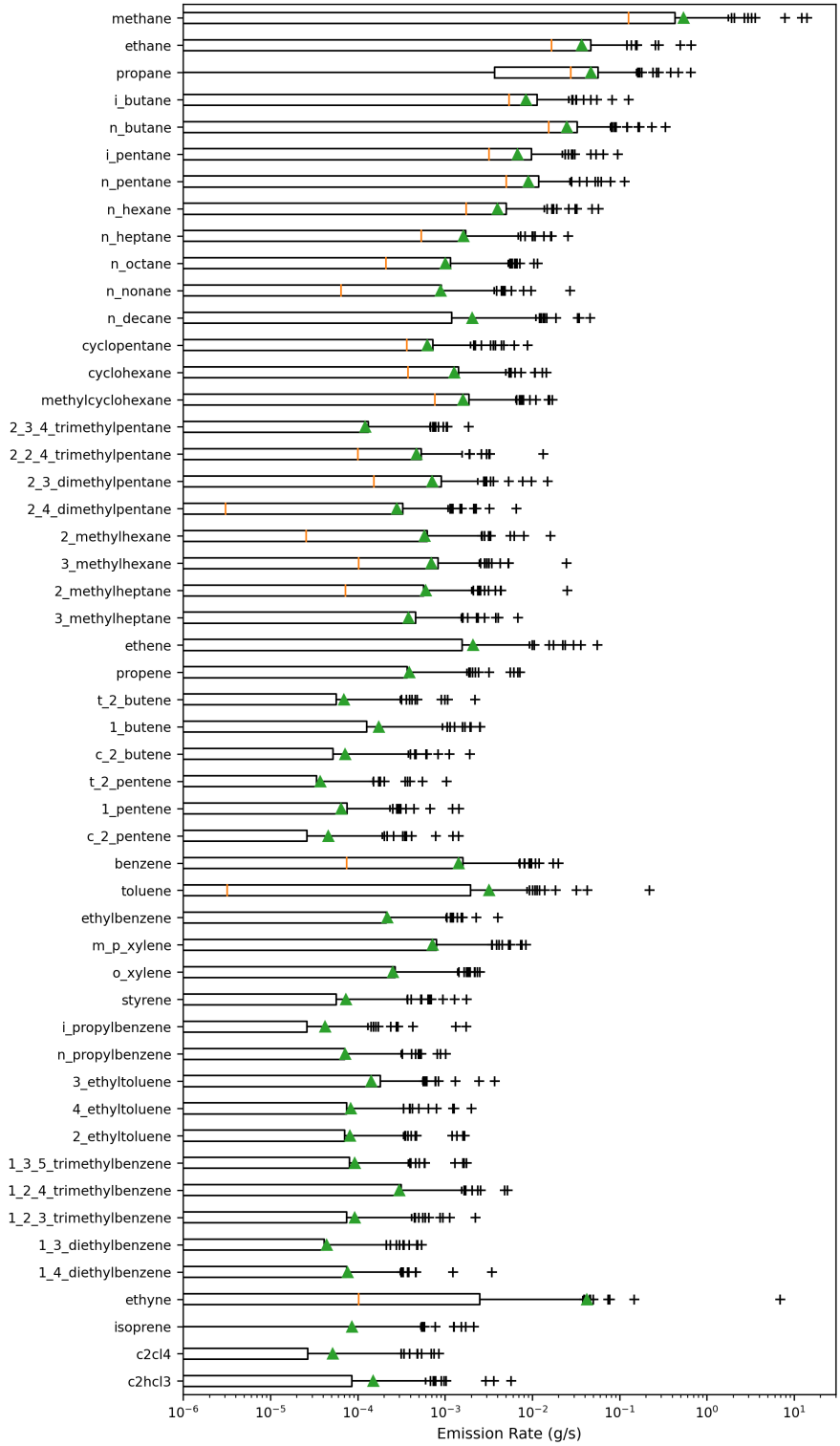

Figure C.9: Emission rates of 51 VOCs using weekly canister samples during production. Green triangles and orange lines are mean and median values, respectively. Boxes and whiskers are 5^{th}, 25^{th}, 75^{th}, and 95^{th} percentiles.

Appendix D

Supplementary for Plume-Triggered Samples

Table D.1: Information of plume-triggered canister samples for drilling operations using Neoflo mud.

Triggered #	Triggered Time	Triggered Site	O&G Source
1	2021-09-16 22:47:00	NWP03	NWB
2	2021-09-17 08:12:00	NWP02	NWB
3	2021-09-18 08:24:00	UT02	NWB
4	2021-09-18 10:04:00	UT02	NWB
5	2021-09-18 15:00:00	NWP02	NWB
6	2021-09-18 23:27:00	UT02	NWB
7	2021-09-20 09:57:00	NWP02	NWB
8	2021-09-21 14:59:00	NWP02	NWB
9	2021-09-23 14:19:00	NWP02	NWB
10	2021-09-25 06:01:00	UT02	NWB
11	2021-09-25 14:16:00	NWP02	NWB
12	2021-09-29 08:34:00	NWP02	NWB
13	2021-09-30 11:37:00	NWP02	NWB
14	2021-10-01 11:15:00	NWP02	NWB
15	2021-10-01 12:04:00	NWP02	NWB
16	2021-10-01 22:44:00	NWP02	NWB
17	2021-10-02 21:25:00	NWP02	NWB
18	2021-10-04 13:01:00	NWP02	NWB
19	2021-10-06 22:36:00	NWP02	NWB
20	2021-10-07 18:15:00	NWP02	NWB
21	2021-10-08 04:02:00	UT02	NWB
22	2021-10-08 13:17:00	NWP02	NWB
23	2021-10-08 13:53:00	NWP02	NWB
24	2021-10-09 04:53:00	UT01	NWB
25	2021-10-15 04:51:00	UT02	UT
26	2021-10-15 05:08:00	UT01	UT
27	2021-10-16 00:41:00	UT02	UT
28	2021-10-16 12:16:00	UT01	UT
29	2021-10-16 18:34:00	UT02	UT
30	2021-10-18 14:54:00	UT01	UT
31	2021-10-18 21:22:00	UT02	UT
32	2021-10-22 15:52:00	UT01	UT
33	2021-10-30 13:09:00	UT01	UT
34	2021-11-05 09:21:00	UT01	UT

Table D.2: Information of plume-triggered canister samples for coiled tubing/millout operations.

Triggered #	Triggered Time	Triggered Site	O&G Source
1	2020-02-22 21:14	LS02	LS
2	2020-03-03 19:35	LS02	LS
3	2020-03-06 21:47	LS02	LS
4	2021-12-04 04:08	NWP02	NWA
5	2021-12-04 04:18	NWP03	NWA
6	2021-12-04 16:24	NWP02	NWA

Table D.3: Information of plume-triggered canister samples for flowback operations.

Triggered #	Triggered Time	Triggered Site	O&G Source
1	2020-04-17 20:01	LS01	LS
2	2020-05-25 04:18	LS02	LS
3	2022-01-17 21:53	NWP02	NWA
4	2022-02-03 18:37	NWP02	NWA
5	2022-02-18 01:31	NWP02	NWA
6	2022-02-25 00:10	NWP02	NWA
7	2022-03-04 00:37	NWP02	NWA
8	2022-03-08 04:42	NWP02	NWA
9	2022-07-18 04:28	UT02	UT
10	2022-07-29 01:18	UT02	UT
11	2022-08-16 01:26	UT02	UT
12	2022-08-31 19:40	UT02	UT
13	2022-09-06 19:35	UT02	UT
14	2022-09-26 19:19	UT02	UT

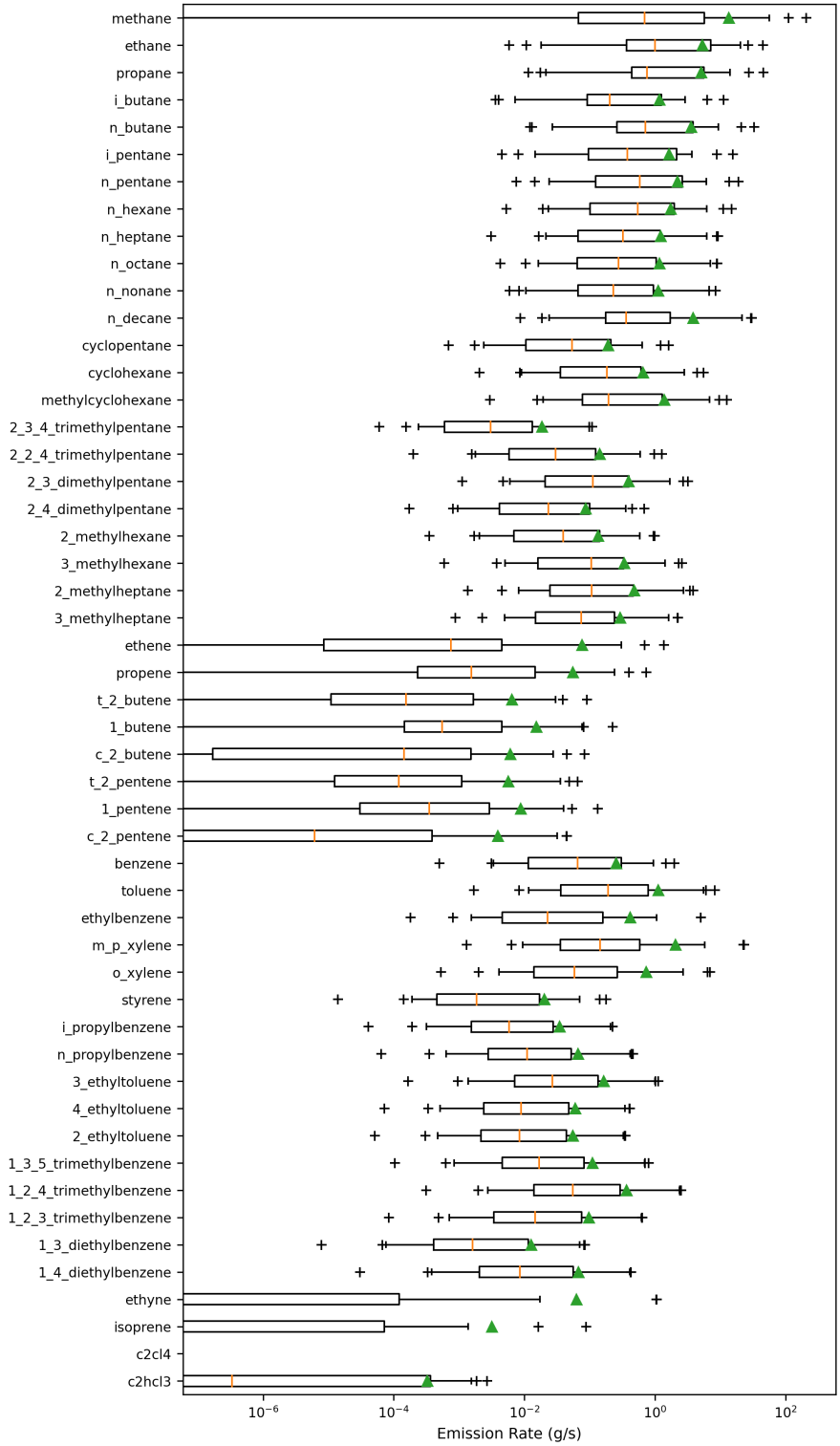

Figure D.1: Emission rates of 51 VOCs using plume-triggered canister samples during drilling operations with Neoflo mud. Green triangles and orange lines are mean and median values, respectively. Boxes and whiskers are 5^{th}, 25^{th}, 75^{th}, and 95^{th} percentiles.

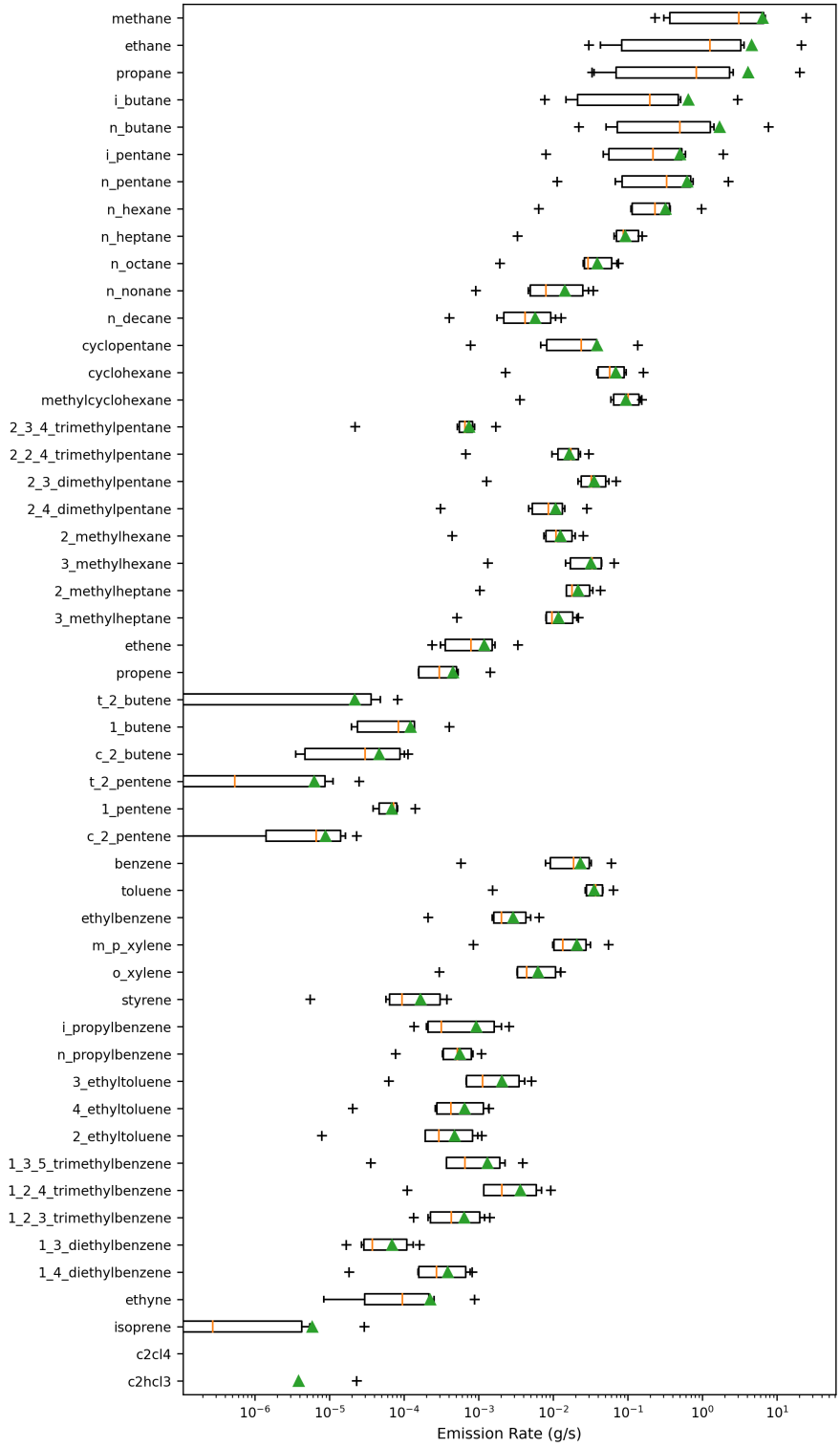

Figure D.2: Emission rates of 51 VOCs using plume-triggered canister samples during coiled tubing/millout operations. Green triangles and orange lines are mean and median values, respectively. Boxes and whiskers are 5^{th}, 25^{th}, 75^{th}, and 95^{th} percentiles.

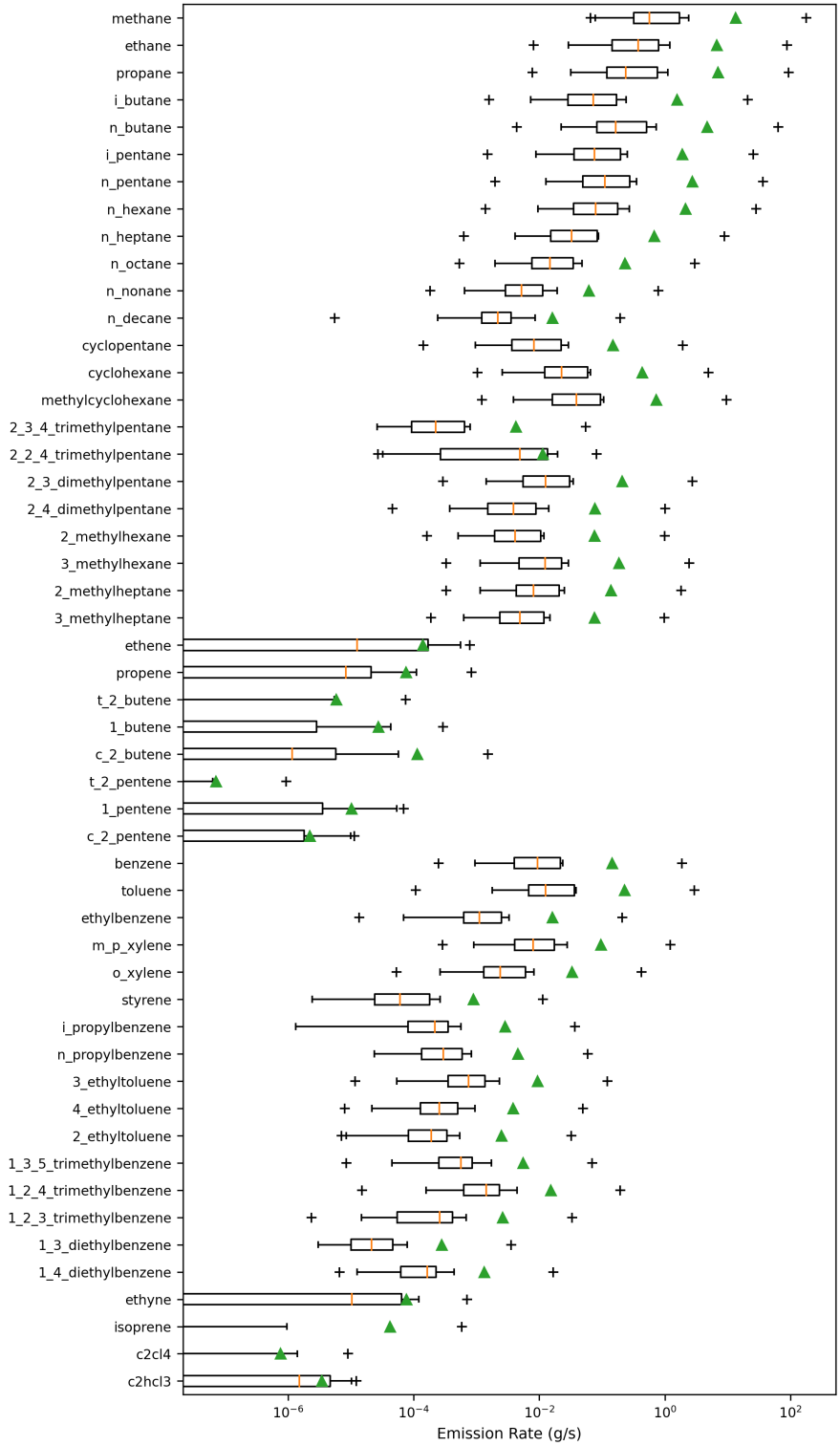

Figure D.3: Emission rates of 51 VOCs using plume-triggered canister samples during flowback operations. Green triangles and orange lines are mean and median values, respectively. Boxes and whiskers are 5^{th}, 25^{th}, 75^{th}, and 95^{th} percentiles.

Appendix E

1-Hour Concentration Extrapolation Method

The PID triggering system collects one canister sample in approximately 15 seconds, while AERMOD provides hourly simulations. To make them comparable when estimating the 1-hour emission rates, VOC concentrations in the triggered samples are extrapolated into 1-hour average concentrations based on the PID reading and VOC concentrations in the triggered canister samples. This method, adapted from Ajax Analytics (2022), assumes that the plume's composition remains consistent during each triggered event. Thus, changes in PID readings during each triggered event are presumed to be proportional to the changes in all plume species concentrations. When calculating the 1-hour estimated concentration for each triggered sample, the plume conversion factor (Equation E.1) and baseline conversion factor (Equation E.2) are essential components.

$$F_{plume} = \frac{[VOC]_{triggered}}{PID_{1-min}} \tag{E.1}$$

$$F_{baseline} = \frac{[VOC]_{baseline}}{PID_{baseline}} \tag{E.2}$$

In Equation E.1, F_{plume} is the plume conversion factor; $[VOC]_{triggered}$ is the VOC concentration in the triggered canister; and PID_{1-min} is the corresponding 1-min reading from the PID sensor at the triggered time. In Equation E.2, $F_{baseline}$ is the baseline conversion factor; $[VOC]_{baseline}$ is the baseline VOC concentration in the weekly canister at the same site during the corresponding monitoring week; and $PID_{baseline}$ is the baseline PID reading which is the average PID reading over a manually selected baseline period. This baseline period, typically ranging from 30 minutes to 1 hour, should fall within 48 hours prior to the triggered time. Furthermore, it is preferable to select a baseline period that is close to the triggered time.

Then, I apply these two conversion factors to the PID reading of every minute within a 120-minute window (1 hour before and 1 hour after the triggered time) using Equation E.3. This

process converts each 1-min PID reading into the corresponding 1-min estimated concentration. In Equation E.3, $[VOC]_{1-min}$ is the estimated 1-min VOC concentration, while F represents the plume or baseline conversion factor, depending on whether this minute is classified as a plume or baseline condition.

$$[VOC]_{1-min} = F * PID_{1-min} \tag{E.3}$$

The determination of whether to use the plume or baseline conversion factor depends on the PID reading's characteristics. Specifically, we apply F_{plume} to minutes with elevated PID readings, indicating the PID sensor measured the plume composition. Conversely, $F_{baseline}$ is applied to minutes without elevated PID readings, indicating the PID sensor measured the background air composition. If the $PID_{1-min} > 1.2 * PID_{baseline}$, we consider the reading as elevated and apply F_{plume}. The $1.2 * PID_{baseline}$ criteria is explained below.

Based on the long-term PID monitoring data, Ku et al. (2024) found that during the typical background conditions in Broomfield, the PID baseline signal ranged from 80 to 150 mV with a ±10 mV drift. Consequently, the maximum percentage of baseline reading drift is ±12.5% ($\frac{\pm 10mV}{80mV}$). Therefore, when the PID reading is between $1.125 * PID_{baseline}$ and $0.875 * PID_{baseline}$, it is categorized as baseline. To ensure accurate handling of PID readings and avoid misclassification (e.g., treating baseline readings as plume or vice versa), we employ the following criterion: when the PID reading exceeds $1.2 * PID_{baseline}$, it is classified as plume, and F_{plume} is applied. Otherwise, $F_{baseline}$ is applied.

Once all one hundred and twenty 1-min PID readings within the 2-hour window have been converted into corresponding estimated 1-min concentrations, we proceed to calculate a 60-min moving average for each minute, covering ±30 minutes of the triggered time within the window. This process obtains 60 moving averages for each triggered event. Subsequently, the maximum concentration among the 60 moving averages is identified as the extrapolated 1-hour concentration for this triggered event.